Edwardsville Supplemental Response

Marathon Pipe Line LLC

October 2023

Table of Contents

Overview

This document is the Marathon Pipe Line LLC (MPL) party submission to the National Transportation Safety Board (NTSB) regarding the March 11, 2021, incident in Edwardsville, Illinois, resulting in a release of crude oil. With cooperation from MPL, NTSB led the investigation of the incident to develop its investigation report for the accident.

MPL takes this accident seriously and provides this document to explain further its conclusions regarding the release and steps that it took to prevent a recurrence. Based on the Edwardsville Release, MPL reevaluated its Integrity Management Program and improved its processes. Specifically, MPL improved and standardized its method of identifying geohazard threats. MPL enhanced usage of in-line inspection to locate pipeline segments at risk from geohazards. Using lessons learned from the Edwardsville release, MPL expanded training and provided advanced tools to identify geohazards. MPL also reviewed and contributed to Pipeline Hazardous Materials Safety Administration (PHMSA) and industry research projects related to geohazards, including formal geohazard information-sharing events with seven pipeline companies.

Incident

Summary of Incident

At approximately 08:15 CST on March 11, 2022, the WoodPat 22-inch crude system (Woodpat) operated by MPL experienced a girth weld failure six miles downstream of Roxana station along Cahokia Creek near Edwardsville, Illinois. The ruptured pipeline discharged approximately 3,500 barrels of crude oil. No people were injured or structures damaged as a result of the release. The site had previously been remediated to address the geological hazard (geohazard) caused by the shifting of the bank of Cahokia Creek due to erosion. This supplemental response discusses MPL's response to the release, investigation of the release, and subsequent changes to prevent a recurrence.

Initial Response and Isolation of Rupture Site

MPL responded quickly to minimize the release of crude oil from the ruptured pipeline. MPL operates Woodpat from a remote Pipeline Operation Center (POC). At the time of the incident, Pipeline Controller A was responsible for operating the Woodpat. Controller A had worked for MPL for just over three years at the time of the incident. Controller A was performing normal pipeline control responsibilities at the time of the incident.[1]

Instantaneous to the release at 08:15 CST, the mainline unit of the pipeline, Unit 3, went down on low suction while the booster feeding Unit 3, Booster 8, was showing abnormal suction pressure. Attempting to stabilize the line in response to losing Unit 3, Controller A issued a start command to another Woodpat mainline unit, Unit 2**.** During the next three minutes, several flow and pressure alarms were activated at both the receipt and delivery ends of the Woodpat system. However, the Computational Pipeline Monitoring (CPM) leak did not alarm during this timeframe**.** Controller A interpreted the alarms coming in through the Supervisory Control and Data Acquisition (SCADA) system. The SCADA system monitors and automatically checks for potential pipeline leaks based on metered volumes and line pack calculations. Controller A identified the line conditions as an Abnormal Operating Condition (AOC) at

[1] Consistent with PHMSA and DOT regulations, Controller A was drug and alcohol tested, with negative test results.

08:19 CST and initiated a shutdown of the Woodpat system, which included isolation of both ends of the system via headgate valves. The system was shut down and isolated at both ends at 08:23 CST on March 11, 2022. Controller A's response was in alignment with MPL training and procedures.

At 08:45 CST, the POC notified Area Operations of a potential incident on the Woodpat system and dispatched personnel to investigate. Area Operations confirmed an active release of crude oil approximately six miles downstream of Roxana Station and entering Cahokia Creek at 09:50 CST. MPL employees further isolated the compromised pipeline location by closing the nearest upstream block valve, Roxana Equilon, at 09:51 CST and the nearest downstream block valve, Grant Fork, at 10:07 CST. The first containment boom was placed in Cahokia Diversion Channel at approximately 10:30 CST, with additional first responders completing boom deployment closer to the release location at 11:10 CST. The leading edge of the release was contained approximately one mile upstream of Cahokia Diversion Channel's confluence with the Mississippi River near the Highway 3 bridge at 21:23 CST. No released crude oil reached the Mississippi River.

Emergency response activities continued, including additional release countermeasures, agency notifications, and establishing a Unified Command consisting of MPL, United States Environmental Protection Agency (EPA), Illinois Environmental Protection Agency (IEPA), and Edwardsville Fire Department in addition to cooperating agencies consisting of United States Coast Guard (USCG), Pipeline and Hazardous Materials Safety Administration (PHMSA), United States Fish and Wildlife Services (USFWS), Illinois Department of Natural Resources (IDNR), Illinois Emergency Management Agency (IEMA), and Madison County Emergency Management for the response. The response identified the release location as a failed girth weld with evidence of pipeline bending strain due to earth movement. With approval from PHMSA, a repair plan was developed and implemented, resulting in the system restarting on March 15, 2022, at 07:32 CST.

The initial response/remediation efforts spanned from the originating location of the discharge, which included impacts to the shoreline, pipeline ROW, and adjacent wetland, as well as approximately ten miles of Cahokia Creek and Cahokia Diversion Channel to the confluence with the Mississippi River. The incident response began on March 11, 2022, and with the approval of Unified Command, transitioned to a post-response clean-up project on March 19, 2022. Gross contamination removal activities continued through May 16, 2022.

During the response, MPL deployed internal and external Oil Spill Removal Organizations (OSROs) to respond to the incident. Oil containment and recovery equipment began to arrive on the scene and was deployed within one hour to control the source and intercept the leading edge to prevent it from traveling further downstream. During the first 24 hours following the release, MPL had established ten oil spill containment locations along Cahokia Creek Cahokia Diversion Channel, extending to its confluence with the Mississippi River.

Emergency response personnel utilized boats, vacuum recovery trucks, frac tanks, booms, and skimmers at various locations along approximately ten miles of Cahokia Creek Cahokia Diversion Channel. Intermittent sheen and stained debris were observed along the banks and manually removed via on-water teams of personnel and boats. These teams used recirculation pumps to rinse impacted soils and vegetation and direct oil to absorbent booms and recovery equipment. Saturated absorbent booms were replaced as necessary, and impacted vegetation was removed as observed. Additionally, the Shoreline Cleanup and Assessment Technique (SCAT) was performed over twelve segments of Cahokia

Creek Cahokia Diversion Channel to the Mississippi River confluence.

Response activities at the point of the release included the vacuum recovery of crude and contact water and the removal of impacted vegetation and soil. Additionally, with approval from the IEPA, MPL installed and operated a water treatment system to aid in managing and treating accumulated surface water throughout the wetland, allowing further removal of impacted soil and debris.

MPL utilized trained personnel, environmental consultants, and EPA and IEPA employees to assess damage to the impacted areas. The response plans, including the following, were approved and executed during the initial response/remediation:

- Surface Water Sampling Plan
- Pipeline Corridor Soil Sampling Plan
- Wildlife Management Plan
- Shoreline Cleanup and Assessment Technique (SCAT) Plan
- Solid Waste Management Plan
- Private Water Well Sampling Plan
- Sediment Assessment Poling Plan
- Transition Plan
- Temporary Spill Prevention Control and Countermeasure (SPCC) Plan
- Site Safety and Air Monitoring Work Plan

The initial response/remediation efforts resulted in the recovery of approximately 96% (3362 bbls) of the material released. Ongoing cleanup efforts are being completed under the direction of the IEPA.

On the day of the incident, March 11, 2022, three MPL ROW Specialists were immediately engaged to support the incident. MPL ROW Specialists support pipeline incidents and emergencies by identifying and communicating with impacted stakeholders and informing parties how to file claims. The ROW Specialists traveled to the site and filled the Liaison and Community Relations roles within the Incident Command Structure. The first ROW Specialist was onsite at 15:25 CST; the other two arrived around 19:30 CST. As the ROW Specialist arrived at the site, they quickly got up to speed on the incident facts and contacted stakeholders. Due to the progression of the incident, three more ROW Specialists were brought to the incident to provide further support to the Liaison and Community Relations roles.

Existing Processes and Programs

MPL takes its obligation to prevent and respond to releases seriously. To this effect, MPL has implemented programs to ensure its pipeline's integrity and protect against geohazards.

Pipeline Integrity Management at MPL

MPL's Integrity Management Program (IMP), detailed in *MPL-Hazardous Liquids Integrity Management Program (IMP) Plan* (MPL-DOT-01167-POL), provides the framework for the management of pipeline and facility integrity activities delivering a comprehensive assessment and analysis of pipeline integrity. Our annual risk modeling systematically identifies potential hazards to each pipeline as well as their relative significance, from which preventative and mitigative measures are developed. These risks may include third-party damage, corrosion, cracks, dents, operator error, manufacturing defects, equipment failure, geohazards, or weather events.

MPL completes periodic inspections, testing, and preventative maintenance on its pipelines and associated equipment to confirm they are of sound integrity and functioning properly. MPL makes repairs and implements additional risk mitigation to maintain safe operations when necessary. Utilizing state-of-the-art methods, MPL assesses the integrity of its pipeline systems, including but not limited to:

- In-line inspection tools travel through pipelines, scanning and measuring a pipe's walls for signs of dents, corrosion, cracking, or bending strain. These tools can detect anomalous conditions associated with the pipeline. This technology allows MPL to address possible integrity issues in its systems proactively. These inspections are conducted at least once every five years for liquid pipelines in accordance with 49 CFR Part 195.
- Above-ground inspections involve visually inspecting pipeline routes with air and/or ground patrols to detect land disturbances and pipeline spills. These inspections are conducted at least once every three weeks for liquid pipelines in accordance with 49 CFR Part 195.
- Waterway crossing inspections use high-resolution sonar equipment to inspect underwater pipelines to determine whether erosion and water channel changes may impact the pipe. These inspections are conducted at least once every five years for liquid pipelines in accordance with 49 CFR Part 195.

The Geohazard Program at MPL at the Time of The Release

MPL's geohazard program was based on the *Guidelines for Management of Landslide Hazards for Pipeline*s, a joint industry project (JIP) completed in collaboration with the Interstate Natural Gas Association of America (INGAA) and its sponsors, including MPL. This document was developed to assist operators with establishing a Geohazard Management Program.

Based on the *Guidelines for Management of Landslide Hazards for Pipelines* framework, MPL's Geohazard Management Program is led by the Geohazard Integrity Engineer (GIE). This position is responsible for the overall management of the program.

MPL used and continues to use inertial measurement unit (IMU) data to complete bending strain assessments as a foundation for geohazard assessments. Following the recommendations in the *Guidelines for Management of Landslide Hazards for Pipelines*, strain features were analyzed for 0.35% total strain and 0.15% horizontal strain. In addition to this criterion, the GIE analyzed the bending strain data per *MPL-Responding to Strain Features* (MPL-MNT-01568-PRS). The output of the analysis was a prioritization of the bending strain calls.

- Priority 1 Feature: A feature that was likely affected by geohazards. A desktop study and site assessment were completed to confirm if the geohazard was active and affecting the pipeline.
- Priority 2 Feature: A feature that may be affected by geohazards but lacks confirmation. A desktop study and site assessment were completed to confirm if the geohazard was active and affecting the pipeline.
- Priority 3 Feature: A feature was likely not a geohazard. The location was provided to Integrity Analysis Services (IAS) and used for data integration.

Field investigations, led by a surveying or geological consultant, gathered pipe depths, alignment, topographic, and soil information to identify whether a geohazard was present at the location. The information was compiled into a report and submitted to the GIE. The GIE reviewed field reports and determined if the site was flagged for monitoring or mitigation.

Systems determined to be susceptible to geohazards were assessed via an In-Line Inspection (ILI) tool with IMU every five years at a minimum. Pipe movement between ILI tool runs were analyzed, and strain changes greater than 0.04% were flagged for prioritization and investigation. MPL also conducted laser imaging, detection, and ranging (LiDAR) on lines determined to be susceptible to geohazard threats. All potential geohazard locations are stored in MPL's integrity database, including ILI tool data, strain inspection, and geohazard mitigation information.

Leak Detection at MPL

MPL is required by 49 CFR §195.444 to have an effective system for detecting leaks and to evaluate the system capability to protect the public, property, and environment. Per 49 CFR §195.444(b), at a minimum, this evaluation must consider the length and size of the pipeline, the type of product carried, the swiftness of detection, the location of response personnel, and the leak history of the pipeline being monitored. MPL utilizes the Leak Detection Adequacy Process to comply with 49 CFR §195.444 (b). This process reviews and selects different leak detection systems based upon defined requirements and Subject Matter Expert (SME) review. This review is completed at a minimum of once every five years for all pipeline systems. In addition, 49 CFR §195.134 requires that any installed leak detection system adhere to API RP 1130, an industry document outlining the maintenance and testing of Computational Pipeline Monitoring (CPM) Systems. MPL complies with CPM Selection criteria according to API RP 1130 Section 4.2, installs and maintains the proper infrastructure to support the use of CPM Systems according to API RP 1130 Section 5, and operates, maintains, and tests CPM Systems according to API RP 1130 Section 6.

MPL utilizes leak detection systems using field-captured telemetry including flow rate, pressure, and temperature. On the Woodpat system MPL uses "AVEVA SimSuite 6.7®". This system is a real-time transient model system that utilizes hydraulic calculations to accurately calculate the inventory of the pipeline, otherwise known as line pack. The line pack value is then summed with the flow difference between receipt and delivery meters to calculate a leak rate. This leak rate is calculated in a series of averaging periods with a decreasing alarm threshold. The current thresholds in use by MPL are one minute, five minutes, 30 minutes, and 2 hours. As the timeframe decreases, the level at which the system will alarm also decreases. The thresholds are calculated based on the accuracy of measurement equipment, including flow meters, pressure transmitters, and temperature sensing equipment. The method of baseline threshold calculation is based upon the calculations provided by API 1149; from this point the baselines are tuned by CPM Engineers to provide a balance of sensitivity, a measure of how small of a leak can be detected, and reliability, a measure of how many false positives are generated by the system. The system is based on servers at the primary and backup operations center and has multiple levels of redundancy.

MPL Hydraulics Group supports the leak detection system, and the scope of work includes the development of new models, modifications to models as field changes are required, and supporting the day-to-day interpretation of leak detection alarms. Personnel are trained both by MPL subject matter experts and training sessions hosted by the AVEVA company. After-hours leak detection system support is provided by the same engineers responsible for developing the models and is based on a four-week call-out schedule. Multiple levels of support are utilized, including an on-call primary, on-call backup,

second-level support, and third-level SME support. When needed, support from AVEVA is utilized. MPL continues to review new technologies for use in our leak detection program, including new forms of computerized leak detection as well as externally based point-specific systems.

Improvements to leak detection implemented after the Edwardsville incident include:

- Removing “additive” threshold increases when overlapping transient events occur.
    - Pre-release thresholds increased when pumps changed status, control valve position significantly changed, system started and stopped.
    - These increases could potentially all occur at the same time yielding a detection threshold that was above the potential flow rate of the system.
- Removing threshold increases based on delivery change.

Pipeline Operations Center (POC) Training Overview

The objective of the POC Training Program is to ensure that we have consistent and reliable operations throughout all POC personnel. This is accomplished by implementing our formalized training program that guarantees all POC personnel are trained and qualified to operate under normal, abnormal, and emergency conditions.

The Training Program is initiated with our onboarding class, where we introduce general pipeline operations to new controllers. The onboarding class takes around three weeks to complete and introduces new controllers to our company, culture, and operating philosophy as well as basic operating concepts and terminology. During this onboarding class, we utilized different applications such as our SCADA system as well as our simulator to help develop the knowledge the controllers will need for pipeline operations.

After completion of the onboarding class, controllers will then transition to the on-console portion of the training, where they are introduced to a specific console and specific pipeline systems. They start to take a more hands-on approach to learning as they will engage with a qualified controller about more complex operations through day-to-day operations and are required to take assessments along the way to confirm comprehension of the material. The overall Training Program lasts around six months, and the controller is required to demonstrate they understand pipeline operations during normal, abnormal, and emergency situations through the certification process at the end of their training.

The certification process involves passing a written test consisting of console-specific information as well as completing an evaluation on OQ-covered tasks. Lastly, the controller must also demonstrate their understanding through a panel evaluation discussion conducted by the Training Department and POC Supervision. A passing grade is required on the written certification test, the panel evaluation, and the OQ-qualified tasks to officially qualify on a specific console.

Emergency Response Program

MPL has developed and implemented various leak prevention and detection methodologies and standards utilized on MPL's PHMSA-regulated pipeline systems. The majority of pipelines operated by MPL are controlled by the company's Pipeline Operations Centers via a SCADA system. The SCADA system monitors and automatically checks for potential pipeline leaks based on metered volumes and line pack calculations. The measured volumes are compared at specific time intervals, and an alarm

condition will alert the Pipeline Operations Center Controller to potential problems. According to MPL's *Martinsville Response Zone Emergency Response Plan*, these alarm responses direct controllers and field personnel on measures to be taken for each type of alarm that could be received. Response plan procedures described initial response objectives that included personnel and public safety, securing the source, containing released product, ignition control, and notifications.

Per the Oil Pollution Act of 1990 (OPA90) National Preparedness for Response Exercise Program (NPREP) guidelines, Wood River Operations performed equipment deployment exercises. Wood River Operations deployed boom on Cahokia Creek and Cahokia Diversion Channel on September 25, 2018, and October 31, 2016.

Following the accident, MPL performed a post-incident review to identify actual or potential deficiencies in the applicable emergency response plan and determine the changes required to correct any deficiencies. The Edwardsville post-incident review did not identify any deficiencies with the Martinsville Response Zone Emergency Response Plan and noted potential improvements in local first responder incident management training, wildlife rehabilitation service providers, and shoreline cleanup assessment technique training.

Damage Prevention ROW Inspection and Monitoring

MPL's ROW Inspection program includes routine aerial or ground patrols that target a weekly inspection. This program requires at least 26 inspections each calendar year, not exceeding three weeks between inspections for 49 CFR Part 195-regulated systems. Additional inspections are performed as needed for emergencies or special events. Qualified individuals look for and report third-party threats, potential leaks, indications of natural force threats, encroachments, and any other operational concerns. These are reported as conflicts through MPL's ticket management software, investigated in the field, and closed or resolved.

MPL has also pursued an investment in Flyscan to partner on the development and implementation of an Advanced ROW Inspection solution for the industry. This solution leverages hardware mounted on a fixed-wing aircraft to capture high-resolution visual and hyperspectral imagery of the entire rights of way during flight. The imagery is analyzed in real time using artificial intelligence threat detection models to detect pipeline conflicts, including mechanical equipment, encumbrances, and other third-party threats. Additional models are currently in development and testing to identify leaks, geohazards, pipe exposures, and farming practices post-flight. Leveraging imagery capture and artificial intelligence will help improve the effectiveness of inspections and minimize human error.

Public Engagement

MPL's Public Engagement program, named "Earning Your Trust", began in 2016 to build better relationships with its external stakeholders to improve communications, transparency, and trust between the company and its external stakeholders. Areas of focus include schools, public officials, emergency responders, landowners, and the communities in which we operate. MPL set out to make these improvements via an innovative five-year mail campaign that used unique packaging meant to minimize the discarding of materials and encourage the stakeholders to open and review educational materials. Topics covered in these mailers included the importance of calling 811, pipeline maintenance practices, what to do in the event of a pipeline emergency, the difference between 811 and 911, and rules and guidelines for the development of pipeline rights of way.

One of the key components of the Earning Your Trust program was the sharing of single points of contact for external stakeholders. MPL's Right-of-Way Specialists became the point of reference for most external stakeholders as their names, likenesses, e-mail addresses, and mobile phone numbers were shared with every landowner along an MPL right-of-way. MPL also committed that all inquiries and concerns would be responded to within three business days to establish this two-way communication. MPL then built out several tools to make this outreach easier, starting with providing contact information on www.marathonpipeline.com and setting up landowner e-mail and voicemail inboxes. Interactions continue to be tracked through MPL's Public Inquiry system to ensure accountability for this commitment to two-way communication.

Causation

Pipeline Attributes, Original Testing, Subsequent Testing, and MOP

The Woodpat pipeline begins in Wood River, Illinois, and ends in Patoka, Illinois. The pipeline was constructed in 1949 with carbon steel pipe coated with coal tar enamel. Crude oil of various grades is transported through the pipeline. The section of the Woodpat pipeline involved in the accident is predominately comprised of 0.344-inch wall thickness, API 5L Grade X-46 line pipe with electric resistance welded (ERW) longitudinal seams manufactured by the Youngstown Sheet and Tube Company.

MPL has conducted extensive integrity testing of the Woodpat pipeline. Figure 1 provides an overview of the line's integrity assessment history since 1990 and is summarized below.

Figure 1: Integrity Assessment History

Year	Technology	Vendor
1990	Hydrotest	N/A
1991	Hydrotest	N/A
2002	CAL	Enduro
2003	UTWM	Pii
2004	Hydrotest	N/A
2007	CAL/MFL	CPIG
2009	Hydrotest	N/A
2012	CAL/IMU/UTCD/CMFL/UTWM	GE
2013	Hydrotest	N/A
2017	CAL/IMU/CMFL/UTWM	GE
2018	IMU/EMAT	Rosen
2018	UTCD	GE
2018	Hydrotest	N/A

2018	UTCD	GE
2019	UTCD (Eclipse)	NDT
2020	UTCD (Eclipse)	NDT
2021	CAL/IMU	Rosen
2021	UTCCD	NDT
2021	CMFL/MFL/PGS	Rosen

- **August 1990, System Hydrotest**. A system hydrotest occurred in August of 1990. The full system was hydrotested, except for the piping between mile post (MP) 46 – MP 51.
- **August 1991, System Hydrotest.** In August of 1991, the full system was hydrotested. This test established the maximum operating pressure (MOP) for the segment and assessed for geometric anomalies, metal loss, and manufacturing defects.
- **November 17, 2002, Enduro Caliper (CAL) ILI Assessment.** An Enduro CAL assessment was completed on November 17, 2002, to assess for geometric anomalies and mechanical damage. This represented the first geometric anomaly-focused ILI assessment for the pipeline segment.
- **January 21, 2003, Pii Ultrasonic Wall Measurement (UTWM) ILI Assessment.** A Pii UTWM assessment was completed on January 21, 2003, to assess for metal loss. This represented the first metal loss focused ILI assessment for the pipeline segment.
- **April 2004, System Hydrotest.** A full system hydrotest occurred in April of 2004. This test reestablished the MOP for the segment and assessed geometric anomalies, metal loss, and manufacturing defects.
- **September 21, 2007, CPIG CAL/Magnetic Flux Leakage (MFL) ILI Assessment.** A CPIG CAL/MFL assessment was completed on September 21, 2007, to assess for geometric anomalies, mechanical damage, and metal loss. This assessment was the first assessment where ILI data was integrated together from the vendor.
- **March/April 2009, System Hydrotest.** A full system hydrotest occurred in March/April of 2009. This test reestablished the MOP for the segment and assessed geometric anomalies, metal loss, and manufacturing defects.
- **August 21 - September 18, 2012, GE CAL/IMU/Ultrasonic Crack Detection (UTCD)/Circumferential MFL (CMFL)/UTWM ILI Assessment.** A GE CAL/IMU assessment was completed on August 21, 2012, to assess for geometric anomalies and mechanical damage. The IMU tool collected global positioning system (GPS) data at the girth welds across the system to assist with locating anomalies. A GE UTCD assessment was completed on August 23, 2012, to assess for manufacturing-related defects in the long seam and pipe body crack defects. This assessment represented the first crack-focused ILI assessment for the pipeline segment. A GE CMFL assessment was completed on September 6, 2012, to assess for metal loss and manufacturing defects in the long seam. This represented the first long seam magnetic focused ILI assessment for the pipeline segment. In addition to the CMFL assessment, MPL elected to complete the Kinder Morgan assessment protocol (KMAP) using the CMFL data. The KMAP analysis is a Kinder Morgan proprietary analysis service that uses CMFL data to prioritize CMFL signals in the long seam. A GE UTWM assessment was completed on September 18, 2012, to assess for metal loss.
- **May 2013, System Hydrotest.** A full system hydrotest occurred in May 2013. This test reestablished the MOP for the segment and assessed for geometric anomalies, metal loss, and manufacturing

defects.

- **February 28 – March 15, 2017, GE CAL/IMU/CMFL/UTWM ILI Assessment.** A GE CAL/IMU assessment was completed on February 28, 2017, to assess for geometric anomalies and mechanical damage. The IMU was run to provide GPS positions across the system. A GE CMFL assessment was completed on March 8, 2017, to assess for metal loss and manufacturing defects in the long seam. In addition to the CMFL assessment, MPL elected to complete the KMAP analysis using the CMFL data. A GE UTWM assessment was completed on March 15, 2017, to assess for metal loss.
- **January 5, 2018, Rosen IMU/Electro Magnetic Acoustic Transducer (EMAT) ILI Assessment.** A Rosen EMAT assessment was completed on January 5, 2018, to assess for manufacturing-related defects in the long seam and pipe body crack defects. This IMU data was collected to complete a pipeline bending strain assessment and assess for geohazard threats on the segment.
- **January 19, 2018, GE UTCD ILI Assessment.** A GE UTCD assessment was completed on January 19, 2018, to assess for manufacturing-related defects in the long seam and pipe body crack defects.
- **March 2018, System Hydrotest.** Both January 2018 EMAT and UTCD assessments were completed before the hydrotest. A full system hydrotest occurred in March 2018. This test reestablished the MOP for the segment and assessed for geometric anomalies, metal loss, and manufacturing defects.
- **May 24, 2018, GE UTCD ILI Assessment.** A GE UTCD assessment was completed after the hydrotest on May 24, 2018. This assessment was completed to compare variability between subsequent UTCD inspections and identify any crack-like flaws that may have progressed during the hydrotest.
- **March 20, 2019, NDT UTCD ILI Assessment.** An NDT UTCD Eclipse assessment was completed on March 20, 2019, to assess for manufacturing-related defects in the long seam and pipe body crack defects. The Eclipse technology was developed between NDT and MPL and designed with the additional capability to detect and size long seam defects that have a tilt/skew (hook type features) from the manufacturing process.
- **February 24, 2020, NDT UTCD ILI Assessment.** An NDT UTCD Eclipse assessment was completed on February 14, 2020, to assess for manufacturing-related defects in the long seam and pipe body crack defects. This tool run served as a comparison to the 2019 NDT UTCD Eclipse assessment and provided information to prioritize pipe joints for removal and analysis. These pipe joints were sent to a lab for destructive testing and UTCD Eclipse validation.
- **August 31, 2021, Rosen CAL/IMU ILI Assessment.** A Rosen CAL/IMU assessment was completed on August 31, 2021, to assess for geometric anomalies and mechanical damage. This IMU data was used to complete a bending strain assessment and pipeline movement analysis based on this and the 2018 IMU data set.
- **September 20, 2021, NDT Ultrasonic Circumferential Crack Detection (UTCCD) ILI Assessment.** An NDT UTCCD assessment was completed on September 20, 2021, to assess for crack-like and construction flaws oriented in the circumferential direction. The tool has the capability of detecting and sizing circumferential flaws present in girth welds as well as the pipe.
- **October 13 – 27, 2021, Rosen CMFL/MFL/Pipe Grade Specification (PGS) ILI Assessment.** A Rosen CMFL assessment was completed on October 13, 2021, to assess for metal loss and manufacturing defects in the long seam. A Rosen MFL/PGS assessment was completed on October 27, 2021, to assess for metal loss. The PGS was run to provide additional data on each joint's pipe grade specification.

The most recent hydrostatic test was completed in 2018 at a pressure of 1,100 psi. MPL set the MOP at 80% of the hydrotest pressure, which is 881 psi. At the time of the accident, the pressure on Woodpat

was calculated to be 423 psi at the release location based on the upstream pump station corresponding to approximately 41% of the specified minimum yield strength (SMYS).

Calculation of Tensile Strain Capacity

MPL retained a third-party engineering firm to perform testing and analysis to evaluate the girth weld tensile strain capacity (TSC) of the pipeline segment. Two girth welds were tested as part of the analysis. The strain capacity report was received on October 18, 2021, and the strain capacity of the girth welds was found to be 0.73% and 1.5%, respectively, which is consistent with the strain capacity of welds constructed during this time period.

Geohazard Identification and Assessment at the Incident Site

In addition to integrity testing, MPL evaluated Woodpat for geohazard risks. The following is a timeline of interactions with the accident site from a geohazard assessment perspective:

- **January 5, 2018, IMU ILI Assessment.** An IMU assessment was completed on January 5, 2018, to collect the data to be used to complete a pipeline bending strain assessment for the segment, assessing the geohazard threat on the system.
- **April 23, 2019, Bending Strain Assessment**. MPL hired a third-party to complete a bending strain assessment based on the 2018 IMU dataset. The bending strain assessment report was received on April 23, 2019.
- **May 10, 2019, Site Identification**. The area involved in the accident was first identified as a potential geohazard on May 10, 2019, as part of the bending strain assessment report analysis. The analysis of this data set resulted in Item 765 being a Priority 1 Feature.
- **April 17, 2020, Site Investigation Project Created**. MPL initiated a project on April 17, 2020, to complete a desktop study and site investigation of the Priority 1 Feature to confirm if the geohazard is active and affecting the pipeline.
- **April 15, 2021, Site Investigation**. MPL hired a third-party geotechnical engineering firm to begin the desktop study and site investigation for the Priority 1 Feature.
- **July 4, 2021, Girth Weld Strain Capacity Testing**. MPL retained a third-party engineering firm to perform an analysis to evaluate the girth weld TSC of the pipeline and compare against the Item 765 reported strain. Two girth welds were tested as part of the analysis.
- **July 7, 2021, Site Investigation Final Report.** MPL received the third-party geotechnical engineering firm desktop study and site investigation report on July 7, 2021. The site investigation resulted in a recommendation to increase monitoring of the bank stability, repeat depth of cover surveys, and consider additional armoring of the south bank to decrease ongoing bank instability.
- **August 31, 2021, IMU ILI Assessment**. Based on the recommendations of the third-party geotechnical engineering firm site investigation, MPL completed a second IMU assessment on August 31, 2021. A bending strain assessment and pipeline movement analysis was planned for 2022 based on this data and the 2018 IMU data set. The pipeline movement and bending strain assessment final report was not received until March 30, 2022.
- **October 18, 2021, Girth Weld Strain Capacity Final Report.** MPL received the third-party engineering firm strain capacity final report on October 18, 2021, and the strain capacity of the two girth welds was found to be 0.73% and 1.5%, respectively. The estimated TSC of the girth welds was more than twice the indicated bending strain of Item 765 at 0.34%.
- **March 11, 2022, Woodpat release occurred.**

Site Work at the Incident Site

Beginning in 2014, MPL acted at the site of the release to reduce the risk of erosion at the site and address integrity concerns. On August 11, 2014, MPL hired a third-party contractor to line the south bank of Cahokia Creek with concrete mats to stabilize the bank and to cover and protect the pipeline. The bank and washout area were reshaped to create gentle, stable slopes within the project area. The freshly grated creek and washout area was covered with geotextile material, followed by the installation of a concrete mattress system. The mats were extended down the bank for approximately 175 feet and covered the washout area to prevent further erosion. The mats were anchored into the bank elevation in excavated two-foot-deep termination trenches to prevent undercut. The upstream leading edge of the mattress system was terminated in an excavated three-foot deep anchor trench. They used 35 total mats that were 8 feet by 20-foot in size.

On May 13, 2014, MPL completed a rehab dig based on the 2012 GE CMFL ILI report. Four Type B sleeve repairs were made to remediate the lack of fusion features 9%-15% in depth. A 30% deep metal loss feature was also recoated as part of this work.

On April 20, 2017, MPL hired a third-party contractor to repair the existing matting, regrade the bank, and install additional mats to ensure the pipeline had adequate cover and protection in the bank and washout area near Cahokia Creek. In the years since the 2014 remediation was installed, there was evidence that the mattress system had started to slide toward the creek. Of the about 175 feet of matting, around 125 feet on the repair's west side showed signs of slippage and erosion on the leading edge closest to the creek. Fourteen mats were removed, and the area beneath them was regraded before they were replaced. Three of the existing mats were removed and not put back into service. An additional row of nine mats was added to the south side of the matting system to reach level ground before anchoring to prevent future slippage. Twenty cubic yards of rip rap were added to the edges of the mats. Lastly, duck bill anchors were installed to secure the mats further. Pipeline depth of cover across this area was noted as consistently around four feet.

Significant Rain Events at the Incident Site

MPL completed a review of significant rain events at the incident site from January 1, 2008, through December 31, 2022. The gage height data for Cahokia Creek at Edwardsville (05587900) started collecting data on October 1, 2007. The banks of Cahokia Creek overflow at approximately 12.5 feet. Figure 2 of the significant rain event review does not show a significant trend. The blue line represents the number of events where water was at or above 12.5 feet over the 15 years. Note that only two of the 2022 events occurred before the accident.

Figure 2: Significant Rain Events at the Incident Site

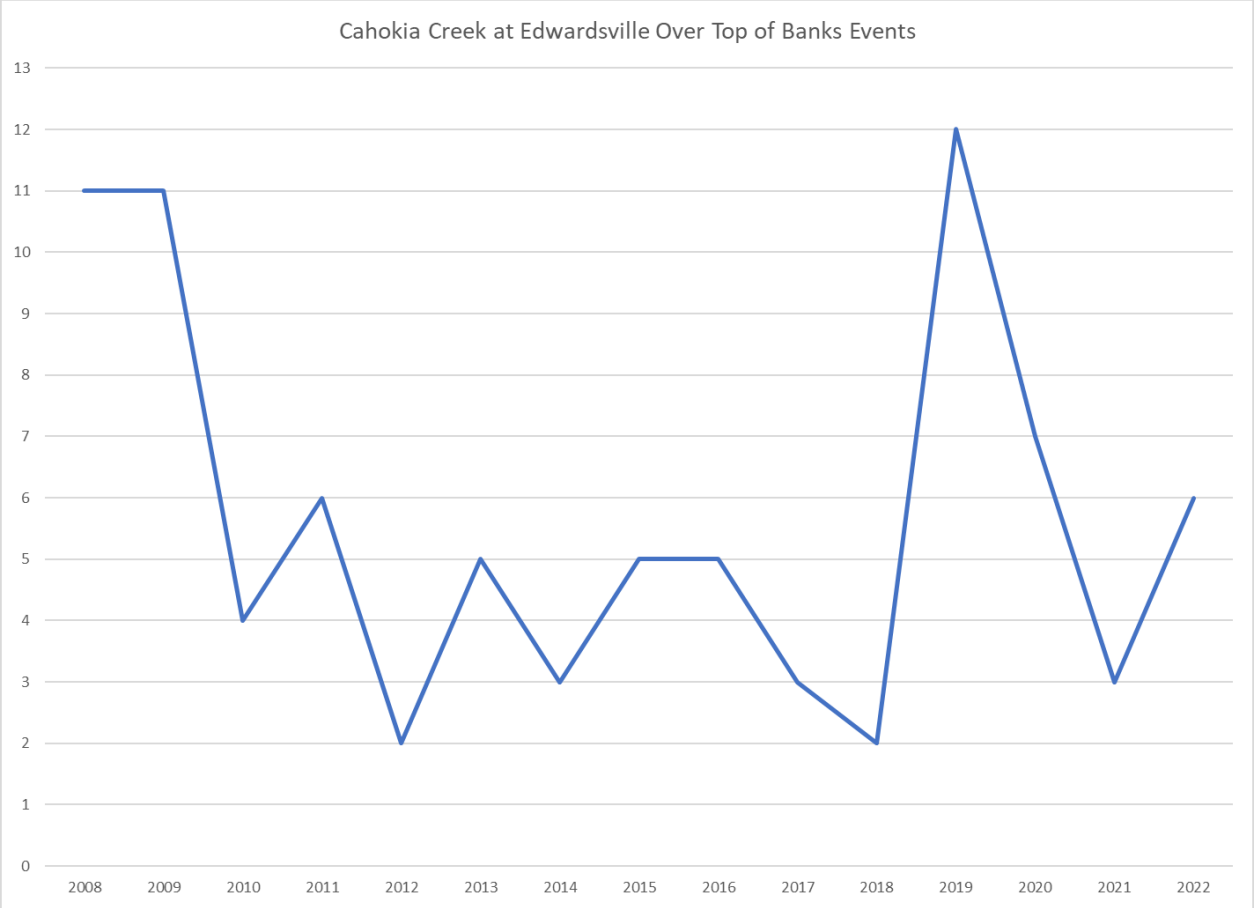

Water in Cahokia Creek passes underneath the bridge east of the incident site, and flows directly toward the south stream bank, towards the location of the failure. Sandy flood deposits were observed along the streambank more than 15 feet above the observed water elevation, suggesting that episodic high-flow and associated erosional events occur within Cahokia Creek. Streambank deposits along Cahokia Creek are alluvial deposits susceptible to scour. It is suspected that a single flood event is not responsible for the scour that led to the conditions at the incident site, but rather a series of several small events.

Land Movement and Pipe Deflection

IMU ILI assessments were completed in 2018 and 2021. The bending strain assessment of the 2018 tool data shows strain and displacement. The maximum total bending strain of 0.34% was at the maximum movement point, but the girth weld failure did not occur at this location. The failed girth weld was outside the 196-foot strain envelope. Displacement and strain increased over time as the pipe moved towards the creek. From the pipeline movement and bending strain assessment of the 2021 tool data and comparison to the 2018 data set, the pipe moved four feet diagonally towards the creek between 2018 and 2021. In 2021, the maximum total bending strain had increased to 0.41%, and the girth weld that failed was now inside the 348-foot strain envelope.

Figure 3: 2018 Total Bending Strain

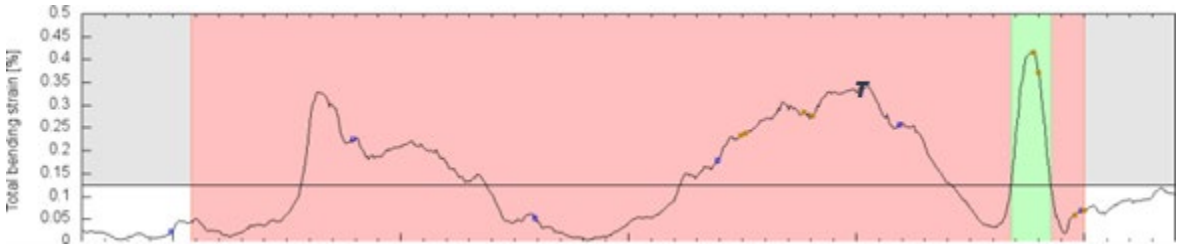

Figure 4: 2021 Total Bending Strain

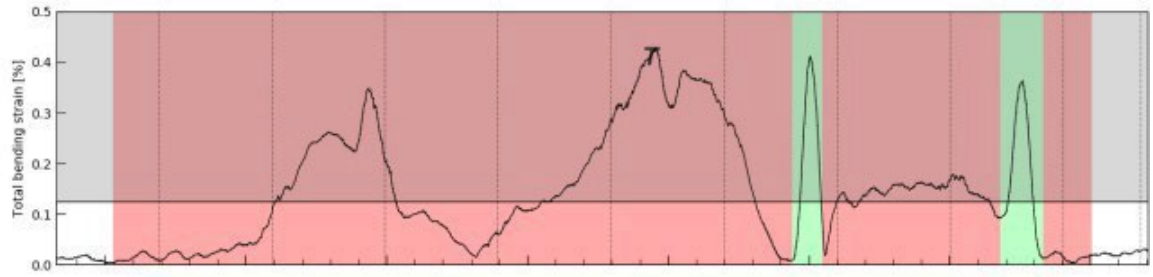

Figure 5 below shows the eight-foot deflection of the pipeline from deviation to a straight line just prior to the accident on March 11, 2022.

Figure 5: 2018 and 2021 Deviation to a Straight Line

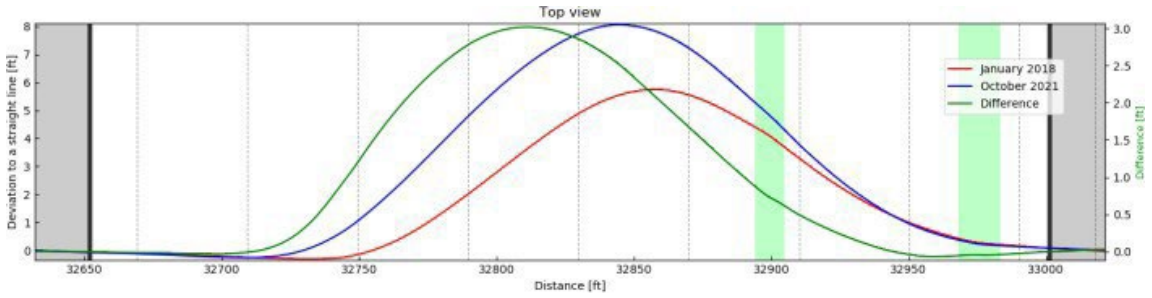

Analysis

Regulatory Requirements

PHMSA requires the consideration of hazards in the operation of pipelines and for operators to act when they identify conditions, such as geohazards, that could impact the pipeline's safe operation. 49 CFR §195.401(b)(1).

The PHMSA regulations are silent regarding specific steps an operator must take to protect hazardous liquid pipelines from geological hazards. Rather, PHMSA relies upon performance-based standards to address threats like those posed by geological hazards. The applicable regulation, 49 CFR §195.401(b)(2), however, provides operators with flexibility in how they address geological hazards and does not impose strict liability on operators if unanticipated conditions were to cause a release. *See ExxonMobil Pipeline Co. v. U.S. Dep't of Transp.*, 867 F.3d 564, 577-78 (5th Cir. 2017). Therefore, to determine whether an operator complied with PHMSA's requirements for geological hazards, one cannot rely upon a checklist of mandated mitigation practices applicable to all hazardous liquid

pipelines or even the fact that a release occurred. To determine compliance when addressing geological hazards, it is necessary to consider whether the operator took appropriate, practicable steps to protect the line from abnormal loads caused by geological hazards.

Section 49 CFR §195.401(b)(1) of the pipeline safety regulations for hazardous liquid pipelines states that ''[w]henever an operator discovers any condition that could adversely affect the safe operation of its pipeline system, it must correct the condition within a reasonable time. However, if the condition is of such a nature that it presents an immediate hazard to persons or property, the operator may not operate the affected part of the system until it has corrected the unsafe condition.'' Section 49 CFR §195.401(b)(2) further states that ''[w]hen an operator discovers a condition on a pipeline covered under [the integrity management requirements in] §195.452, the operator must correct the condition as prescribed in §195.452(h).'' Land movement, severe flooding, river scour, and river channel migration are the types of unusual operating conditions that can adversely affect the safe operation of a pipeline and require corrective action under 49 CFR §195.401(b). Additional guidance for identifying risk factors and mitigating natural force hazards on pipeline segments, which could affect high-consequence areas, are outlined in Appendix C, Section B, to Part 195. 49 CFR §195.452(i) requires an operator to take additional preventative and mitigative measures to prevent a pipeline failure and to mitigate the consequences of a pipeline failure that could affect a high-consequence area.

In 2019, PHMSA issued an advisory bulletin addressing the risks of geohazards, *Pipeline Safety: Potential for Damage to Pipeline Facilities Caused by Earth Movement and Other Geological Hazards*, [Docket No. PHMSA–2019–0087]. In the bulletin, PHMSA made recommendations to address the serious safety-related issues that can result from geohazards. Specifically, the bulletin made six recommendations:

1) Identify areas surrounding the pipeline that may be prone to large earth movement, including but not limited to slope instability, subsidence, frost heave, soil settlement, erosion, earthquakes, and other dynamic geologic conditions that may pose a safety risk.
2) Utilize geotechnical engineers during the design, construction, and ongoing operations of a pipeline system to ensure that sufficient information is available to avoid or minimize the impact of earth movement on the integrity of the pipeline system. At a minimum, this should include soil strength characteristics, ground and surface water conditions, propensity for erosion or scour of underlying soils, and the propensity of earthquakes or frost heave.
3) Develop design, construction, and monitoring plans and procedures for each identified location, based on the site-specific hazards identified. When constructing new pipelines, develop and implement procedures for pipe and girth weld designs to increase their effectiveness for taking loads, either stresses or strains, exerted from pipe movement in areas where geological subsurface conditions and movement are a hazard to the pipeline integrity.
4) Inclusion of certain considerations in monitoring plans, such as conducting stress/strain analysis utilizing in-line inspection tools equipped with Inertia Mapping Unit technology and High-Resolution Deformation in-line inspection for pipe bending and denting from movement, utilizing aerial mapping light detection, and ranging or other technology to track changes in ground conditions.
5) Develop mitigation measures to remediate the identified locations.
6) Mitigation measures should be based on site-specific conditions and include options such as reducing the steepness of potentially unstable slopes, including installing retaining walls, soldier

piles, sheet piles, wire mesh systems, mechanically stabilized earth systems and other mechanical structures.

MPL took PHMSA's advisory bulletin seriously and implemented the recommendations. As described in detail, MPL made further improvements to its geohazard program based on lessons learned from the Edwardsville release.

Probable Cause and Contributing Factors

The failure of the Woodpat pipeline that occurred on March 11, 2022, was the result of the tensile strain demand of the area adjacent to Cahokia Creek exceeding the tensile strain capacity of the pipeline. The factors attributed to the strain demand include creek bank instability and the formation of a plastic hinge at the area near the failed girth weld. The creek bank instability was caused by a combination of water flow directed toward the south stream bank as a result of a rip rap peninsula that was installed off the north bank immediately downstream of the Edwardsville Road bridge, episodic high-flow erosional flood events, and the creek bank consisting of alluvial deposits, which are susceptible to scour. This location saw a rapid change (89% increase) in strain between 2021 and the time of the failure. The strain capacity of the failed girth weld was reduced due to the presence of a defect measuring 7.2 inches long and a peak depth of 88% deep located at the 1:15 – 1:30 o'clock orientation on the pipeline. The combination of the rapidly increasing strain demand from earth movement and reduced strain capacity of the failed girth weld caused the Woodpat failure. For more information on the cause and contributing factors, see attached Edwardsville Failure Analysis (Exhibit A) and Memorandum Addressing Cause of Ground Movement (Exhibit B).

Post-Incident Improvements

MPL has an extensive IMP that identifies and manages integrity threats to the pipeline systems and is known in the industry for leading integrity improvements. Threats include corrosion, third-party damage, dents, cracks, manufacturing defects, and geohazards. Based on the Edwardsville release, MPL reevaluated its Integrity Management Program and improved its processes. Specifically, MPL 1) performed site stabilization at the location of the release, 2) improved and standardized its method of identifying geohazard threats, 3) enhanced usage of in-line inspection to locate pipeline segments at risk from geohazards, 4) used lessons learned from the Edwardsville release to expand training and provide advanced tools to identify geohazards, and 5) reviewed and contributed to PHMSA and industry research projects related to geohazards.

Earth Stability

To prevent a recurrence of the geohazard conditions that caused the release, MPL completed site stabilization improvements. To prevent further erosion, a 190-foot-long super-sack wall filled with sand three sacks high was placed along the stream bank near the accident location. MPL placed sloped imported clay fill at no greater than a three horizontal to one vertical slope with a preference to reduce the slope inclination as much as practical while still establishing the minimum depth of cover on the repaired pipeline. To prevent water from crossing the pipeline, MPL constructed a temporary berm. The rip rap peninsula installed off the north bank immediately downstream of the Edwardsville Road bridge was removed with the approval of Illinois Department of Transportation (IDOT) to divert the water flow away from the impacted stream bank. The figure below shows the water flow with the peninsula intact. Notice the water's trajectory toward the south bank, which coincides with the failure's location.

Figure 6: Cahokia Creek Flow with Peninsula

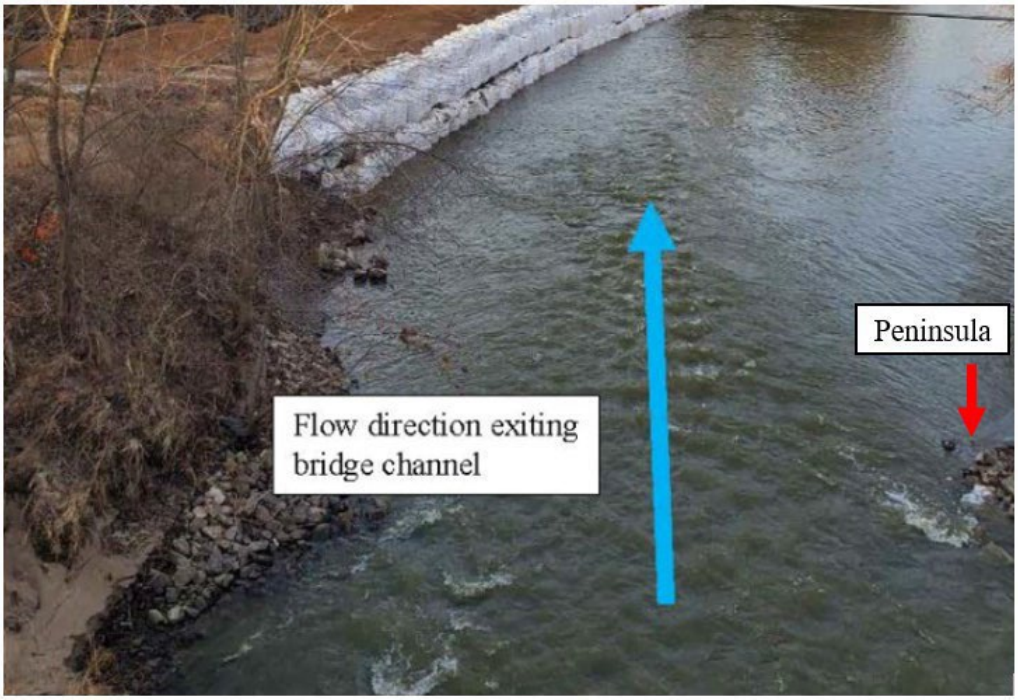

The figure below shows the water flow after the rip rap peninsula was removed. Notice the turbulent flow of the creek staying in the center of the creek as opposed to being diverted towards the south bank. Also note the lack of turbulence around the edge of the creek bank, indicative of slower-moving water velocities.

Figure 7: Cahokia Creek Flow without Peninsula

In collaboration with the United States Army Corps of Engineers (USACE), IDNR, and USFWS, MPL received all permits required to complete the long-term stabilization efforts at the incident site. Construction commenced on November 29, 2022. The site stabilization work was completed on May 30, 2023.

Figure 8: Cahokia Creek with Final Stabilization

MPL Improved and Standardized Its Method of Identifying Geohazard Risks

To standardize its evaluation of geohazards, MPL updated its Strain Feature Prioritization Flow Chart (Exhibit C). The updated Flow Chart includes improvements such as using an integrated approach with LiDAR for threat identification and revised total bending strain action limits. Specifically, MPL expanded its LiDAR usage to survey the entire Woodpat pipeline and completed an additional 4500 miles across all our assets to enhance geohazard threat identification. The LiDAR data for the entire Woodpat pipeline system was analyzed, and no new locations of land movement were identified.

To provide an outside review of its geohazard program, MPL hired third-party geotechnical and engineering consultants to review the program's identification of geohazard threat protocols, strain analysis protocols, and to identify gaps. Based on the final report, MPL's prioritization for immediate action was lowered to 0.28% total bending strain from 0.35%. The lower prioritization level will result in additional site investigations and remediation projects for locations that could be at risk of geohazard-related damage. MPL also started collecting deviation from straight values during bending strain analysis to be included in the analysis of bending strain features, which assists with analysis of baseline IMU runs. Based on the final report, MPL has also expanded the use of LiDAR to proactively identify geohazards threats and formalized the protocol to calculate total strain demand on pipelines from strain features.

On June 2, 2022, PHMSA published an updated advisory bulletin addressing the potential of geohazard damage. See *Pipeline Safety: Potential for Damage to Pipeline Facilities Caused by Earth Movement and Other Geological Hazards* (Docket No. PHMSA-2022-0063). Based on the advisory bulletin, MPL continued to improve its geohazard management practices. MPL reviewed its pipelines for geohazard susceptibility under improved susceptibility criteria, including lessons learned from the Edwardsville release. This review included waterways running parallel to the pipeline right-of-way, erosion, and increased flood potential. MPL initiated a comprehensive susceptibility assessment of all MPL right-of-way for geohazard threats with a geotechnical engineering consultant. This work is expected to be completed in 2023.

MPL Used Enhanced In-Line Inspections to Better Find Pipeline Segments at Greater Risk from Geohazards

MPL utilizes various ILI technologies to identify and measure integrity threats identified by the IMP processes. For geohazard threats, MPL uses IMU ILI tools to identify the pipe's location, bending strain, and pipeline movement.

In addition, MPL revised its geohazard assessment frequency based on system susceptibility. This includes annual geohazard assessments for segments “Observed”, geohazard assessments every three years for segments determined to be “Susceptible”, and geohazard assessments every five years for segments that are “Monitor” for geohazards. Pipeline movement between multiple IMU ILI runs is also analyzed in our integrated approach.

In 2022 and 2023 to present, MPL conducted 41 IMU ILI runs to complete baseline bending strain assessments. In addition, 35 bending strain reports were completed from previously completed IMU ILI runs. To date, MPL has completed baseline bending strain assessments for 6,385 of 6,561 miles susceptible to earth movement (97%). MPL utilized the Pipeline Research Council International (PRCI) TSC estimation tool to calculate the TSC of the pipeline at the strain feature. With the assistance of a third-party engineering firm, MPL developed a method of using site assessment data and IMU bending strain data to estimate total strain demand from the bending strain feature. The TSC and total strain demand values were compared to determine the necessary mitigation for the strain feature. Extensive analysis of all bending strain reports resulted in 242 geotechnical site assessments, 22 new sites being monitored with strain gauges and inclinometers, and 23 mitigation projects initiated.

MPL Used Lessons Learned from the Edwardsville Release to Expand Training and Provide Advanced Tools to Identify Geohazards

MPL has improved the content of its formal geohazard training program based on lessons learned and incorporating the threats identified by the recent geohazards PHMSA bulletin. To ensure that it reaches all employees who could identify a geohazard, MPL expanded groups being trained for holistic threat recognition to aerial patrol, and additional field resources to improve geohazard identification. Additionally, MPL has reviewed and enhanced its right-of-way inspection program and training. Through its Right-of-Way Management Program, MPL identifies the indications of potential geohazard threats and reviews the findings with the Integrity and Corrosion Engineering Department to identify potential threats. MPL’s process and training packet for its right-of-way inspection patrollers incorporates examples and indications of slope stability and erosion. These visual indications and examples of potential threats have been reinforced with MPL’s right-of-way inspection patrollers. In addition, MPL

has added new functionality to MPL's right-of-way inspection tablets to allow patrollers to view images of previously reported sites and report if any observable change has occurred between inspections.

MPL has begun piloting and developing an advanced right-of-way inspection program, leveraging aerial imagery and Artificial Intelligence (AI) models to help automate and improve the effectiveness of inspections. Natural force threats remain a top focus of the program's roadmap for AI model development. MPL works with a third party to collect aerial imagery during quarterly flights. The technology is being tested to validate 100% right-of-way coverage during inspection, automated AI detection for mechanical equipment and encumbrances, and supplemental passive leak detection. In addition, AI models are currently in development to identify visual indications of pipe exposures, deep tilling, and geohazards within the collected imagery. This technology is being evaluated to incorporate with routine aerial patrols.

Additionally, MPL used lessons from the Edwardsville release to improve training at its POCs. In 2022, due to the Edwardsville release, MPL added content to its existing leak detection training to include scenarios like those at Edwardsville to help controllers recognize a release event. Previously, MPL's training focused on more complicated systems that included booster stations that helped new controllers understand what would occur in a leak scenario. The new material helps operators on systems that do not have booster stations. MPL also modified its existing leak detection training for new controllers to include horsepower values as another data point to detect when and where a release could occur. In addition, MPL added language to the CPM leak alarm response to reference horsepower and how it will react in a leak scenario. To enhance awareness, MPL created a lesson-learned training detailing the events of the release that was shared with all the controllers. The lessons learned training focused on the different ways to recognize a release, especially when there are not any booster stations on the system. It also focused on using all resources to gather data as controllers evaluate abnormal events.

MPL Has Contributed to Efforts to Advance Knowledge of Geohazards

To improve the knowledge of geohazards, MPL has participated in projects related to geohazards and applied lessons learned to geohazard management practices. These geohazard projects include:

- Interstate Natural Gas Association of American (INGAA) Phase I project to develop Guidelines for Management of Landslide Hazards for Pipelines (2020)
- PHMSA/Gas Technology Institute (GTI) Development and Validation of a Probabilistic Method for Estimating Accumulated Strain and Assessing Strain Demand and Capacity on Existing Pipelines project (2023)
- INGAA Phase II project to develop a Recommended Practice for Pipeline Integrity Management of Landslide Hazards (2022-2023)
- American Petroleum Institute (API) development of Recommended Practice 1187 for pipeline geohazards (2022-2023)

While the investigation was ongoing, MPL took the initiative to share approved learnings from the incident with the industry and industry regulators.

MPL orchestrated an operator-to-operator info share with the NTSB and PHMSA within 3.5 weeks of the incident. At the request of the company's president, the NTSB and PHMSA fully supported his desire to accelerate the sharing and learning process. Both highly supported holding a webinar weeks after the incident, allowing operators to learn and apply key takeaways much earlier than normal. The program

included opening remarks from Robert Hall, NTSB Director of the Office of Railroad, Pipeline, and Hazardous Material Investigations, Alan Mayberry, PHMSA Associate Administrator of Pipeline Safety, and the company's president. The industry sharing event was highly attended, with approximately 900 attendees on the webinar. MPL shared with the industry the details of the incident, initial learnings, and the steps that were taken to mitigate this situation in the future.

Another industry-sharing opportunity came when the company's president was invited to be on a panel at the Pipeline Safety Trust 2022 annual conference to discuss geohazard management and associated challenges. The key takeaways and learnings from the incident the company had experienced months prior were among the panel's topics. Geohazard events can occur slowly over time, and while the industry is finding ways to leverage technology to better predict these events, industry sharing is an important tool to improve geohazard management. He stated, "One thing that we thought was critical was to share these things as quickly as possible. We will learn together, and we will learn better, the quicker we get this information out". He continued to discuss how a Geohazard Management Program was in place when the incident occurred, and this spurred them into action and made changes to the program within weeks.

Finally, the company organized and led formal geohazard information-sharing events with seven pipeline companies. The operator-to-operator dialogue continues over one year later, illustrating the power of sharing for the betterment of the industry and in the name of public safety.

Conclusion

The cause of earth movement was a combination of the rip rap peninsula placed by a third-party on the north bank to protect the Edwardsville Road bridge, directing water in the creek to flow towards the south stream bank, and episodic high-flow erosional flood events, which reduced the strength in the alluvial soils due to softening and repeated shearing. The progressive earth movement deflected the pipeline horizontally and vertically toward the creek and increased the strain demand to the point that it exceeded the tensile strain capacity of the girth weld and caused a rupture.

MPL wants to thank NTSB and its investigators for their time and effort in this investigation. MPL further appreciates the work of PHMSA, EPA, IEPA, Edwardsville Fire Department, USCG, USFWS, IDNR, IEMA, and Madison County Emergency Management for the response and its investigation. While MPL regrets that this release occurred, it has learned from the incident and has made every effort to share its lessons learned with other operators.

Exhibits

ADVINTEGRITY

ADVANCING INDUSTRY TOGETHER

Exhibit A

Edwardsville Failure Analysis

Final Report

Prepared for

Marathon Pipe Line LLC

~~100440-RP01-Rev1-071723~~

July 2023

WHEN TECHNOLOGY WORKS, TREMENDOUS THINGS ARE POSSIBLE.

Edwardsville Failure Analysis

Final Report

Prepared for

Marathon Pipe Line LLC

Findlay, OH

July 2023

Reviewed by: [redacted]

Reviewed by: [redacted]

[redacted]

[redacted]

ADVINTEGRITY

ADVANCING INDUSTRY TOGETHER

100440-RP01-Rev1-071723

Rev	Date	Description	Prepared	Reviewed
0	07.17.2023	Issued for Use	[redacted]	[redacted]
1	07.17.2023	Issued for Use with Minor Revisions	[redacted]	[redacted]

EXECUTIVE SUMMARY

On March 11, 2022, an incident occurred involving a 22-inch diameter crude oil pipeline operated by Marathon Pipeline, LLC (MPL) near Edwardsville, IL adjacent to Cahokia Creek. At the time of the accident, the pipeline was transporting Wyoming Asphaltic Sour Crude. The failed pipeline was the northernmost of three parallel pipelines that shared the right-of-way, and the closest to the creek. Soil stabilization had been previously completed in 2014 in the area where the failure occurred. The affected pipeline was constructed from [redacted].

Numerical analysis was performed using calibrated models based on information collected from previous IMU inspections in 2018 and 2021 in addition to information collected after the incident. The numerical models considered representative soils and operating conditions at the time of failure. The following conclusions were made based on the results of the numerical analysis.

1. The area near the failure had a maximum combined bending strain of 0.33% based on the 2018 bending strain results with a 5.7-ft horizontal deviation from straight. The same area exhibited change between 2018 and 2021 with the combined bending strain increasing to 0.41% and the horizontal deviation increasing to 8-ft. The data collected at the time of failure showed a marginal increase in horizontal deviation to 8.2 feet.

2. Calibrated numerical models were developed representing both undrained (clay) and drained (sand) soil conditions; however, the models were easier to calibrate for the undrained conditions indicating that the soil behavior is more likely representative of undrained conditions at the time of failure, which is consistent with the soil conditions observed near the incident.

3. Both the drained and undrained models showed that the pipeline developed a fully yielded cross section (i.e., a plastic hinge) near the failed girth weld between the 2021 IMU inspection and the time of failure. The strains rapidly increased at this location as the membrane and bending strains accumulated at the location of the plastic hinge.

4. The numerical models showed that the location and magnitude of the strains at the plastic hinge depend on soil properties and the extents of the movement profile. However, interaction of the plastic hinge with the failed girth weld is considered likely.

5. The maximum total strain within the plastic hinge ranged from 0.61% to 0.83% in the numerical models. The bending strains and membrane strains contributed almost equally to the total strain at this location.

6. As a result of the plastic hinge forming, the strains near the critical location were changing more rapidly between 2021 and the time of the failure than the strains near the peak pipeline displacement or the location of maximum bending strain.

7. The dimensions of the feature in the girth weld exceeded the size limitations of the PRCI SIA-1-7 strain capacity calculator. However, a feature was assessed with a size approximating the identified girth weld feature with respect to the peak depth. The assessed feature had a length of 3.27 inches with a depth of 80% NWT. This assessed feature is shorter than the actual feature, but with a depth near the measured peak depth. The tensile strain capacity (TSC) based on this feature was 0.29%. The calculated tensile strains from the numerical model were greater than this TSC, indicating that the girth weld failed because the increased demand from soil movement exceeded the TSC of the girth weld.

CONTENTS

1.0 BACKGROUND

On March 11, 2022, an incident occurred on a 22-inch diameter crude oil pipeline operated by Marathon Pipeline, LLC (MPL) near Edwardsville, IL adjacent to Cahokia Creek. At the time of the incident, the pipeline was transporting Wyoming Asphaltic Sour Crude. The failed pipeline was the northernmost of three parallel pipelines that shared the right-of-way, and the closest to the creek. Soil stabilization had been previously completed in the area where the failure occurred. The affected pipeline was constructed in [redacted]

The failed pipeline transports refined products from Wood River, IL to Patoka, IL and is referred to as the "WoodPat" system. The incident and subsequent product release occurred because a girth weld failed during operations. Images taken during the remediation of the girth weld failure are shown in Figure 1.1. The image on the left is taken looking upstream across the incident site toward the failed girth weld with Cahokia creek on the right-hand side of the image. The image shows that the WoodPat pipeline experienced both horizontal and vertical displacements. The image on the right-hand side of Figure 1.1 shows an image of the failed girth weld. The pipeline separated both laterally and axially at the failure location. An aerial image of the remediation site is shown in Figure 1.2.

Figure 1.1: Failed Girth Weld During Excavation

Figure 1.2: Aerial Image of Failure Location

2.0 OBJECTIVE

MPL requested that ADV Integrity, Inc. (ADV) help identify the causal factors that resulted in the accident. Specifically, ADV was asked to develop numerical models simulating the condition of the pipeline prior to the incident. The models were expected to account for the as-laid condition of the pipeline and the influence of ground movement near Cahokia Creek. The objective of the numerical analysis is to provide information on the strain demand near the failed girth weld at the time of the incident. Furthermore, the strain demand from the models will be compared to representative strain capacities determined through material testing and the methodology from the Pipeline Research Council International (PRCI) project SIA-1-7 (Wang, 2019).

To achieve these objectives, the scope of work proposed by ADV included the following tasks:

- Task 1: Review historical data, including inspection information, operating conditions, and prior stabilization efforts.
- Task 2: Determine initial as-laid condition based on a review of as-built drawings and historical IMU information.
- Task 3: Construct an FEA model and calibrate the model to measured conditions.
- Task 4: Use the model to investigate variations in soil properties and movement.
- Task 5: Estimate strains near the failed girth weld at the time of failure and compare strain capacities based on metallurgical evaluation and material testing.

3.0 SUPPORTING INFORMATION

This section presents a summary of the information provided to ADV and reviewed as part of Task 1. A summary of the documents is included in Table 3-1.

Table 3-1: Documents Reviewed

Document	Description
22in_Woopat Pipeline_Wood River to Patoka_2021_IMU Data	2021 High Resolution IMU Data
22in_Woopat Pipeline_Wood River to Patoka_2021_Weld Log	2021 Girth Weld Listing
Rosen 2021 Pipeline Movement and Bending Strain Assessment Report 3-30	Strain Comparison Report
22in_Woopat Pipeline_Wood River to Patoka_2018_IMU Data	2018 High Resolution IMU Data
22in_Woopat Pipeline_Wood River to Patoka_2018_Weld Log	2018 Girth Weld Listing
2012 Roxana - Patoka Woodpat (120265_22A) IMU Raw Data	2012 High Resolution IMU Data
2012 GE Pii CAL CMFL	2012 Feature Listing
IR#14 - Alignment Sheet with stationing of Release location	Alignment Sheet
TXG0258_Marathon_Edwardsville Geotech Site Assessment	Geohazard Assessment
TXG0258-MPL Edwardsville-Borehole Logs-Final	Borehole Results
MPL - Cahokia Canal DOC Exhibit	Post-Incident Survey Locations
3-0220457 - Original 03-12-22 Adjusted with LatLong	Post-Incident Geospatial Locations
Post-Accident Excavation Notes -PRELIMINARY	Field Notes

3.1 IMU Data Review

The bending strains based on the inspection from October 28, 2021 are reproduced in Figure 3.1. The maximum combined bending strain at this location is 0.41%. The girth weld that failed is #7630, located at odometer 32709.3 ft, and is annotated in the image with the red arrow. The IMU data indicates approximately 8-ft of horizontal deviation from a straight line across the impacted area and 9.3 feet of vertical deviation from a straight line across the impacted area.

ADV aligned and compared all the available IMU data sets as shown in Figure 3.2. ADV observed that the out-of-straightness (OOS) profiles from the 2012 IMU data do not appear plausible. When the IMU data was examined outside of the area of interest in stable locations, the horizontal and vertical geospatial information from 2012 often showed deviations that were inconsistent with the information from the inspections in 2018 and 2021. However, the bending strain profiles calculated from the pitch and azimuth did appear consistent with the other two data sets. These types of issues with geospatial accuracy are

more common in older IMU data sets. While they do not restrict the ability to compare calculated strains between the data sets, the OOS profiles often cannot be compared.

When comparing the strains in Figure 3.2, a clear progression in the horizontal, vertical, and combined strains is evident from 2012 to 2018 and from 2018 to 2021. This data confirms that the pipeline was experiencing external loads and being subjected to both horizontal and vertical movement in the time between 2012 and 2021.

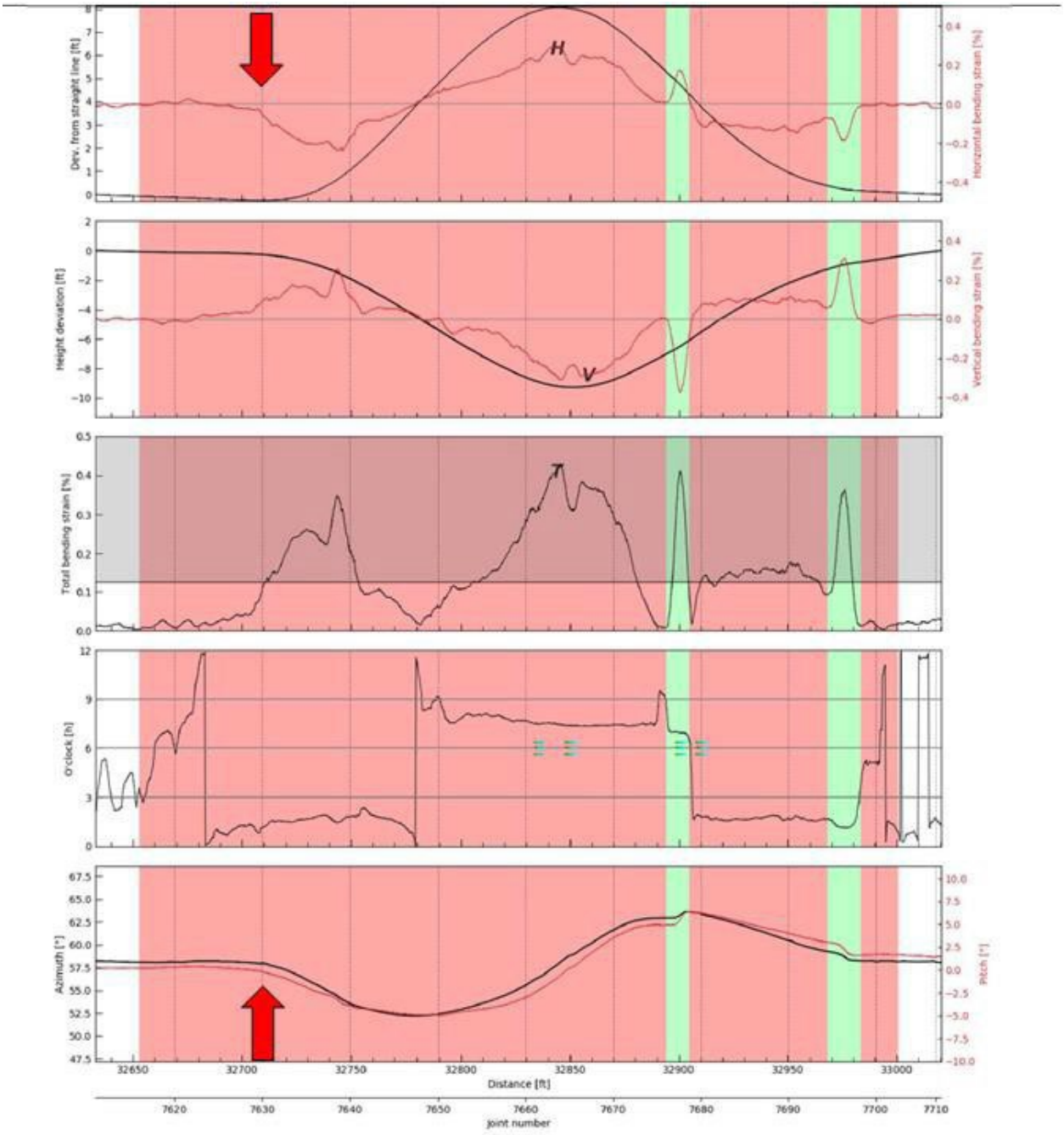

Figure 3.1: Bending Strain Site #7610 (ref: Strain Comparison Report)

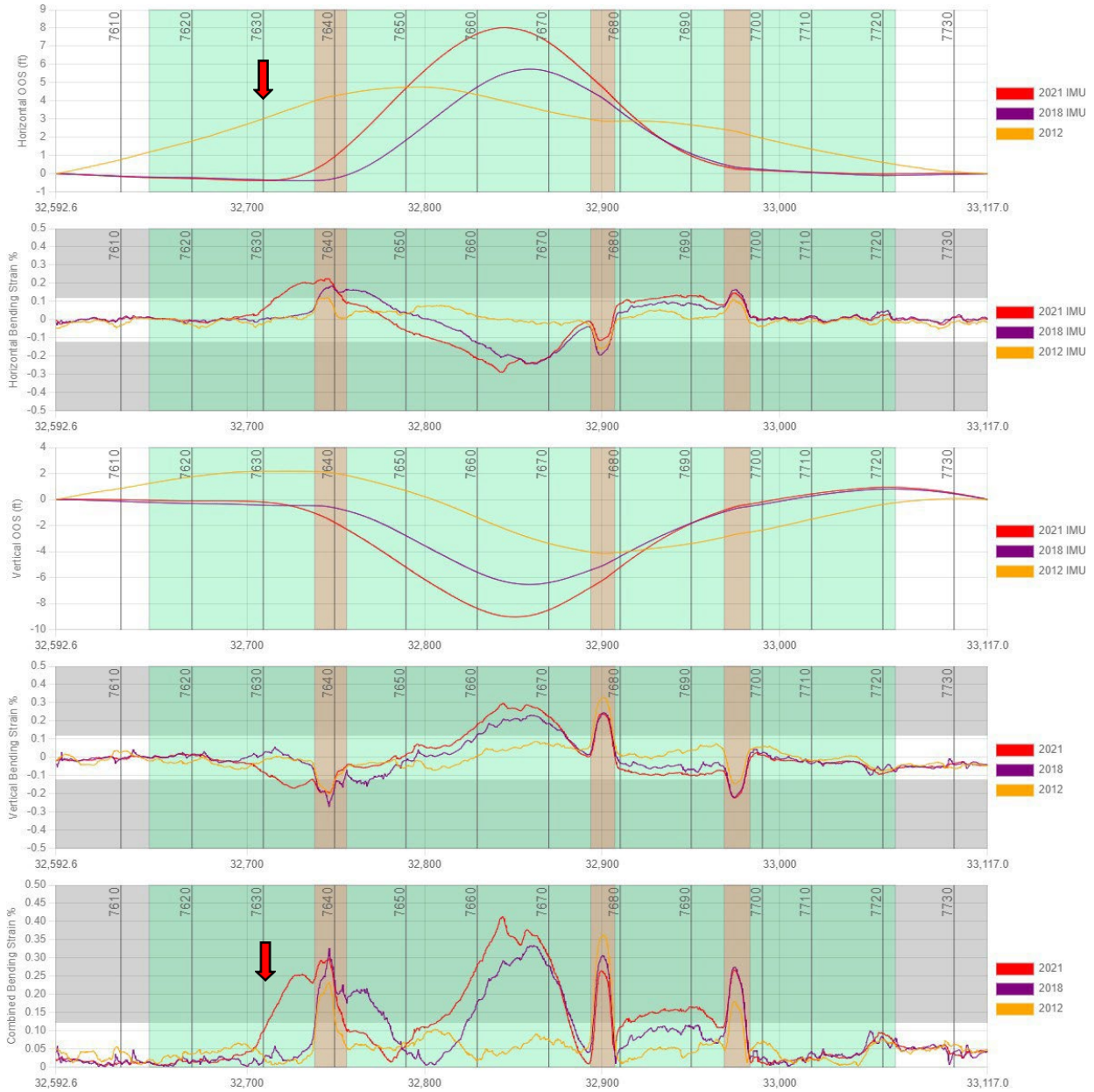

Figure 3.2: IMU Comparison for 2012, 2018, and 2021

3.2 Alignment Sheet Information

Information showing the original pipeline construction location from 1949 was not available. Marathon provided alignment sheets with information on the surface elevation, top of pipe elevation, and depth of cover. The information from the alignment sheet near the failure is enlarged in Figure 3.3. This information does not reflect as-built conditions but was collected prior to the incident (the alignment sheet was dated February 18, 2022). The information shows that the ground elevation near the failure was characteristic of a depression with the low-point approximately 4-6 feet lower than the surrounding area. This

information was confirmed by satellite imagery showing a drainage channel crossed over the pipeline near the failure location. The alignment sheet also confirmed the depth of cover near the failure varies from [redacted].

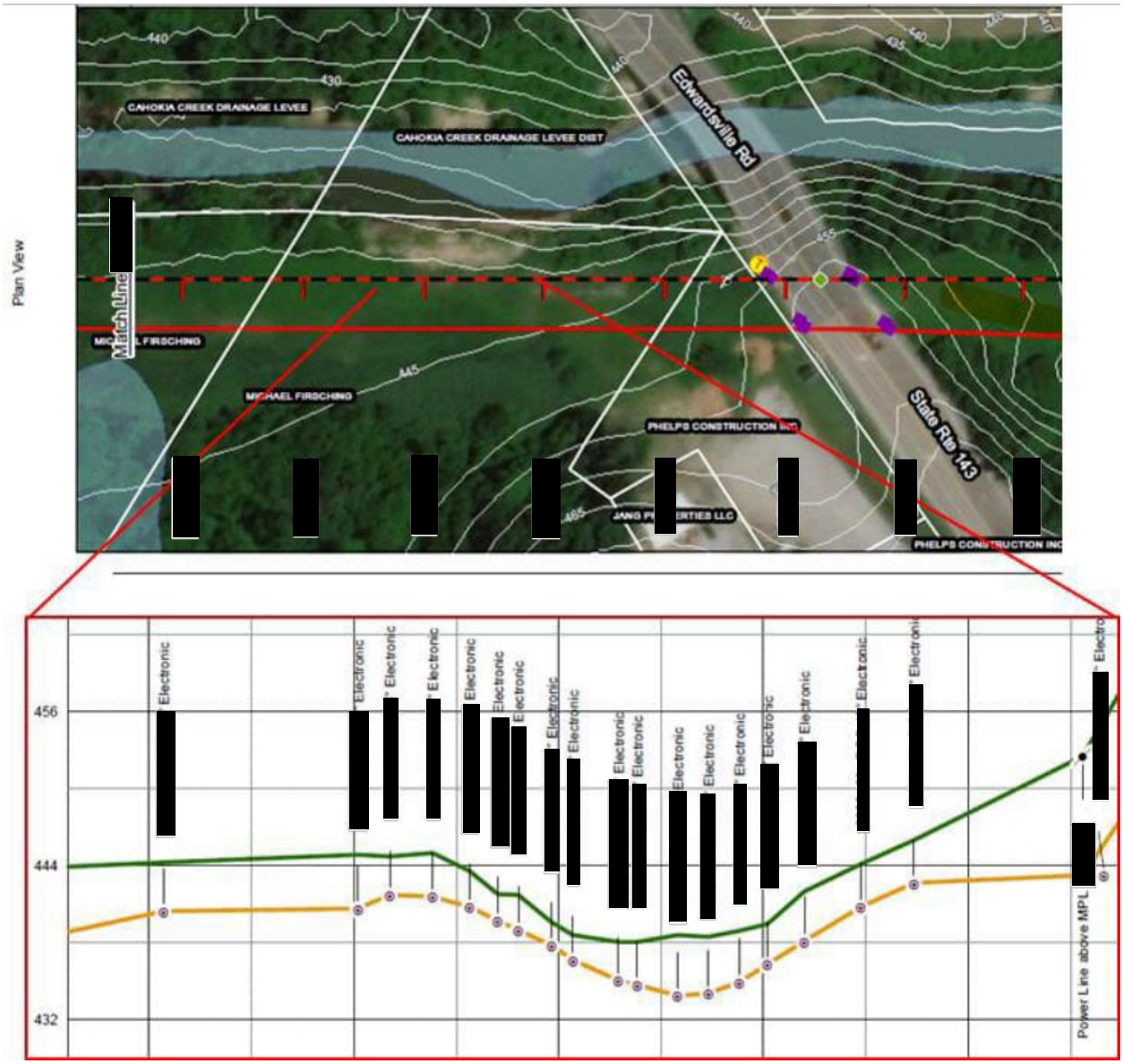

Figure 3.3: Alignment Sheet Information

3.3 Soil Data

Soil characteristics were collected from two boreholes located near the failure as shown in Figure 3.4. Based on the depth of cover survey, the soils of interest would occur between 3 and 8 feet deep. An image of the data from the IN/PZ1 borehole is provided in Figure 3.5. The IN/PZ1 borehole shows soft to medium stiff clays at the pipeline depth. The information from the IN/PZ2 borehole is provided in Figure 3.6,

showing soft clay at the pipeline depth. The pocket penetration values for unconfined compressive strength varied from 0.5 to 1 ton per square foot between the two boreholes. The lab results indicated a dry unit weight of 100.3 pcf and a moist unit weight of 125.8 pcf.

Figure 3.4: Borehole Locations

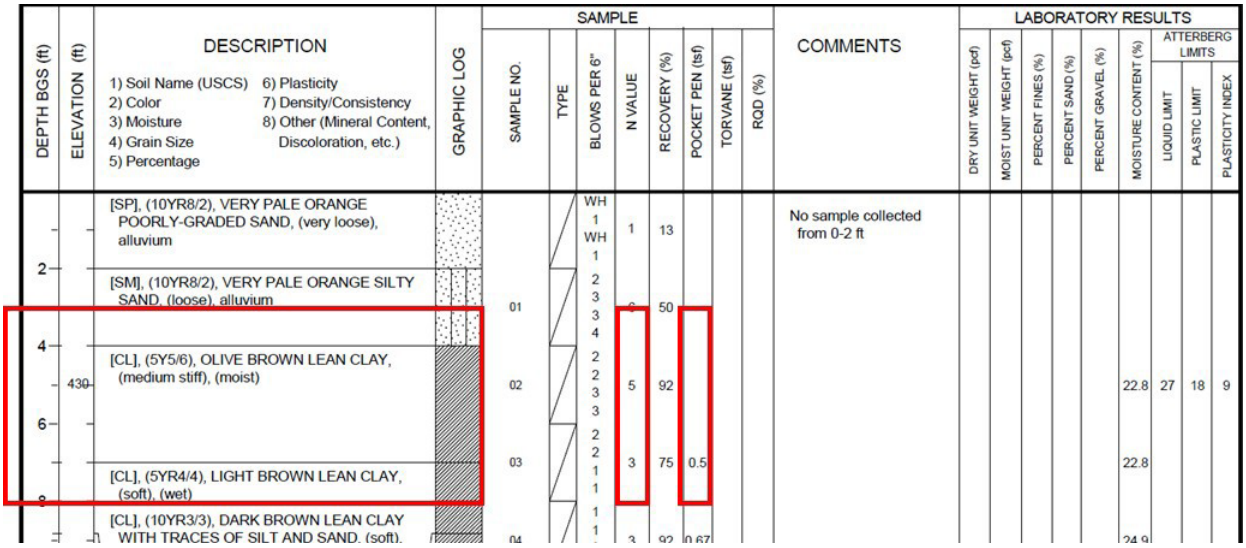

Figure 3.5: IN/PZ1 Borehole Information

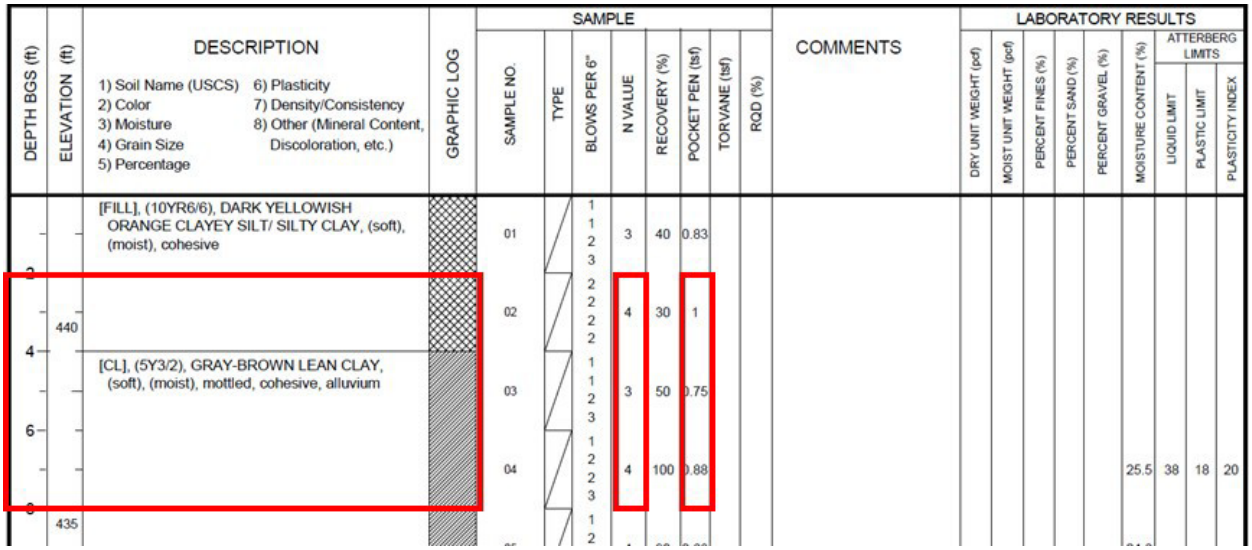

Figure 3.6: IN/PZ2 Borehole Information

3.4 In-Situ Information

ADV received information describing the geospatial location (latitude, longitude, and elevation) of the pipeline post-failure at select locations. Additionally, field notes taken during the remediation captured information pertaining to the pipe "separation" at the failed girth weld. The information is reproduced in Table 3-2.

Table 3-2: Pipe Separation Measurements

Orientation	Separation Distance
12 o'clock (TDC)	7 ½ inches
3 o'clock (south)	8 inches
6 o'clock (bottom)	7 inches
9 o'clock (north)	6 ¾ inches
Lateral (12 o'clock)	4 ¼ inches
Lateral (6 o'clock)	7 ¾ inches

The information from the as-found survey was aligned and overlaid with the available IMU data sets. The comparison for the horizontal and vertical out-of-straightness profiles are shown in Figure 3.7. The survey information shows that the Woodpat pipeline exhibited slight additional movement after the 2021 survey with a total horizontal out-of-straightness of 8.2 feet. The vertical out-of-straightness did not show a measurable difference when compared to the 2021 IMU data set with a total vertical deviation of 9-feet.

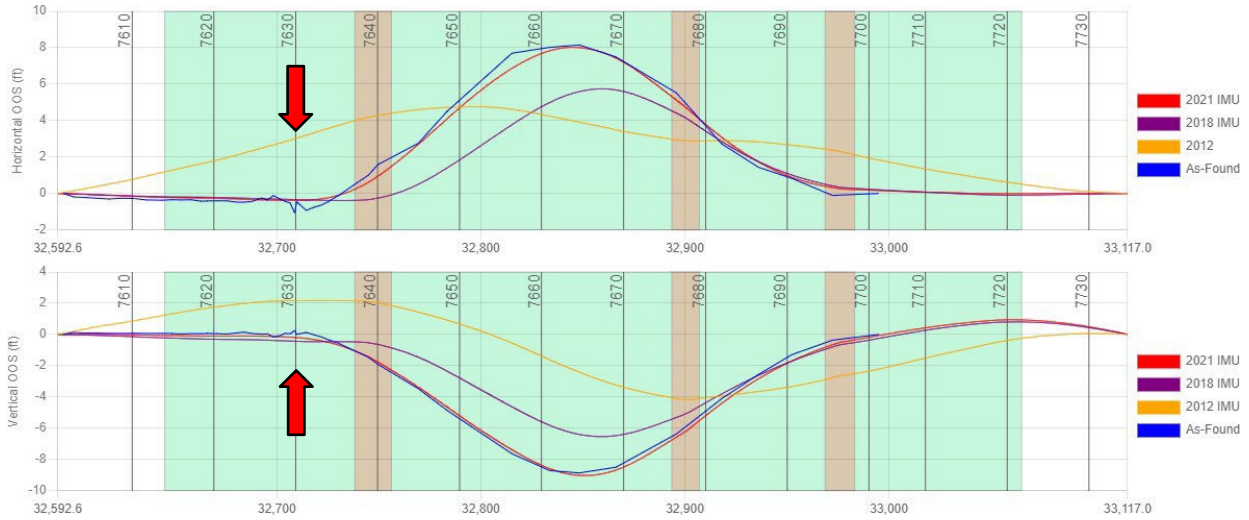

Figure 3.7: As-Found Survey

3.5 Operating Conditions

The WoodPat system is composed of 22-inch Diameter, 0.344 NWT, [redacted] pipe material at the location of the incident. At the time of the failure, the Woodpat system was transporting crude oil with an API Gravity of 21.6°. The pressure at the Roxana discharge station was recorded as 476 psi at 8:15 AM.

4.0 NUMERICAL MODEL

4.1 Structural Properties

The numerical model was evaluated using the Abaqus general-purpose finite element code and utilized beam elements (type PIPE31) to represent the pipeline. The beam elements were modeled as 22-inch outer diameter with a nominal wall thickness of 0.344-inches. The effective weight of the elements was modeled as 1,370 lb/in^3 accounting for the weight of the steel pipe and internal contents. Elastic-plastic material properties were specified for the pipe material based on the specified minimum properties for [redacted] pipe material. A Ramberg-Osgood formulation was used to generate the true stress – true strain curve based on a yield strength of 46,400 psi and an ultimate tensile strength of 63,100 psi. The resulting material curve is shown in Figure 4.1.

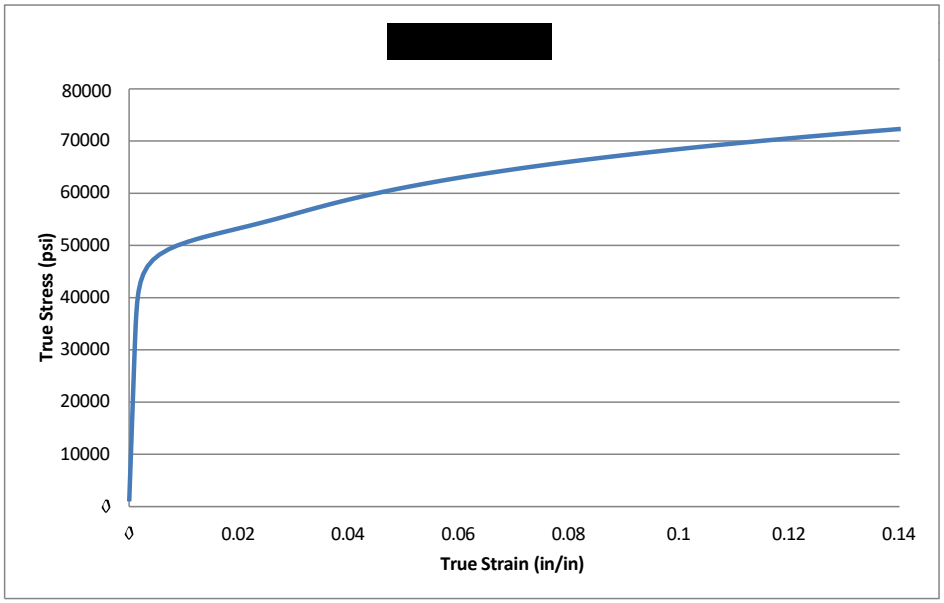

Figure 4.1: API [redacted] Elastic Plastic Material Properties

4.2 As-Laid Configuration

Identifying the as-laid condition of the pipeline consisted of three tasks. First, the heading angles (pitch and azimuth) recorded by the IMU during inspections were reviewed to identify which components of the pipeline within the bending strain area are consistent with manufactured bends. Second, the heading angles were reviewed to identify a plausible as-laid trajectory, and then the heading angles were reconstructed to fit this as-laid trajectory. Finally, the reconstructed heading angles were used to generate an as-laid centerline for the pipeline.

Figure 4.2 provides a comparison of the horizontal out-of-straightness profiles and azimuth angles from the 2018 and the 2021 inspections. The 2012 data was not included in the comparison as the heading

angles and out-of-straightness profile were not considered accurate as discussed in the previous section. Both inspections show similar behavior in the azimuth angle consistent with external loads acting on the pipeline. The azimuth angle is approximately 58-degrees near the beginning and end of the bending strain and movement area in both inspections. Two minor 2-degree horizontal manufactured bends appear in the data near odometer 32,900 feet and 39,990 feet. This information suggests that the pipeline was initially laid nearly straight throughout this area with minor deviations. This pattern is typical of most pipelines. Within the displaced area, the azimuth shows a distinct "S"-shaped pattern. This pattern is produced when a pipeline is displaced from its initial location. It is reasonable to conclude that the pipeline was initially laid straight through the area and account for the two minor manufactured bends in the recreated heading profile as shown with a dashed line in Figure 4.2.

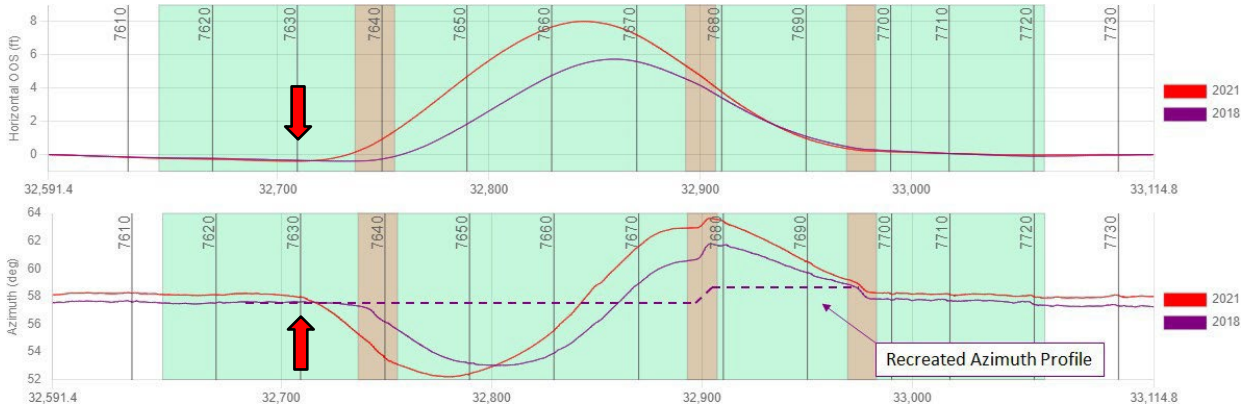

Figure 4.2: Azimuth Recreation

Figure 4.3 provides a comparison of the vertical out-of-straightness profiles and the pitch angles from the 2018 and the 2021 inspections. Both inspections show similar behavior in the pitch angle consistent with external loads acting on the pipeline. Near the beginning of the movement area, both tools enter with a near-flat pitch of approximately 0.5-degrees and exit the movement area with a pitch of approximately 2-degrees. Within the movement area, three small vertical bends can be seen near odometer 32750 feet, 32,900 feet, and 33,990 feet. These vertical bends form an overbend-sagbend-overbend combination that is typical of pipeline construction at shallow crossings. The presence of these vertical manufactured bends confirms the information from the depth of cover assessment that showed a shallow drainage area at this location. It is reasonable to conclude that the pipeline was constructed with shallow bends to cross the drainage. Similar to the azimuth heading angles, the pitch angles in both inspections show the characteristic "S" shape within the movement area as a result of external loads. The recreated pitch profile is shown in Figure 4.3 with the dashed line. The recreated profile preserves the manufactured bends near 32,900 feet and 33,990 feet.

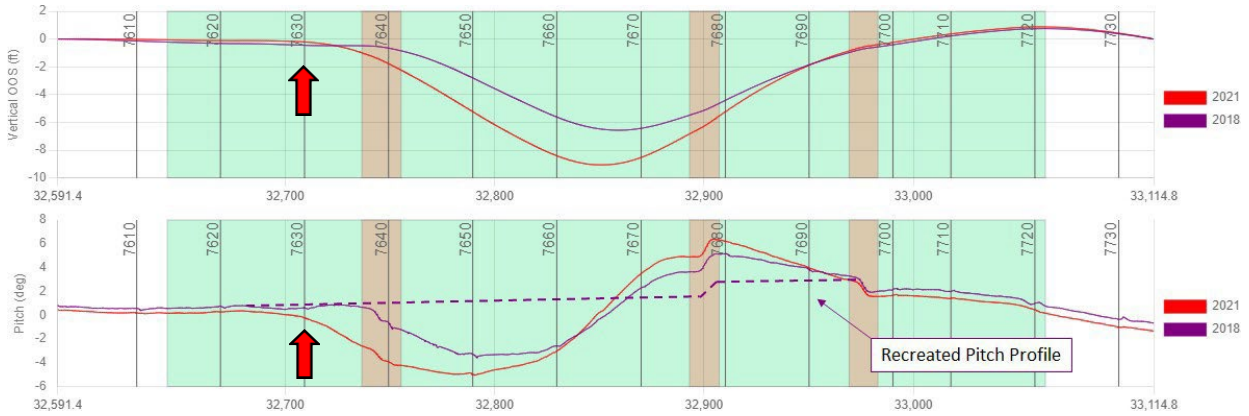

Figure 4.3: Pitch Recreation

The resulting as-laid condition used for the baseline is shown in Figure 4.4 for both the horizontal and vertical profiles. The recreated as-built profile is shown as a green line. The horizontal out-of-straightness shows a near straight trajectory with less than 1-ft of deviation, and the vertical out-of-straightness shows an initial vertical change of approximately 3-ft. This agrees well with the depth of cover information which showed similar deviations in the ground elevation near the drain crossing.

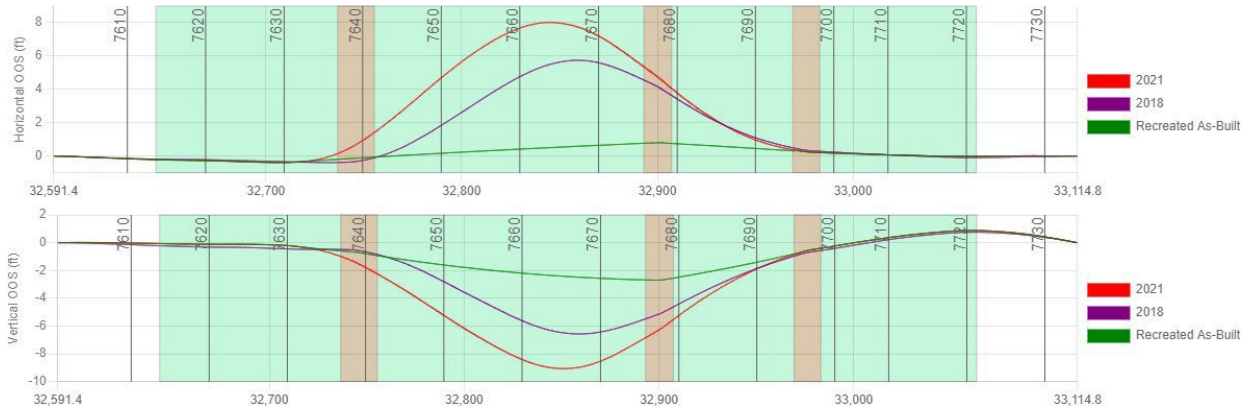

Figure 4.4: Recreated Out-of-Straightness Profiles

4.3 Soil Properties

The Abaqus model used pipe-soil interaction elements (type PSI34) to capture the behavior of the soil at the WoodPat system based on the data captured in the borings. PSI34 elements represent the interaction between the pipeline and the soil as a series of non-linear springs in the horizontal, vertical, and axial direction. The formulations for the soil springs are based on documentation from the American Lifelines Alliance document (American Lifelines Alliance, 2005). The soil was indicated to be primarily made of clay at the pipeline depth with stiffness ranging from soft to firm. Therefore, analysis models were developed using clay (i.e., undrained soil response) formulations that are based on the shear strength of the soil. The upper and lower bound properties used in the assessment are shown in Table 4-1.

Table 4-1: Clay (Undrained) Properties

Property	Lower Bound (weak) Undrained Values	Upper Bound (firm) Undrained Values
Shear Strength	3.62 psi (25 kPa)	7.25 psi (50 kPa)
Alpha	0.94	0.69
Nch (horizontal factor)	6.25	6.25
Ncv (uplift factor)	5.4	5.4
Nc (bearing factor)	5.14	5.14

While the borings did not show sandy material near the depth of the pipeline, the geotechnical review did observe coarse-grained materials (i.e., sand) near the water line. Therefore, the analysis also considered soil properties using sand (i.e., drained soil response) formulations that are based on unit weight and friction angle. Like the clay properties, upper and lower bound values were generated as shown in Table 4-2. The soil friction angle was taken from publicly available sources as this value is not typically characterized for clay soils (Oswell, 2016).

Table 4-2: Sand (Drained) Properties

Property	Lower Bound (weak) Drained Values	Upper Bound (firm) Drained Values
Effective Unit Weight	63.4 pcf	63.4 pcf
Θ, Friction Angle	10°	30°
Nqh (lateral factor)	3.0	7.6
Nqv (uplift factor)	1.0	2.0
Nq (bearing factor)	2.4	18.4
Nγ (bearing factor)	0.5	18.1

4.4 Assessment Methodology

The analysis utilized an iterative approach to determine the strain demand placed on the weld prior to failure. This approach is shown graphically in Figure 4.5. The as-laid configuration as described in the previous section was taken as the starting point for the analysis. The as-laid configuration was assumed to be constructed in a stress-free condition. Displacements were applied to the soil nodes which in turn produce pipeline displacements. The soil displacements are incrementally applied to match the conditions from the 2018 and 2021 inspections as well as the as-found measurements. The strains and resulting pipeline displacements from each increment are compared to the displacements captured from the IMU tool or the as-found survey measurements. If a good match is obtained, the strains at the girth weld of interest are extracted from the model. If a match is not obtained, the displacement profile is iteratively

adjusted until a match is obtained. For the purposes of this report, only the final calibrated models and associated results are presented.

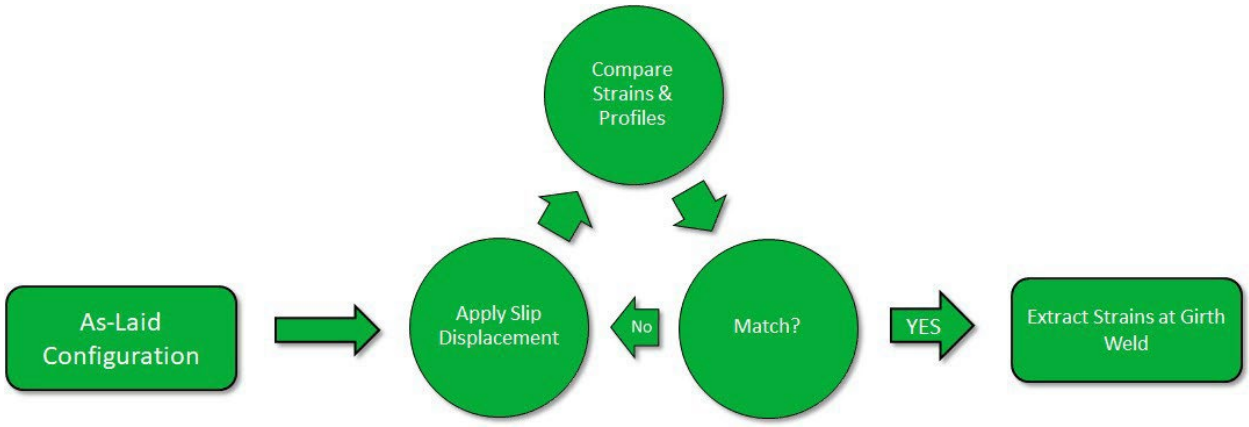

Figure 4.5: Analysis Methodology

4.5 Load Cases

The assessment of the Edwardsville failure addressed four load cases, which are described in Table 4-3. Four load cases were assessed considering variations in the soil type and properties. All load cases included gravity and an internal pressure specified as 476 psi.

Table 4-3: Load Case Description

Load Case	Description
Load Case 1	Upper Bound Undrained (Clay) properties
Load Case 2	Lower Bound Undrained (Clay) properties
Load Case 3	Lower Bound Drained (Sand) properties
Load Case 4	Upper Bound Drained (Sand) Properties

4.6 Post Failure Simulation

The response after the failure was modeled for each load case by “deleting” the elements near the girth weld and allowing the pipeline to respond. The separations observed in the model were then compared to the results recorded during the response shown in Table 3-2.

5.0 RESULTS

The results from the numerical analysis are presented in detail for Load Case 1 and then summarized more briefly for each of the remaining load cases. The process for evaluating the Load Cases is shown graphically in Figure 5.1. The numerical analysis proceeded in steps, and the results are compared for each of the following steps: 2018 alignment, 2021 alignment, and as-found Alignment. Iterative adjustments were made as needed to achieve the results shown for each load case.

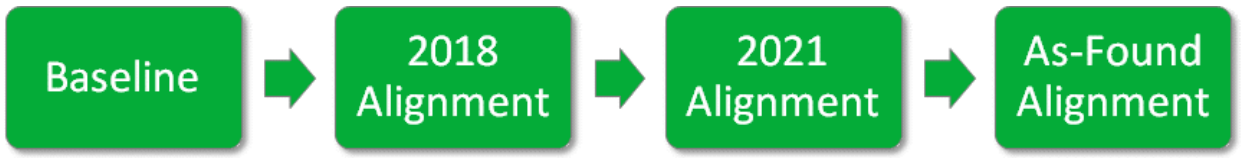

Figure 5.1: Results Comparisons

It is also important to clarify the nomenclature regarding strains. The bending strains determined from the heading angles recorded by the IMU tool and presented in the previous sections are calculated based on curvature in the horizontal and vertical planes. These bending strains do not include membrane strains, which reflect how much the pipe may have "stretched" or "compressed" because of uniform axial loading.

In contrast, the numerical models can provide bending, membrane, and total strains by post-processing the available axial strains at locations around the pipe circumference. The total strain includes both the bending and membrane components. When the results from the numerical models are compared to the IMU bending strain data, the axial strains are processed to render the bending strain components in the horizontal and vertical directions providing an equivalent comparison. When the results present the total strains from the numerical models, these values are inclusive of the membrane and bending strains. The total strains are not compared to the bending strains calculated from IMU.

5.1 Load Case 1 – Upper Bound Undrained Properties

The results for Load Case 1 are shown in Figure 5.2. Except for the total strain panel, each panel compares the results from the IMU tool (or as-found field measurements) to the numerical models with matching colors. Results from the numerical model are shown with dashed lines while the results from the IMU or field measurements are shown with solid lines. It should be noted that strains are not available for the as-found field measurements, but they are presented for the calibrated numerical model representing the same condition. The results of each comparison based on the information in the panels are summarized below:

- Horizontal OOS: The horizontal OOS shows excellent agreement for the 2018, 2021, and as-found data sets. The peak displacements match to within 0.1-ft for each of these conditions.

- Horizontal Bending Strain: The horizontal bending strains show excellent agreement with the available IMU data sets from 2018 and 2021. The horizontal strains for the as-found condition from the numerical model show a sharp increase from the 2021 values near the upstream flank of the landslide with peak horizontal bending strains of 0.38%.

- Vertical OOS: The vertical OOS shows agreement for the 2018, 2021, and as-found data sets.

- Vertical Bending Strain: The vertical bending strains show excellent agreement with the available IMU data sets from 2018 and 2021. There are no significant changes in the vertical strains from 2021 to the as-found condition in the numerical model.

- Combined Bending Strain: The combined bending strains show excellent agreement with the available IMU data sets from 2018 and 2021. The combined strains for the as-found condition from the numerical model show a sharp increase from the 2021 values near the upstream flank of the landslide with peak bending strains of 0.42%. This increase is primarily due to the increase in the horizontal bending strain.

- Total Strain: The total strains show progressive increases from 2018 to 2021 and the as-found condition in the numerical models. The maximum total strain in 2018 was 0.61% located near the peak displacement in the landslide. The maximum total strain in 2021 was 0.76% also located near the peak displacement in the landslide. In addition, the 2021 value shows rapidly changing total strains in the bend near odometer 32,900 feet. This rapid change is due to the "straightening" of the 2-degree field bend at this location. The numerical model also shows significant change near the upstream flank of the landslide adjacent to the failed girth weld 7630 at odometer 32,709 feet. At this location, the total strains show a sharp increase with total strains of 0.83%. This rapid change in total strain near the failure is attributed to the pipe cross section becoming fully yielded (i.e., forming a plastic hinge) near the upstream flank of the landslide thereby creating a location where strains can accumulate.

In summary, the comparison for Load Case 1 shows that the horizontal bending and total strains changed rapidly near the upstream flank of the landslide adjacent to the location of the failed girth weld. While the actual total strains are 0.18% at the location of the failed girth weld, the peak total strain occurs less than 10-feet away from the girth weld. Given the uncertainties with the precise position of the WoodPat pipeline prior to failure with respect to the landslide extents, it is possible that the strains were as high as 0.83% in the weld if the upstream flank of the landslide is shifted slightly upstream from where it is located based on the 2021 IMU data.

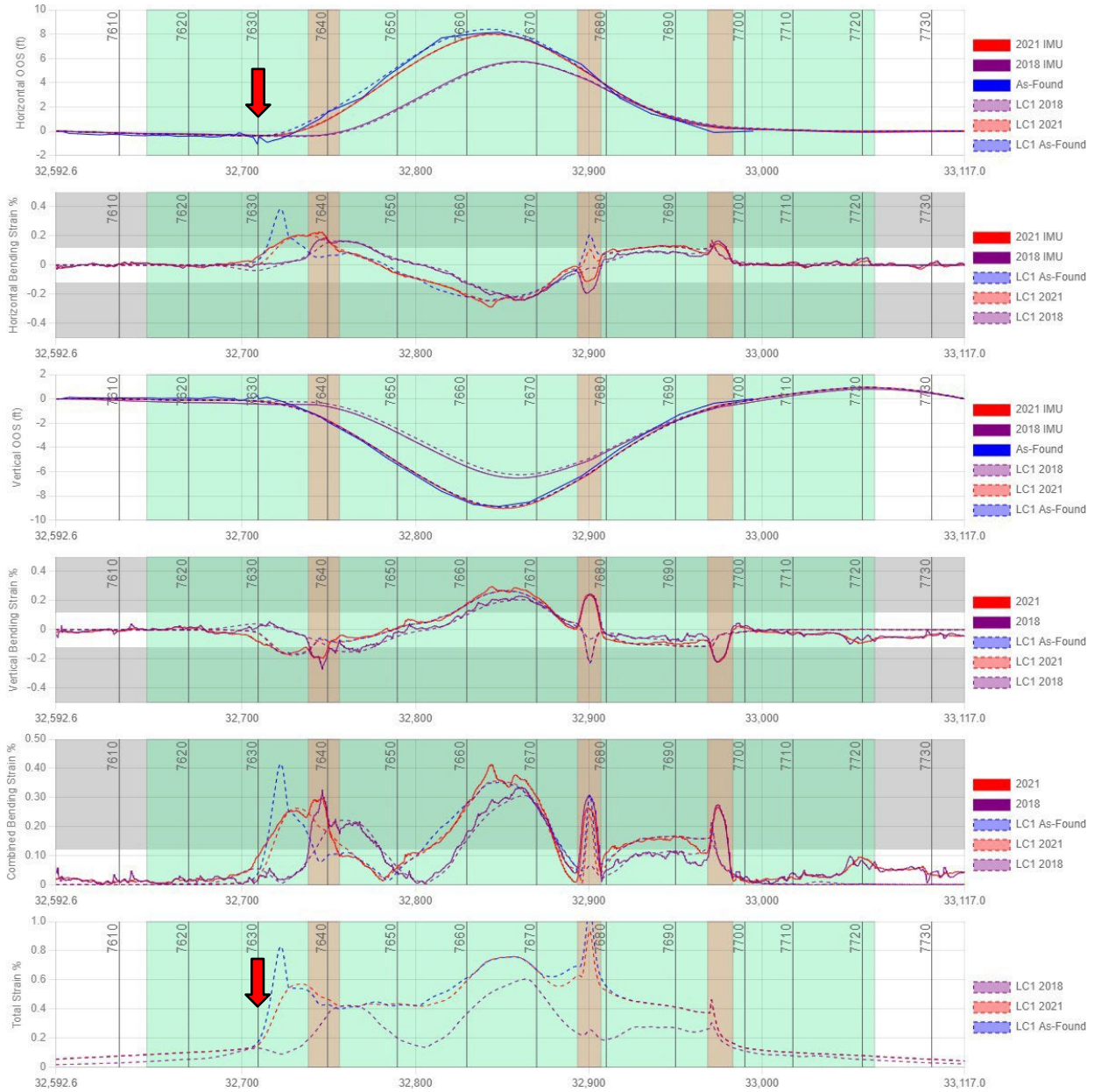

Figure 5.2: Load Case 1, Upper Bound Undrained, Results Comparison

5.2 Load Case 2 – Lower Bound Undrained Properties

The results for Load Case 2 with lower bound undrained properties are shown in Figure 5.3. Except for the total strain panel, each panel compares the results from the IMU tool (or as-found field measurements) to the numerical models with matching colors. Results from the numerical model are shown with dashed lines, while the results from the IMU or field measurements are shown with solid lines. It should be noted that strains are not available for the as-found field measurements, but they are presented for the calibrated numerical model.

With respect to the out-of-straightness plots, the results from Load Case 2 are nearly identical to the results from Load Case 1. Both the horizontal and vertical out-of-straightness plots show excellent agreement with the 2018, 2021, and as-found data sets. However, the results do show differences in the horizontal, combined, and total strains. The sharp peak observed in Load Case 1 is more muted for Load Case 2 with lower overall strains near the upstream flank of the landslide. The horizontal bending strain near the upstream flank is 0.26% while the total strain is 0.61%. The strains are lower for Load Case 2 because the axial and bending resistance of the soil is weaker for the lower-bound load properties. The weaker properties delay the formation of the plastic hinge, but do not prevent its formation.

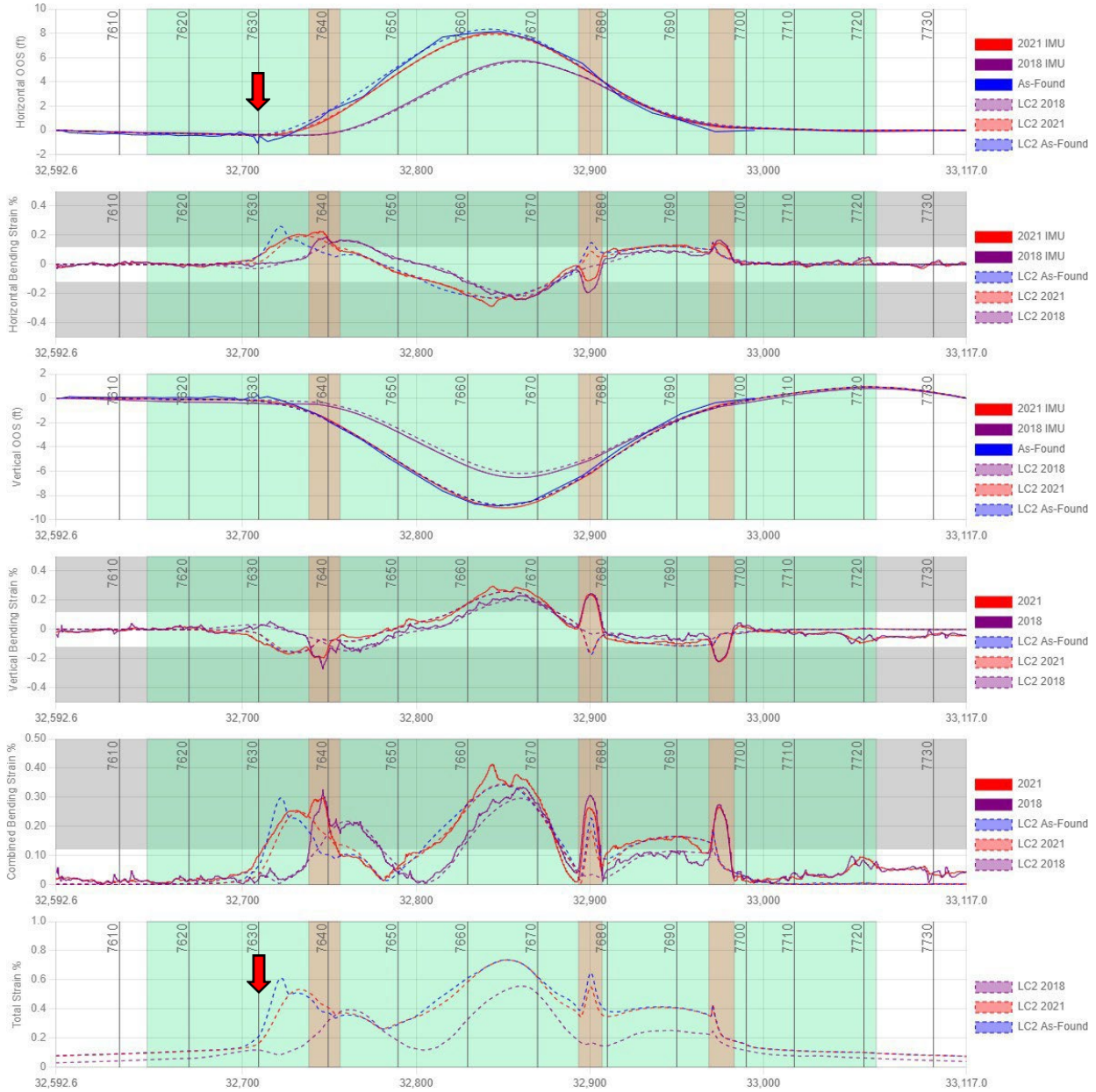

Figure 5.3: Load Case 2, Lower Bound Undrained, Results Comparison

5.3 Load Case 3 – Upper Bound Drained Properties

The comparison of the results for Load Case 3 with upper bound drained properties are shown in Figure 5.4. Except for the total strain panel, each panel compares the results from the IMU tool or as-found field measurements to the numerical models with matching colors. Results from the numerical model are shown with dashed lines while the results from the IMU are shown with solid lines. It should be noted that strains are not available for the as-found field measurements, but they are presented for the calibrated numerical model.

With respect to the out-of-straightness plots, the results for the horizontal displacements from Load Case 3 are nearly identical to the previous results. However, the vertical displacements do not match quite as well. Additionally, the calibration of the vertical displacements required the use of the saturated unit weight (125.4 pcf) rather than the equivalent unit weight (63 pcf). Since the vertical strength of drained materials is a function on the unit weight and the burial depth, this has the effect of increasing the vertical soil resistance. In this assessment, an increase in the unit weight was required to achieve agreement in the displacements.

Regarding the strains, the results from Load Case 3 show similar results to Load Case 1. A localized peak in the strains is evident near the upstream flank of the landslide. The horizontal bending strain near the upstream flank is 0.29% while the total strain is 0.64%. These strains are slightly lower than the results for the upper bound undrained properties in Load Case 1.

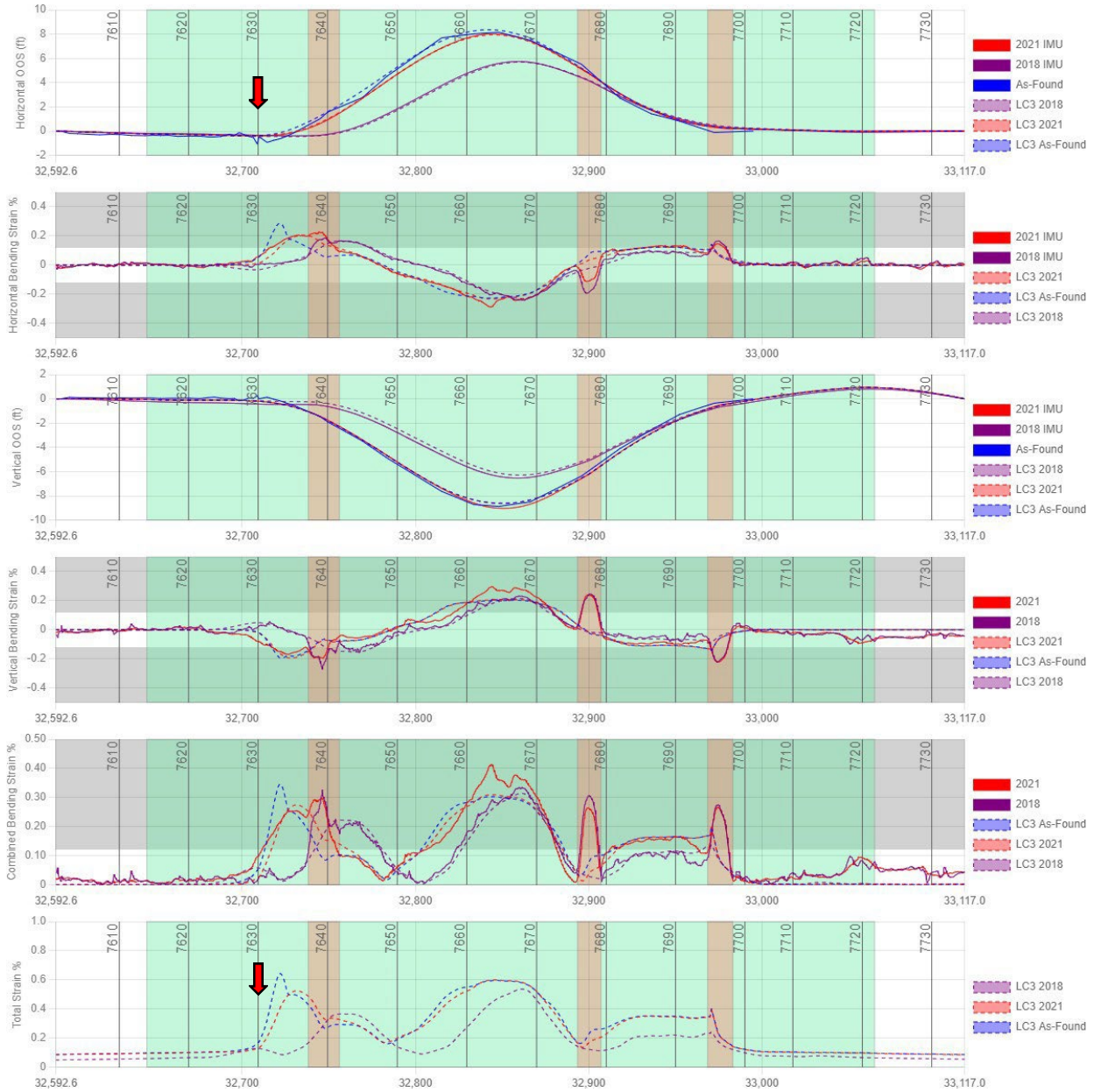

Figure 5.4: Load Case 3, Upper Bound Drained, Results Comparison

5.4 Load Case 4 – Lower Bound Drained Properties

The results for Load Case 4 with lower bound drained properties are shown in Figure 5.5. Except for the total strain panel, each panel compares the results from the IMU tool or as-found field measurements to the numerical models with matching colors. Results from the numerical model are shown with dashed lines while the results from the IMU are shown with solid lines. It should be noted that strains are not available for the as-found field measurements, but they are presented for the calibrated numerical model.

Calibrating the numerical models to the measured strains and displacements based on the recorded IMU data was challenging for Load Case 4. Even with the alteration to the unit weight as described in the previous section, the displacements and strains did not match well. Additionally, the model proved to be numerically unstable at displacements beyond the 2021 values. The comparisons showed that the displacements for the 2018 load case had reasonable agreement, but the comparisons did not match as well as any of the other load cases. In addition, the displacements near the peak and upstream flank of the landslide do not show good agreement for the 2021 load case. The weaker horizontal strength of the soil resulted in a noticeably smoother profile with lower strains near the upstream flank of the landslide.

Regarding the strains, the results for Load Case 4 show significantly lower strains than the other load cases. The vertical and horizontal strains for the 2021 condition show poor agreement with the IMU data. While additional modifications to the soil properties may provide improvements to the comparison, it is unlikely that the vertical displacements will be able to be calibrated. These results indicate that the lower bound drained properties are not an accurate representation of the conditions observed at the failure location based on the 2021 IMU data and information collected at the time of failure. Therefore, the results from Load Case 4 were disregarded for future use.

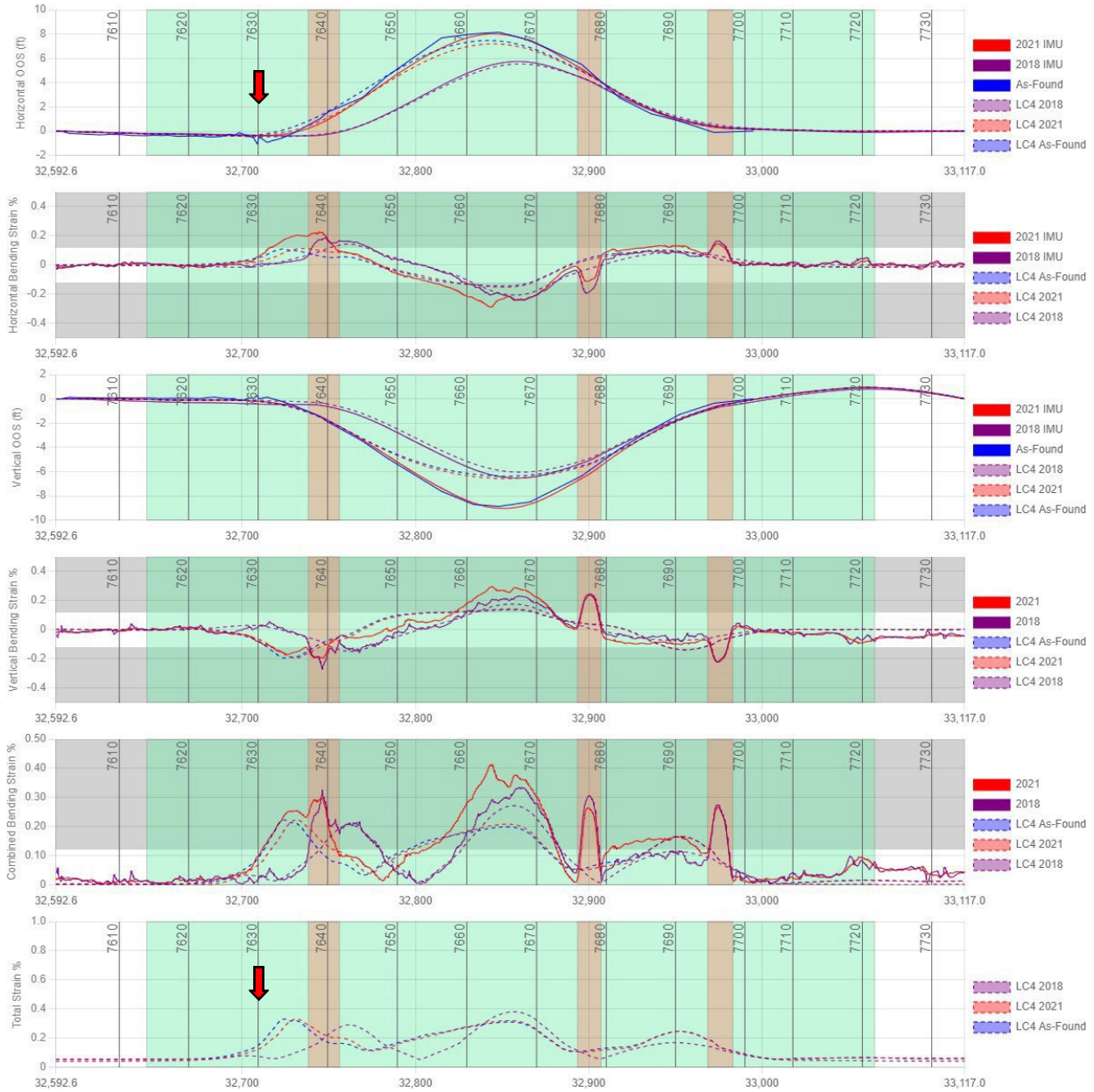

Figure 5.5: Load Case 4, Lower Bound Drained, Results Comparison

5.5 Post Failure Axial Separation

For Load Cases 1 through 3, the analysis models were progressed to simulate the conditions at the time of failure. This was accomplished by deleting the element nearest the girth weld and allowing the pipeline to separate as the soil elements relaxed. It is important to recognize that the results from this step are only considered appropriate when used as a qualitative order-of-magnitude type assessment. The conditions just prior to the failure are not likely to resemble the conditions during the response from 2012 to 2021. The conditions near the girth weld are expected to change as the soil interacts with released

hydrocarbons, and some excavation is required for access to the girth weld. Both conditions will change the local restraint near the girth weld. Nevertheless, the measurements recorded during the investigation provide a useful point of comparison to judge the accuracy of the models.

An average axial separation of 7.3-inches was recorded during the remediation activities. In comparison, Load Case 1 showed a separation of 4.8-inches, and Load Case 2 showed a separation of 6.5-inches. Load Case 3 showed a separation of 6.6-inches. It is interesting that the lower bound undrained properties and the upper bound drained properties showed better agreement than the upper bound undrained properties; however, all the results show reasonable agreement given the challenges in replicating the actual conditions after the failure.

5.6 Other Analysis Considerations

Two additional considerations were addressed in the analysis at the request of MPL. First, the sensitivity of the results to the soil displacements near GW 7630 at the upstream flank of the landslide was investigated. The results from the initial assessments produced a “sharp” change near the upstream flank of the landslide between the 2021 and the as-found simulations. This change was tapered over a 10-ft length to “soften” the change. The results showed no significant difference in the out-of-straightness profiles; however, the total strains did reduce from 0.83% to 0.69% for Load Case 1. These results confirm that the region where the plastic hinge forms adjacent to the girth weld will be sensitive to soil properties and applied displacements.

The second consideration addressed in the analysis was whether repair sleeves installed in 2014 within the displaced section could have influenced the results. Four repair sleeves varying from 1 to 2 feet in length were installed in 2014. The sleeves were located near the following odometers: 32,840 feet, 32,851 feet, 32,900 feet, and 32,911 feet. The failure was located at odometer 32,709 feet, or 131 feet from the nearest sleeve. The sleeves were included in the model by locally increasing the wall thickness for the elements at the sleeve location to account for the additional material. The results showed no difference in the peak strains observed for Load Case 1. Therefore, it was concluded that the presence of the installed sleeves did not contribute to the failure.

5.7 Numerical Analysis Results Summary

The results from the numerical analysis are summarized in Table 5-1. All the load cases showed a sharp increase in strain approximately 10-ft from the girth weld where the incident occurred. The total strains in the girth weld ranged from 0.61 – 0.83%, with the membrane strains accounting for approximately half of these total strains in each load case. While the strains at the girth weld within the model were lower than the maximum values near the girth weld (0.17 – 0.21%), uncertainties in the precise extents of the landslide profile combined with the sharp changes in strain near the girth weld make it likely that the girth weld was experiencing strains higher than the exact values predicted at the girth weld.

Table 5-1: Results Summary

	LC1	LC2	LC3
Total Strain at Girth Weld 7630	0.18%	0.21%	0.17%
Max Bending Strain Near Girth Weld 7630	0.42%	0.30%	0.35%
Max Membrane Strain Near Girth Weld 7630	0.41%	0.31%	0.29%
Max Total Strain Near Girth Weld 7630	0.83%	0.61%	0.64%
Simulated Displacement After Failure (As-found 7.3 inches)	4.8-inches	6.5-inches	6.6-inches

6.0 DISCUSSION

The metallurgical examination (ADV Integrity, 2023) of the girth weld identified two planar features near the failure origin. The largest feature had a length of 7.2-inches with an average depth of 50% nominal wall thickness (NWT) and a peak depth of 88% NWT. The material testing determined that the weld properties and pipe properties were within specifications. The full-size equivalent Charpy energies for the weld centerline and heat affected zone were 58.2 ft-lb and 55.2 ft-lb, respectively. The metallurgical report is included in the appendices.

The tensile strain capacity (TSC) was estimated using PRCI SIA-1-7 with an apparent CTOD value of 0.0177 inches. The exact dimensions of the feature (7.2-inch x 88% NWT) could not be specified as a feature size due to limitations in the SIA-1-7 method. However, a feature was assessed with a size approximating the identified feature with respect to the peak depth. The assessed feature had a length of 3.27 inches with a depth of 80% NWT. This assessed feature is shorter than the actual feature, but with a depth near the measured peak depth. The predicted TSC based on this feature and the measured properties was 0.29%. It is reasonable to conclude that the TSC of the actual feature is not likely to be larger than this value.

This calculated TSC of 0.29% is exceeded by the predicted strains from the numerical model. All the calibrated numerical models indicated that the pipe cross section as fully yielded at a location near the failed girth weld. As a result of the fully plastic cross section, the strains are shown to accumulate rapidly near the failed girth weld with only small increases in additional movement. For example, the peak total strain near the failed girth weld in Load Case 1 was estimated as 0.44% at odometer 32722 feet based on the 2021 IMU inspection. While the pipeline displacements were not substantially different between the 2021 inspection and those recorded after the failure (8 ft vs. 8.2 ft), the peak total strain from the as-found simulation had increased to 0.83% at this same location. These results indicate that the strains near the girth weld increased by 89% with only small changes in movement. The peak total strains at the same location were only 0.1% based on the 2018 inspection.

It is also noteworthy that the maximum overall bending strain did not change as significantly from 2018 to 2021 as the bending strains near the girth weld. The maximum bending strain from the 2018 IMU was 0.33% (total strain 0.60%) while the maximum bending strain in 2021 was 0.41% (total strain 0.76%). This represents an increase of approximately 25% in the reported maximum bending strains. However, the change in bending strain near the girth weld that failed was more significant. The bending strain near the girth weld changed from 0.02% in 2018 to 0.25% in 2021. The bending strain from the as-found condition was estimated at 0.42% representing a 61% increase from 2021 to the time of failure. This information supports the fact that the strains near the critical location were changing more rapidly than the strains near the peak displacement or the location of maximum bending strain within the previously identified area.

Another noteworthy observation in this analysis is that the membrane strains were equal to the calculated bending strains. It is common for pipeline operators to manage geohazard threats based on calculated bending strains alone. For most bending strain locations with smaller displacements and lower strain

values, the membrane strains are not significant and add less than 0.1% strain to the bending strain value. However, at larger displacements, the membrane strains can become significant with magnitudes equal to or greater than the calculated bending strain values as seen in this assessment.

7.0 REFERENCES

ADV Integrity. (2023, June). Woodpat Pipeline Girth Weld Testing, Edwardsville Illinois Pipe Sample .

American Lifelines Alliance. (2005, February). Guidelines for the Design of Buried Steel Pipe.

Oswell, J. M. (2016). *Soil Mechanics for Pipeline Stress Analysis.*

Wang, Y.-Y. (2019). Characterization of Mechanical Properties of Vintage Girth Welds.

APPENDIX A

Metallurgical Report

ADVINTEGRITY

ADVANCING INDUSTRY TOGETHER

Woodpat Pipeline Girth Weld Testing, Edwardsville Illinois Pipe Sample

Final Report

Prepared for

Marathon Pipe Line, LLC

100794-RP01-Rev0-061623

June 2023

WHEN TECHNOLOGY WORKS, TREMENDOUS THINGS ARE POSSIBLE.

Woodpat Pipeline Girth Weld Testing, Edwardsville Illinois Pipe Sample

Final Report

Prepared for

Marathon Pipe Line, LLC

Findlay, OH

June 2023

Prepared by:

[redacted]

Reviewed by:

[redacted]

ADVINTEGRITY

ADVANCING INDUSTRY TOGETHER

100794-RP01-Rev0-061623

Rev	Date	Description	Prepared	Checked	Reviewed
B	06.09.2023	Issued for Client Review	[redacted]	[redacted]	[redacted]
0	06.16.2023	Issued for Use	[redacted]	[redacted]	[redacted]

Texas Registered Engineering Firm F-19081

www.advintegrity.com

ADV INTEGRITY

ADVANCING INDUSTRY TOGETHER

Friday, June 16, 2023 100794-RP01-Rev0-061623

[redacted]
Marathon Pipe Line, LLC
539 S Main St, Findlay, OH 45840

[redacted]

Enclosed is our report documenting the mechanical testing and tensile strain capacity estimation of an intact girth weld removed from the Woodpat pipeline segment. This girth weld was removed due to the Edwardsville, Illinois incident occurring on March 11, 2022. Marathon reported that the pipeline in question was installed in 1949 using nominal 22-inch [redacted] pipe material. Marathon reported that the pipeline transports crude oil at a maximum allowable operating pressure of 881 psig, and the failure occurred at 479 psig.

Thank you for the opportunity to complete this work and please do not hesitate to contact us with any questions.

Regards,

[redacted] | Director, Materials Engineering

ADV Integrity, Inc.
4027 Pinehurst Meadow | Magnolia, TX 77355
Office: [redacted] | E-mail: [redacted]
Texas Registered Engineering Firm F-19081

Reviewed by: [redacted] | Chief Engineer – Pipeline Integrity

CONTENTS

LIST OF FIGURES

LIST OF TABLES

1.0 INTRODUCTION AND BACKGROUND

Marathon Pipe Line, LLC (Marathon) contracted ADV Integrity, Inc. (ADV) to perform mechanical testing of an intact girth weld removed from the Woodpat pipeline segment. This girth weld was removed due to the Edwardsville, Illinois incident occurring on March 11, 2022. The National Transportation Safety Board (NTSB) performed a metallurgical examination of the failed girth weld and a partial examination of the intact weld provided. Marathon reported that the pipeline in question was installed in 1949 using nominal 22-inch [redacted] pipe material. Marathon reported that the pipeline transports crude oil at a maximum allowable operating pressure of 881 psig and the failure occurred at 479 psig.

Marathon requested that ADV perform a series of examinations and mechanical testing to determine the weld's quality and estimate the tensile strain capacity of the weld. To do so, ADV suggested a test matrix to include: pipe body and girth weld tensile tests, Charpy v-Notch testing of the girth weld per API 1104, CTODs of the welds per API 1104, girth weld macros, and full hardness maps. The cross girth weld tensile tests were monitored via digital image correlation (DIC) to provide additional details regarding strain during the tensile test. The results from each examination are summarized in the sections below.

ADV utilized feature dimensions determined via the NTSB examination on the failed girth weld and the feature dimensions present determined via radiographic testing (RT) of the intact girth weld. Based on review of the NTSB data, ADV determined the following:

- Planar feature length within the failed weld:
  - Incomplete Penetration, 7.2-inch long, 1:15 to 1:30 o'clock orientation (0.6 to 1.2 feet); shown in Figure 1 and Figure 2
    - Metallurgical depth of 7.7 mm at deepest point, average 2-4 mm along the length of feature
  - Incomplete Penetration, 1.2-inch long, 3:20 to 3:32 o'clock orientation (1.6 to 1.7 feet)
  - Incomplete Penetration, 0.5 inch long, 6:46 to 6:53 o'clock orientation (3.25 to 3.3 feet)
  - Incomplete Penetration, 0.5 inch long, 10:25 to 10:32 o'clock orientation (5 to 5.05 feet)
- Intact weld: shown in Figure 3
  - Volumetric Features:
    - Elongated slag inclusions and porosity, 0.5 inch long, 12:47 to 12:52 o'clock orientation (4.5 inch to 5 inch)
    - Elongated slag inclusions, 2 inches long, 2:20 to 2:40 o'clock orientation (13.5 inch to 15.5 inch)
    - Elongated slag inclusions, 1.5 inches long, 3:45 to 4:00 o'clock orientation (21.5 inch to 23 inch)
    - Scattered porosity, 5 inches long, 5:12 to 6:05 o'clock orientation (30 inch to 35 inch)
    - Elongated slag inclusions, 3 inches long, 7:38 to 8:10 o'clock orientation (44 inch to 47 inch)
  - Planar features:

- Incomplete Penetration, 0.5-inch long, 4:15 to 4:21 o'clock orientation (24.5 inch to 25 inch)
    - Metallurgical depth 1.3 mm
- Incomplete Fusion, 0.5-inch long, 6:54 to 7:00 o'clock orientation (39.75 inch to 40.25 inch)
- Burn through, 0.25 inch long, 9:20 to 9:23 o'clock orientation (53.75 inch to 54 inch)

Figure 1: Photograph of fracture surface. Numbered scale divisions are inches.

Figure 2: Photograph of fracture surface.

Figure 3: RT image of intact girth weld.

2.0 EXAMINATION OF INTACT WELD

2.1 Tensile Tests

ADV performed tensile testing of the base pipe from both sides of the intact girth weld and three cross weld tensile tests around the circumference of the girth weld. The tensile straps were removed from the top of the pipe (12:00 o'clock orientation) and either the 3:00 o'clock orientation or 9:00 o'clock orientation, and the bottom of the pipe (6:00 o'clock orientation) guided by the RT images in an attempt to avoid flaws present. The cross girth weld tensile tests were monitored via digital image correlation (DIC). DIC utilizes a defined speckle pattern applied to the viewing surface (in this case the through thickness weld profile) created through black and white spray paint to monitor displacement over a given time. Relationship between the starting pattern and how that pattern deforms relative to adjacent patterns is then later interpreted as strain.

The results were compared to the closest API 5L edition from the time of manufacturing: API 5LX, 5th Edition (1954). Tensile test (per ASTM A370) results, summarized in Table 1, respectively, are consistent with the requirements of [redacted]. The cross girth weld tensile test prepared at the 12:00 and 3:00 o'clock orientation failed in the weld metal with obvious signs of weld flaws (incomplete penetration and porosity). Images of all three tensiles are shown in Figure 4 through Figure 6. Videos of the DIC tests were provided in a separate file. Some of these videos failed outside the virtual extensometer as they failed in the base pipe. These results are considered further in the tensile strain capacity calculations.

Table 1: Tensile Strength Results

Sample	Yield Strength (psi)	Tensile Strength (psi)	Elongation (%)
Pipe Body, Longitudinal, Upstream Pipe	51,200	82,600	30.0
Pipe Body, Longitudinal, Downstream Pipe	55,700	82,000	30.0
API [redacted] 5th Edition (1954)	46,000 (min)	63,000 (min)	23.5 (min)
Cross Girth Weld 1 (12:00)	---	69,400 [1]	---
Cross Girth Weld 2 (3:00)	---	69,400 [1]	---
Cross Girth Weld 3 (6:00)	---	81,200 [2]	---

Longitudinal, 3/4" wide reduced sections
[1] Failed in base material, [2] Failed in girth weld or HAZ

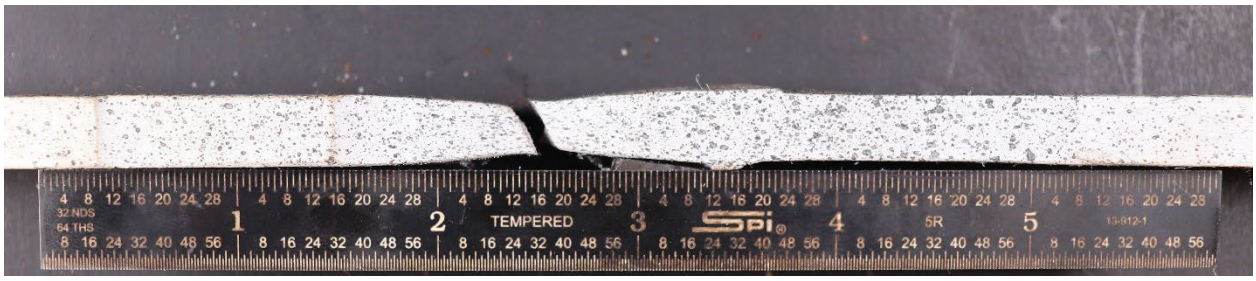

Figure 4: 12:00 o'clock orientation cross girth weld tensile.

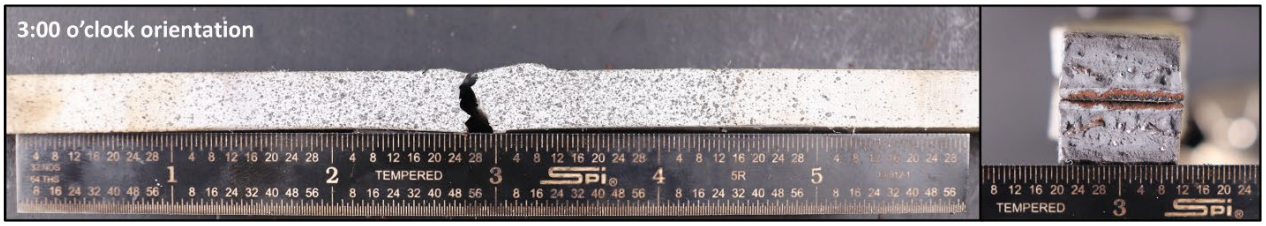

Figure 5: 3:00 o'clock orientation cross girth weld tensile.

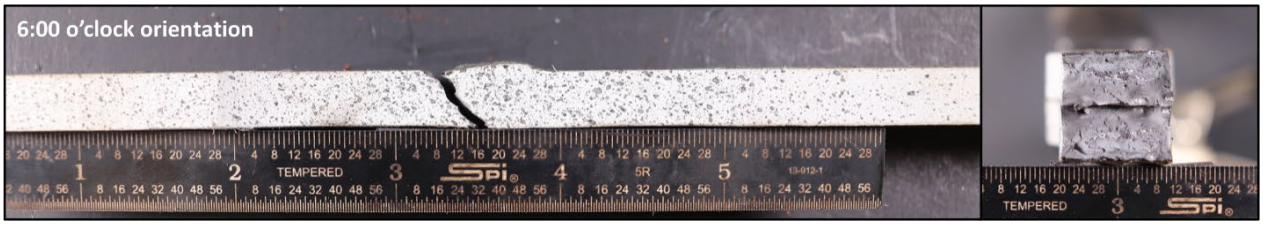

Figure 6: 6:00 o'clock orientation cross girth weld tensile.

2.2 Charpy v-Notch Tests

Girth weld centerline and girth weld heat affected zone (HAZ), two-thirds size Charpy V-notch tests (per ASTM A370) were performed to generate a transition curve; results are summarized in Table 2. Charpy V-notch transition curves were generated using a hyperbolic tangent curve-fit (API 579, Annex 9F) and summarized in Figure 7 and Figure 8.

Table 2: Charpy V-notch Results

Location	Specimen	Temperature	Absorbed Energy (ft-lb)	Approx. Full-Size Equivalent Absorbed Energy (ft-lb)	Percent Shear (%)
Weld Centerline	1	-110	12	17.9	30
	2	-90	4.5	6.7	25
	3	-70	21	31.3	40
	4	-20	22	32.8	60
	5	32	41	61.2	100
	6	74	39	58.2	100
Weld HAZ	1	-70	4	6.0	10
	2	-20	8	11.9	40
	3	32	34	50.7	60
	4	74	37	55.2	70
	5	120	41	61.2	80
	6	170	49	73.1	100

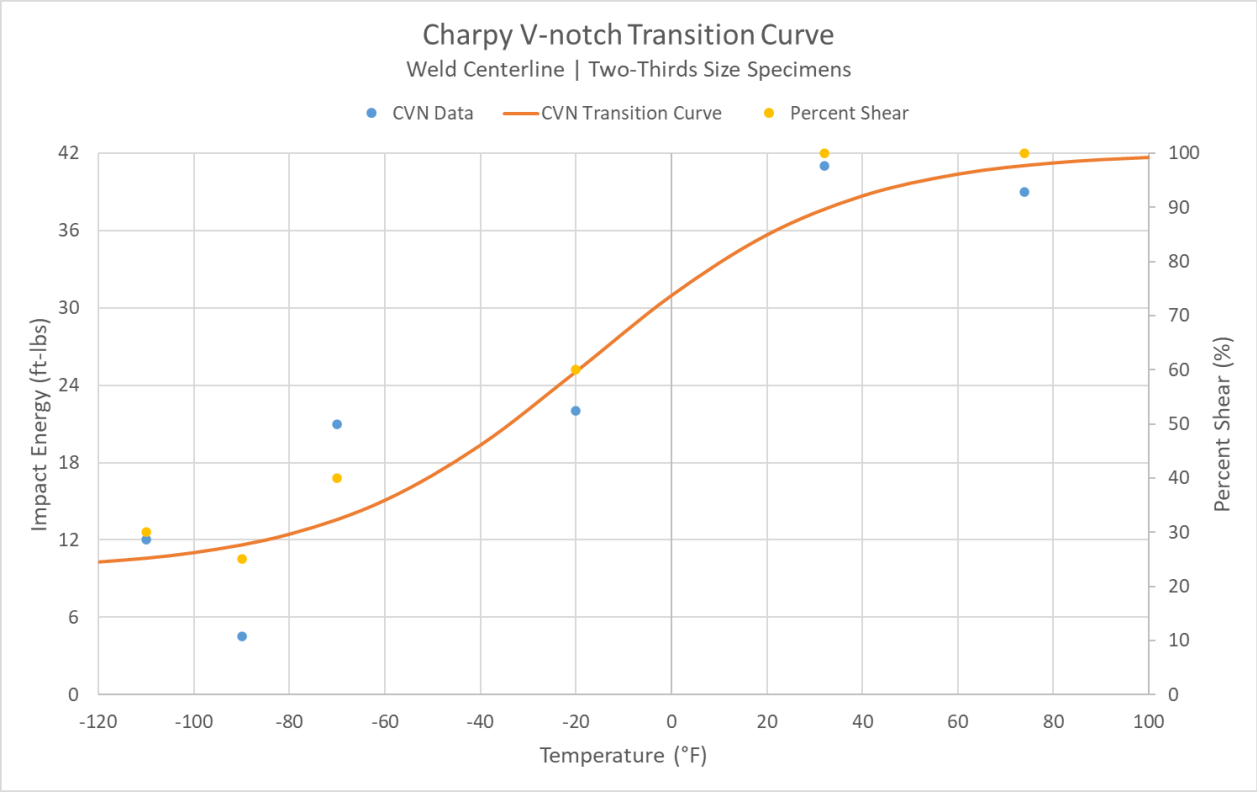

Figure 7: Girth weld centerline CVN transition curve.

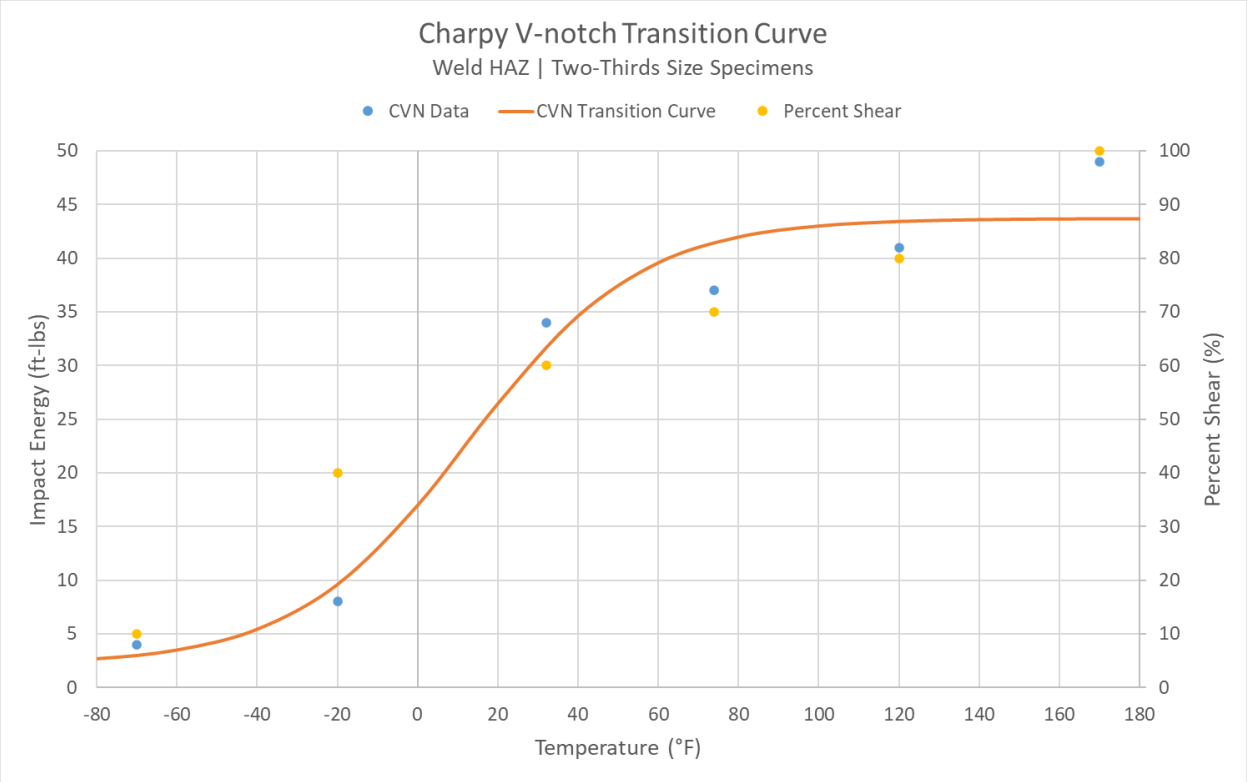

Figure 8: Girth weld HAZ CVN transition curve.

2.3 CTODs

ADV contracted Anderson and Associates to perform Bx2B SE(B) CTODs notched in the weld HAZ and the weld centerline. These tests were performed at ambient temperature at three circumferential locations: 12:00 o'clock, 3:00 o'clock, and 6:00 o'clock orientation. The results are summarized in Table 3.

Table 3: CTOD Results

Location		CTOD (in)	Average CTOD (in)
HAZ	12:00	0.011	0.0097
	3:00	0.0073	
	6:00	0.011	
Weld Centerline	12:00	0.012	0.0109
	3:00	0.011	
	6:00	0.0098 [1]	

[1] Invalid result due to weld flaw present.

2.4 Girth Weld Macros and Hardness Testing

ADV prepared two metallurgical cross sections of the girth weld, one at the 12:00 o'clock and one at the 3:00 o'clock orientation. These cross sections are shown in Figure 9 and Figure 10, respectively. High-lo was identified in the 3:00 o'clock cross section, as annotated in the figure. The high-lo present at the 3:00

o'clock orientation is shown in Figure 11. An area of incomplete penetration was identified connected to the high-lo present. The base pipe microstructure on both sides of the girth weld is consistent with a ferrite-pearlite mixture expected for carbon steel, shown in Figure 12 and Figure 13.

Full hardness maps were performed on the cross sections at a 500-gram load (HV0.5). Images of the hardness traverse are shown in Figure 14 and Figure 15, respectively. No evidence of widespread heat affected zone softening was identified. ADV further calculated a weld strength factor (weld strength / pipe strength) for each macro: both were approximately 0.95. The full hardness reports are attached in Appendix B.

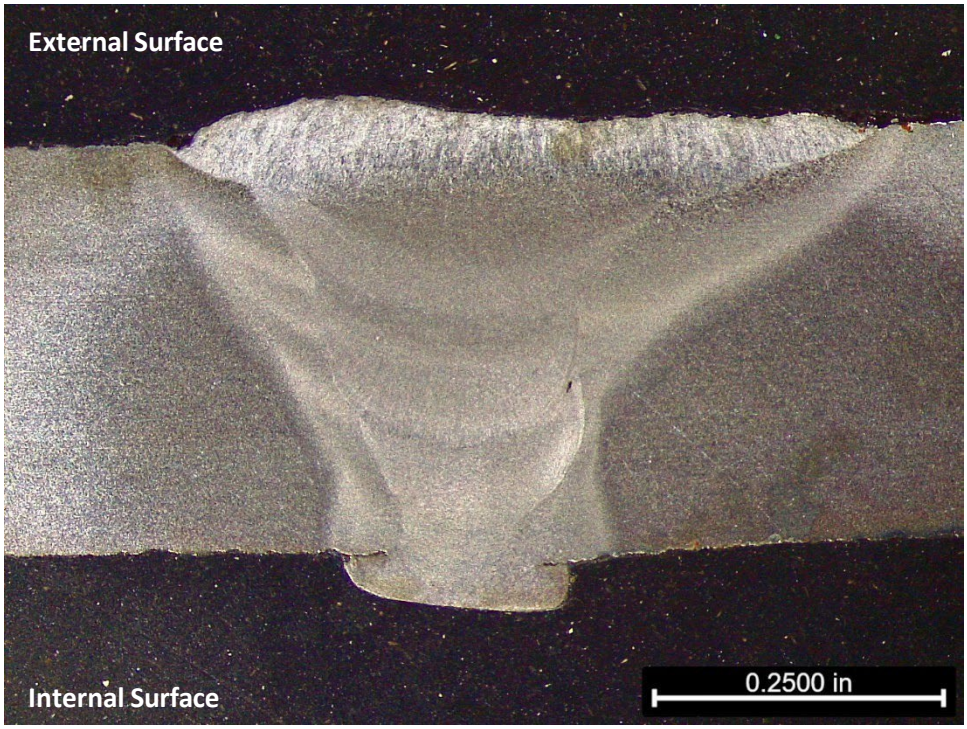

Figure 9: Photomicrograph of across the intact girth weld at the 12:00 o'clock orienation. Etchant is 2% Nital; original mangification is 0.6x.

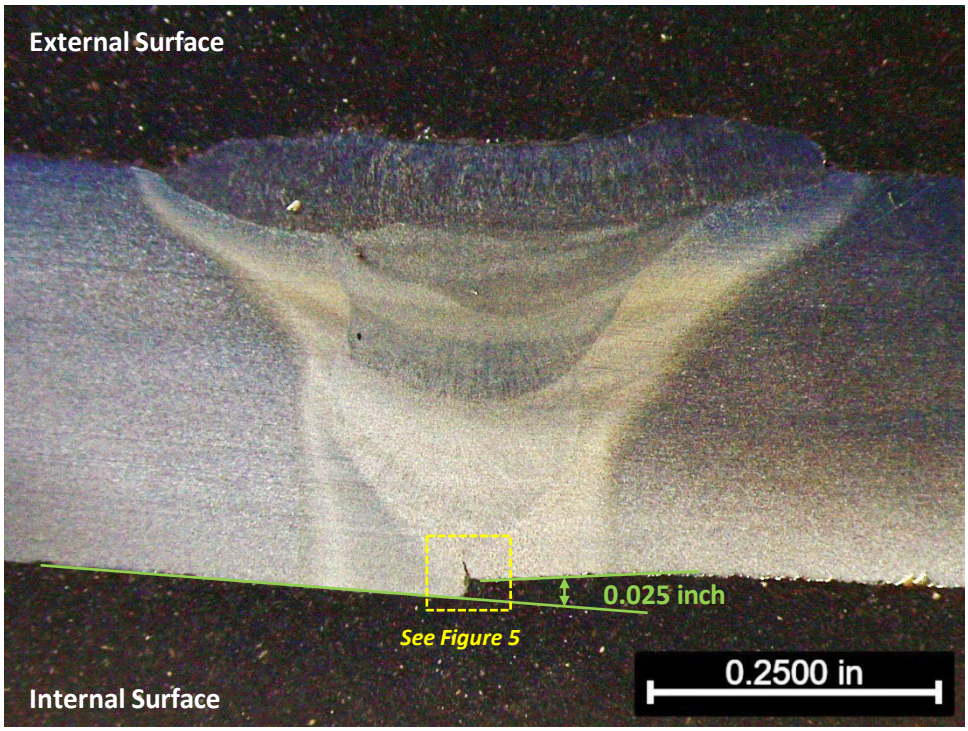

Figure 10: Photomicrograph of across the intact girth weld at the 3:00 o'clock orienation. Etchant is 2% Nital; original mangification is 0.6x.

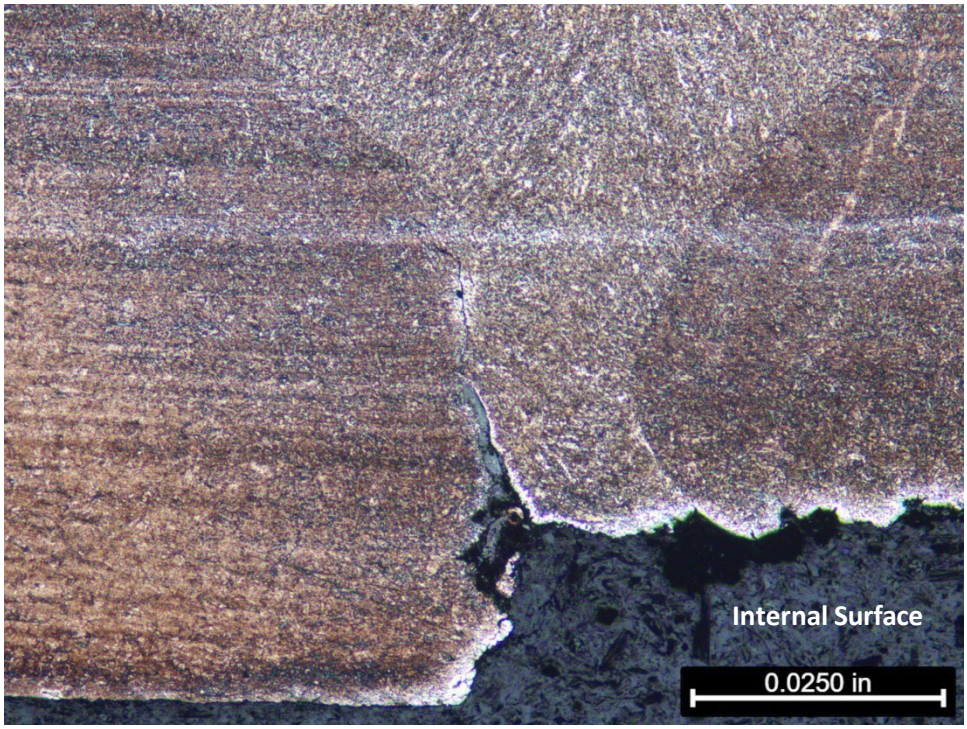

Figure 11: Photomicrograph of girth weld feature present along the internal surface of the 3:00 o'clock cross section. Etchant is 2% Nital; original mangification is 50x.

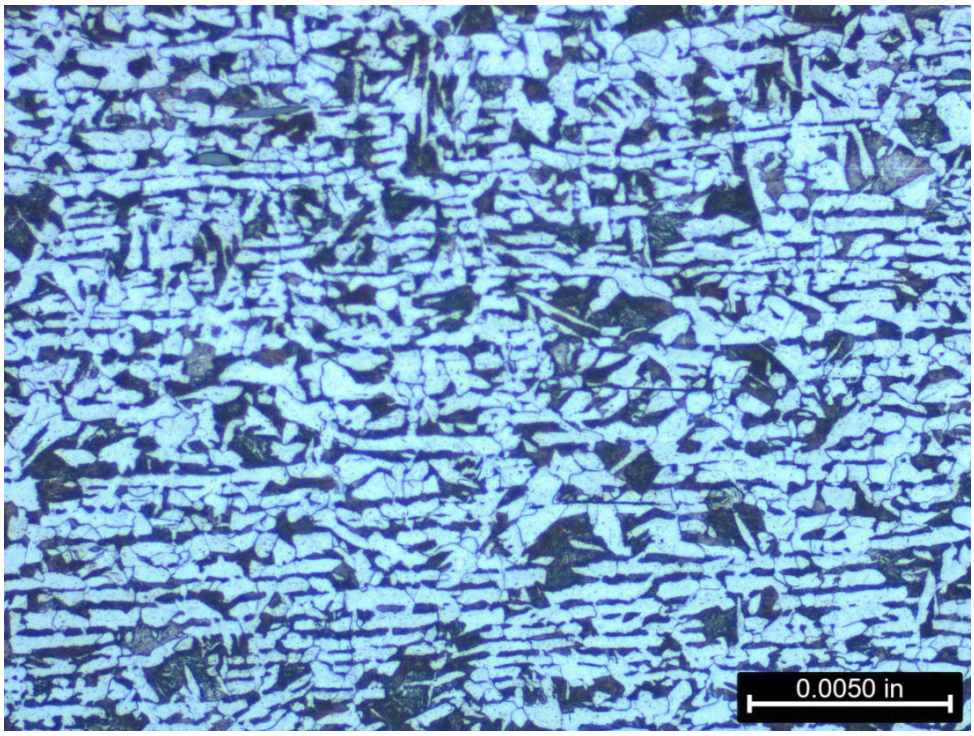

Figure 12: Photomicrograph of the base pipe material upstream of the girth weld. Etchant is 2% Nital; original mangification is 200x.

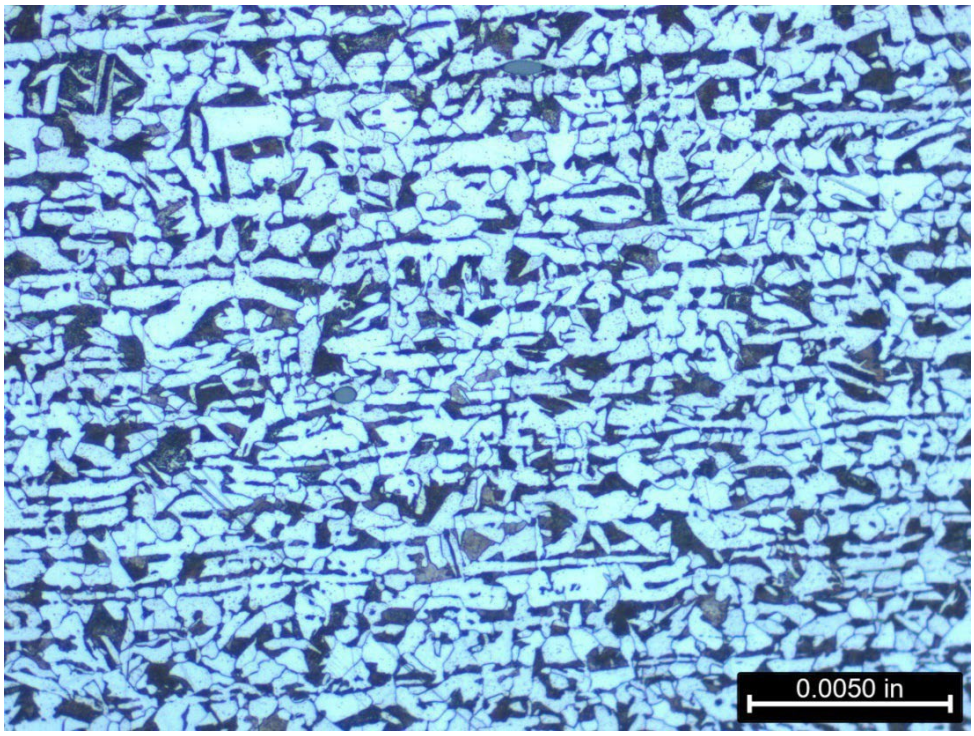

Figure 13: Photomicrograph of the base pipe material downstream of the girth weld. Etchant is 2% Nital; original mangification is 200x.

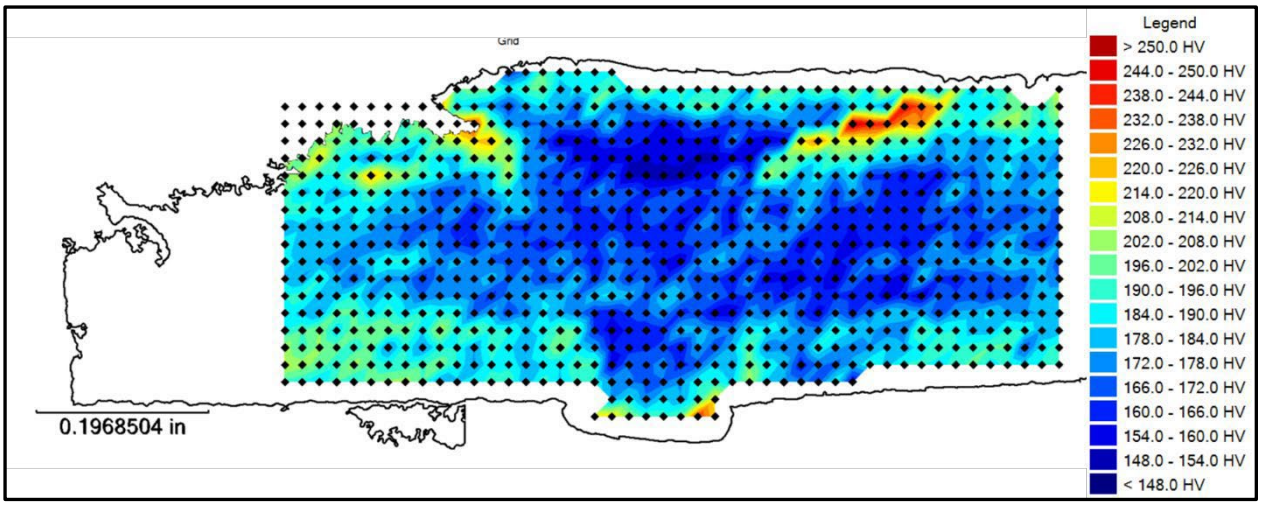

Figure 14: HV0.5 hardness map of weld, 12:00 o'clock orientation.

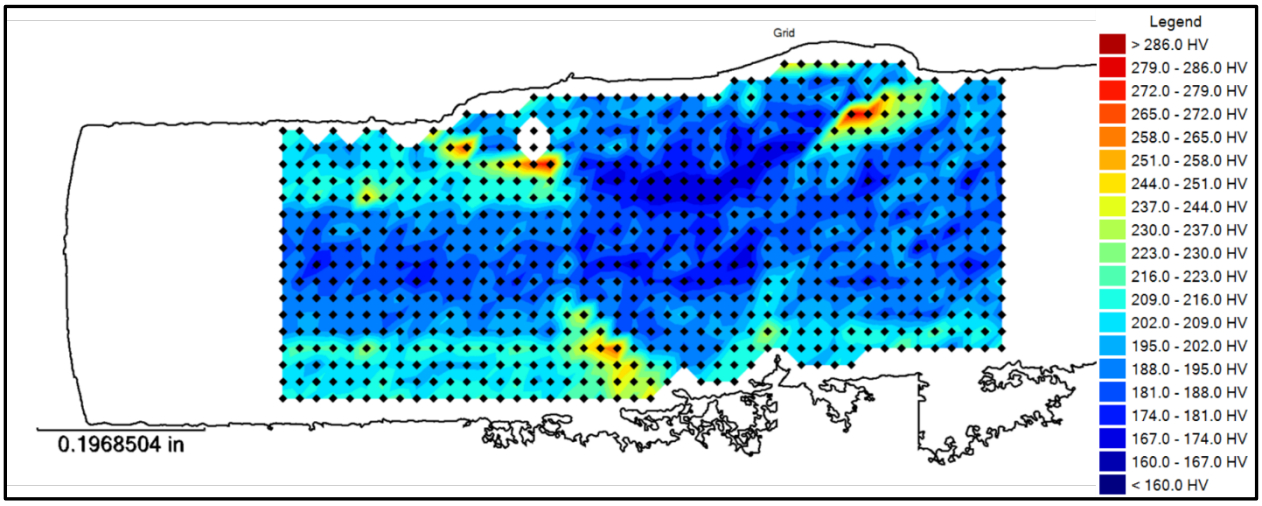

Figure 15: HV0.5 hardness map of weld, 3:00 o'clock orientation.

2.5 Calculated Tensile Strain Capacity (TSC)

ADV followed PRCI SIA-1-7 to estimate the TSC of the weld, which contains a 0.67 safety factor. The assumptions utilized in the calculations are shown in Table 4. These assumptions were based upon the test results described in the subsections above.

Load case 1 was utilized to represent a feature of similar depth to that of the failure origin. The PRCI SIA-1-7 software contains a maximum allowable aspect ratio of 12 and a maximum depth of 80% of the nominal wall thickness. Therefore, the flaw identified is outside the limits of the available industry tool. This limited the analysis to a feature that measured 6.95 mm deep (0.274 inches deep) with a length of 3.27 inches. This resulted in a feature that was slightly shallower (compared to the peak depth) and approximately half the length than found during the metallurgical examination, resulting in a TSC of 0.29. Load case 2 is based on the longest allowable feature within the PRCI SIA-1-7 software with a depth of 3.5

mm (similar to the average depth along the identified feature). Load case 3 is based on the feature length and depth identified via RT and metallography of the intact girth weld provided. These load cases are repeated with the pressure being modified from the MOP (881 psig) to the reported failure pressure (479 psig).

Table 4: Tensile Strain Capacity Inputs and Results

Input	Case					
	1	2	3	4	5	6
Pipe OD (in)	22					
Pipe WT (in)	0.344 (8.7 mm)					
Pipe Grade	[redacted]					
Pressure Factor	0.61 (881 psi)			0.33 (479 psi)		
Misalignment (mm)	0.80					
Weld Strength Factor	0.95					
Flaw Length (in)	3.27	1.65	0.5	3.27	1.65	0.5
Flaw Depth (mm)	6.95	3.5	1.5	6.95	3.5	1.5
CTOD (in)	0.0097 (Avg), 0.0073 (Low)					
Apparent Toughness, CTODa (in)	0.0177					
Result (TSC %)	**0.29**	**0.89**	**>2.0**	**0.35**	**1.1**	**>2.0**

APPENDIX A: HARDNESS TESTING REPORTS

Hardness Map

ADV PN 100794 12:00 o'clock

Date: 05-25-2023
Tester: Admin
Program: Hardness Map

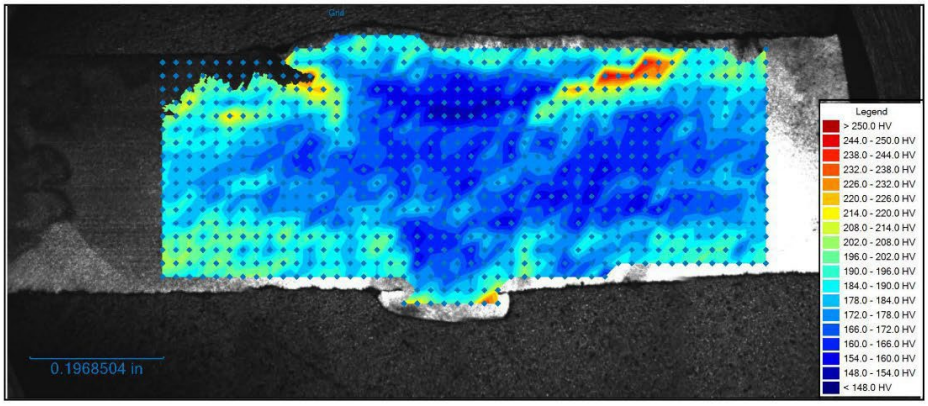

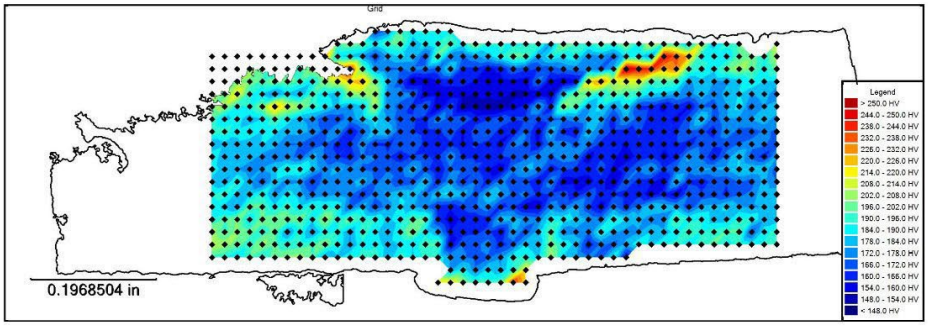

Date: 05-25-2023
Tester: Admin
Program: Hardness Map

Grid

Mean	Minimum	Maximum	Range	Std. deviation
180.3	149.4	252.2	102.9	15.9

Hardness Trace

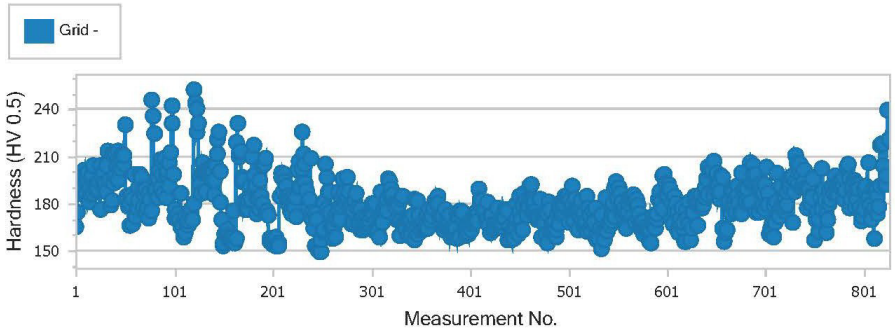

Point	Distance	Hardness	Converted	Diagonal X	Diagonal Y	Comments
1	-	165.0 HV 0.5	85.0 HRB	74.0 µm	75.9 µm	
2	-	174.1 HV 0.5	87.5 HRB	75.9 µm	70.0 µm	
3	-	197.0 HV 0.5	92.4 HRB	68.4 µm	68.8 µm	
4	-	186.1 HV 0.5	90.2 HRB	70.2 µm	70.9 µm	
5	-	192.4 HV 0.5	91.5 HRB	69.6 µm	69.2 µm	
6	-	187.2 HV 0.5	90.4 HRB	70.6 µm	70.2 µm	
7	-	188.9 HV 0.5	90.8 HRB	69.4 µm	70.7 µm	
8	-	195.5 HV 0.5	92.1 HRB	68.7 µm	69.0 µm	
9	-	201.1 HV 0.5	93.2 HRB	68.8 µm	67.0 µm	
10	-	197.8 HV 0.5	92.6 HRB	67.9 µm	69.0 µm	
11	-	186.5 HV 0.5	90.3 HRB	70.6 µm	70.5 µm	
12	-	194.9 HV 0.5	92.0 HRB	68.0 µm	70.0 µm	
13	-	199.4 HV 0.5	92.9 HRB	69.1 µm	67.2 µm	
14	-	180.5 HV 0.5	89.1 HRB	71.7 µm	71.6 µm	
15	-	185.4 HV 0.5	90.1 HRB	72.5 µm	68.9 µm	
16	-	190.6 HV 0.5	91.1 HRB	70.3 µm	69.2 µm	
17	-	197.7 HV 0.5	92.5 HRB	68.7 µm	68.3 µm	
18	-	186.8 HV 0.5	90.4 HRB	70.1 µm	70.8 µm	
19	-	203.9 HV 0.5	93.8 HRB	66.4 µm	68.4 µm	
20	-	191.6 HV 0.5	91.3 HRB	68.3 µm	70.8 µm	
21	-	191.6 HV 0.5	91.3 HRB	68.7 µm	70.5 µm	

Date: 05-25-2023
Tester: Admin
Program: Hardness Map

Point	Distance	Hardness	Converted	Diagonal X	Diagonal Y	Comments
22	-	188.2 HV 0.5	90.6 HRB	70.2 µm	70.2 µm	
23	-	189.0 HV 0.5	90.8 HRB	71.0 µm	69.1 µm	
24	-	194.1 HV 0.5	91.8 HRB	68.3 µm	69.9 µm	
25	-	176.5 HV 0.5	88.1 HRB	72.4 µm	72.6 µm	
26	-	204.2 HV 0.5	93.8 HRB	65.8 µm	68.9 µm	
27	-	196.6 HV 0.5	92.3 HRB	69.6 µm	67.7 µm	
28	-	190.7 HV 0.5	91.1 HRB	70.9 µm	68.6 µm	
29	-	199.1 HV 0.5	92.8 HRB	68.2 µm	68.3 µm	
30	-	193.2 HV 0.5	91.6 HRB	68.0 µm	70.5 µm	
31	-	204.5 HV 0.5	93.9 HRB	67.5 µm	67.2 µm	
32	-	187.4 HV 0.5	90.5 HRB	70.6 µm	70.1 µm	
33	-	213.5 HV 0.5	95.6 HRB	65.8 µm	66.0 µm	
34	-	194.6 HV 0.5	91.9 HRB	70.6 µm	67.5 µm	
35	-	194.9 HV 0.5	92.0 HRB	71.5 µm	66.4 µm	
36	-	179.4 HV 0.5	88.8 HRB	70.3 µm	73.5 µm	
37	-	211.9 HV 0.5	95.3 HRB	65.2 µm	67.1 µm	
38	-	181.6 HV 0.5	89.3 HRB	75.1 µm	67.8 µm	
39	-	192.9 HV 0.5	91.6 HRB	69.5 µm	69.2 µm	
40	-	197.5 HV 0.5	92.5 HRB	68.0 µm	69.0 µm	
41	-	211.0 HV 0.5	95.2 HRB	65.0 µm	67.6 µm	
42	-	203.7 HV 0.5	93.7 HRB	68.7 µm	66.2 µm	
43	-	212.9 HV 0.5	95.5 HRB	67.5 µm	64.5 µm	
44	-	194.5 HV 0.5	91.9 HRB	66.8 µm	71.3 µm	
45	-	205.0 HV 0.5	94.0 HRB	68.6 µm	66.0 µm	
46	-	202.5 HV 0.5	93.5 HRB	67.4 µm	67.9 µm	
47	-	202.3 HV 0.5	93.5 HRB	66.5 µm	68.9 µm	
48	-	211.2 HV 0.5	95.2 HRB	64.8 µm	67.7 µm	
49	-	204.6 HV 0.5	93.9 HRB	65.2 µm	69.4 µm	
50	-	210.9 HV 0.5	95.2 HRB	66.8 µm	65.8 µm	
51	-	230.3 HV 0.5	98.4 HRB	64.2 µm	62.7 µm	
52	-	184.5 HV 0.5	89.9 HRB	71.6 µm	70.2 µm	
53	-	181.5 HV 0.5	89.3 HRB	71.5 µm	71.4 µm	
54	-	178.0 HV 0.5	88.5 HRB	73.1 µm	71.3 µm	
55	-	165.9 HV 0.5	85.2 HRB	75.5 µm	74.0 µm	
56	-	179.5 HV 0.5	88.9 HRB	71.1 µm	72.7 µm	
57	-	185.1 HV 0.5	90.0 HRB	72.6 µm	68.9 µm	
58	-	182.4 HV 0.5	89.5 HRB	71.5 µm	71.1 µm	
59	-	166.9 HV 0.5	85.5 HRB	75.8 µm	73.3 µm	
60	-	198.8 HV 0.5	92.8 HRB	69.3 µm	67.3 µm	

Date: 05-25-2023
Tester: Admin
Program: Hardness Map

Point	Distance	Hardness	Converted	Diagonal X	Diagonal Y	Comments
61	-	173.0 HV 0.5	87.2 HRB	73.4 µm	73.0 µm	
62	-	171.5 HV 0.5	86.8 HRB	74.7 µm	72.4 µm	
63	-	176.7 HV 0.5	88.2 HRB	73.4 µm	71.4 µm	
64	-	181.8 HV 0.5	89.4 HRB	71.5 µm	71.3 µm	
65	-	189.9 HV 0.5	91.0 HRB	69.6 µm	70.2 µm	
66	-	198.4 HV 0.5	92.7 HRB	69.2 µm	67.6 µm	
67	-	196.8 HV 0.5	92.4 HRB	68.7 µm	68.6 µm	
68	-	177.4 HV 0.5	88.4 HRB	73.8 µm	70.8 µm	
69	-	189.0 HV 0.5	90.8 HRB	71.8 µm	68.3 µm	
70	-	185.6 HV 0.5	90.1 HRB	70.9 µm	70.5 µm	
71	-	189.5 HV 0.5	90.9 HRB	70.3 µm	69.6 µm	
72	-	174.3 HV 0.5	87.6 HRB	73.1 µm	72.8 µm	
73	-	177.6 HV 0.5	88.4 HRB	71.8 µm	72.7 µm	
74	-	170.4 HV 0.5	86.5 HRB	73.1 µm	74.5 µm	
75	-	186.4 HV 0.5	90.3 HRB	70.3 µm	70.8 µm	
76	-	183.2 HV 0.5	89.6 HRB	71.8 µm	70.5 µm	
77	-	174.9 HV 0.5	87.7 HRB	72.9 µm	72.7 µm	
78	-	246.0 HV 0.5	-	63.0 µm	59.8 µm	
79	-	235.3 HV 0.5	99.2 HRB	62.1 µm	63.5 µm	
80	-	224.1 HV 0.5	97.4 HRB	64.5 µm	64.1 µm	
81	-	189.2 HV 0.5	90.8 HRB	68.5 µm	71.5 µm	
82	-	188.1 HV 0.5	90.6 HRB	69.2 µm	71.2 µm	
83	-	183.6 HV 0.5	89.7 HRB	72.0 µm	70.1 µm	
84	-	196.3 HV 0.5	92.3 HRB	71.0 µm	66.5 µm	
85	-	201.3 HV 0.5	93.3 HRB	67.8 µm	67.9 µm	
86	-	189.4 HV 0.5	90.9 HRB	69.0 µm	70.9 µm	
87	-	207.6 HV 0.5	94.5 HRB	65.7 µm	67.9 µm	
88	-	198.9 HV 0.5	92.8 HRB	68.4 µm	68.1 µm	
89	-	206.3 HV 0.5	94.3 HRB	69.9 µm	64.2 µm	
90	-	186.6 HV 0.5	90.3 HRB	71.8 µm	69.1 µm	
91	-	208.4 HV 0.5	94.7 HRB	66.2 µm	67.2 µm	
92	-	198.1 HV 0.5	92.6 HRB	68.3 µm	68.6 µm	
93	-	183.8 HV 0.5	89.8 HRB	71.2 µm	70.8 µm	
94	-	200.4 HV 0.5	93.1 HRB	67.2 µm	68.9 µm	
95	-	190.9 HV 0.5	91.2 HRB	68.6 µm	70.8 µm	
96	-	205.7 HV 0.5	94.1 HRB	67.5 µm	66.8 µm	
97	-	212.7 HV 0.5	95.4 HRB	67.0 µm	65.1 µm	
98	-	231.3 HV 0.5	98.6 HRB	64.9 µm	61.7 µm	
99	-	242.1 HV 0.5	-	61.3 µm	62.5 µm	

Date: 05-25-2023
Tester: Admin
Program: Hardness Map

Point	Distance	Hardness	Converted	Diagonal X	Diagonal Y	Comments
100	-	198.7 HV 0.5	92.7 HRB	67.5 µm	69.1 µm	
101	-	176.2 HV 0.5	88.0 HRB	72.7 µm	72.4 µm	
102	-	170.4 HV 0.5	86.5 HRB	73.4 µm	74.1 µm	
103	-	171.5 HV 0.5	86.8 HRB	73.7 µm	73.3 µm	
104	-	173.0 HV 0.5	87.2 HRB	73.4 µm	73.0 µm	
105	-	173.7 HV 0.5	87.4 HRB	72.5 µm	73.7 µm	
106	-	170.0 HV 0.5	86.3 HRB	74.3 µm	73.4 µm	
107	-	186.3 HV 0.5	90.3 HRB	70.3 µm	70.8 µm	
108	-	164.7 HV 0.5	84.9 HRB	76.1 µm	74.0 µm	
109	-	164.5 HV 0.5	84.8 HRB	77.4 µm	72.8 µm	
110	-	158.6 HV 0.5	82.9 HRB	77.3 µm	75.6 µm	
111	-	161.4 HV 0.5	83.8 HRB	75.4 µm	76.2 µm	
112	-	171.5 HV 0.5	86.8 HRB	74.4 µm	72.6 µm	
113	-	167.9 HV 0.5	85.7 HRB	73.1 µm	75.6 µm	
114	-	165.9 HV 0.5	85.2 HRB	75.2 µm	74.3 µm	
115	-	168.5 HV 0.5	85.9 HRB	74.4 µm	74.0 µm	
116	-	172.6 HV 0.5	87.1 HRB	73.2 µm	73.4 µm	
117	-	174.9 HV 0.5	87.7 HRB	74.8 µm	70.8 µm	
118	-	176.0 HV 0.5	88.0 HRB	73.1 µm	72.1 µm	
119	-	169.8 HV 0.5	86.3 HRB	73.2 µm	74.6 µm	
120	-	179.7 HV 0.5	88.9 HRB	70.6 µm	73.1 µm	
121	-	252.2 HV 0.5	-	61.2 µm	60.1 µm	
122	-	243.8 HV 0.5	-	61.8 µm	61.5 µm	
123	-	240.7 HV 0.5	-	61.0 µm	63.1 µm	
124	-	225.1 HV 0.5	97.5 HRB	64.2 µm	64.1 µm	
125	-	231.1 HV 0.5	98.5 HRB	63.7 µm	63.0 µm	
126	-	196.9 HV 0.5	92.4 HRB	69.1 µm	68.2 µm	
127	-	192.1 HV 0.5	91.4 HRB	68.2 µm	70.7 µm	
128	-	186.0 HV 0.5	90.2 HRB	70.9 µm	70.3 µm	
129	-	199.9 HV 0.5	93.0 HRB	67.9 µm	68.4 µm	
130	-	205.6 HV 0.5	94.1 HRB	68.4 µm	65.9 µm	
131	-	200.6 HV 0.5	93.1 HRB	69.2 µm	66.7 µm	
132	-	187.2 HV 0.5	90.4 HRB	70.2 µm	70.5 µm	
133	-	199.3 HV 0.5	92.9 HRB	68.2 µm	68.2 µm	
134	-	199.8 HV 0.5	93.0 HRB	66.3 µm	69.9 µm	
135	-	200.3 HV 0.5	93.1 HRB	68.5 µm	67.6 µm	
136	-	202.6 HV 0.5	93.5 HRB	67.3 µm	68.1 µm	
137	-	200.0 HV 0.5	93.0 HRB	66.7 µm	69.5 µm	
138	-	194.9 HV 0.5	92.0 HRB	68.2 µm	69.7 µm	

Date: 05-25-2023
Tester: Admin
Program: Hardness Map

Point	Distance	Hardness	Converted	Diagonal X	Diagonal Y	Comments
139	-	201.0 HV 0.5	93.2 HRB	68.6 µm	67.3 µm	
140	-	200.6 HV 0.5	93.1 HRB	66.2 µm	69.7 µm	
141	-	194.6 HV 0.5	91.9 HRB	68.0 µm	70.1 µm	
142	-	185.9 HV 0.5	90.2 HRB	68.8 µm	72.5 µm	
143	-	204.0 HV 0.5	93.8 HRB	67.6 µm	67.2 µm	
144	-	211.8 HV 0.5	95.3 HRB	66.3 µm	66.0 µm	
145	-	220.6 HV 0.5	96.8 HRB	64.7 µm	65.0 µm	
146	-	225.8 HV 0.5	97.6 HRB	64.9 µm	63.2 µm	
147	-	200.4 HV 0.5	93.1 HRB	67.4 µm	68.6 µm	
148	-	180.6 HV 0.5	89.1 HRB	71.9 µm	71.4 µm	
149	-	169.5 HV 0.5	86.2 HRB	74.5 µm	73.4 µm	
150	-	152.6 HV 0.5	80.9 HRB	78.4 µm	77.5 µm	
151	-	155.0 HV 0.5	81.7 HRB	76.6 µm	78.1 µm	
152	-	160.2 HV 0.5	83.4 HRB	76.3 µm	75.8 µm	
153	-	162.5 HV 0.5	84.2 HRB	75.0 µm	76.1 µm	
154	-	163.1 HV 0.5	84.4 HRB	75.9 µm	74.9 µm	
155	-	159.6 HV 0.5	83.2 HRB	76.6 µm	75.9 µm	
156	-	156.7 HV 0.5	82.2 HRB	76.6 µm	77.2 µm	
157	-	157.4 HV 0.5	82.5 HRB	76.6 µm	76.9 µm	
158	-	158.5 HV 0.5	82.8 HRB	76.8 µm	76.2 µm	
159	-	156.7 HV 0.5	82.2 HRB	76.4 µm	77.5 µm	
160	-	174.8 HV 0.5	87.7 HRB	73.1 µm	72.6 µm	
161	-	158.1 HV 0.5	82.7 HRB	77.2 µm	76.0 µm	
162	-	154.4 HV 0.5	81.5 HRB	77.5 µm	77.5 µm	
163	-	157.6 HV 0.5	82.5 HRB	75.6 µm	77.8 µm	
164	-	218.7 HV 0.5	96.5 HRB	65.9 µm	64.4 µm	
165	-	231.4 HV 0.5	98.6 HRB	63.5 µm	63.1 µm	
166	-	209.7 HV 0.5	94.9 HRB	66.0 µm	67.0 µm	
167	-	212.4 HV 0.5	95.4 HRB	67.0 µm	65.2 µm	
168	-	213.6 HV 0.5	95.6 HRB	66.2 µm	65.6 µm	
169	-	194.0 HV 0.5	91.8 HRB	69.7 µm	68.6 µm	
170	-	196.9 HV 0.5	92.4 HRB	69.0 µm	68.2 µm	
171	-	195.0 HV 0.5	92.0 HRB	69.1 µm	68.8 µm	
172	-	176.7 HV 0.5	88.2 HRB	72.1 µm	72.8 µm	
173	-	181.9 HV 0.5	89.4 HRB	70.2 µm	72.6 µm	
174	-	177.8 HV 0.5	88.4 HRB	71.4 µm	73.0 µm	
175	-	176.2 HV 0.5	88.1 HRB	69.5 µm	75.5 µm	
176	-	181.8 HV 0.5	89.4 HRB	69.3 µm	73.6 µm	
177	-	190.6 HV 0.5	91.1 HRB	67.5 µm	72.0 µm	

Date: 05-25-2023
Tester: Admin
Program: Hardness Map

Point	Distance	Hardness	Converted	Diagonal X	Diagonal Y	Comments
178	-	184.1 HV 0.5	89.8 HRB	69.7 µm	72.2 µm	
179	-	182.9 HV 0.5	89.6 HRB	72.7 µm	69.7 µm	
180	-	209.3 HV 0.5	94.9 HRB	67.1 µm	66.0 µm	
181	-	197.8 HV 0.5	92.6 HRB	68.1 µm	68.9 µm	
182	-	216.9 HV 0.5	96.1 HRB	62.3 µm	68.4 µm	
183	-	191.4 HV 0.5	91.3 HRB	72.5 µm	66.8 µm	
184	-	183.7 HV 0.5	89.7 HRB	70.5 µm	71.6 µm	
185	-	173.0 HV 0.5	87.3 HRB	70.6 µm	75.8 µm	
186	-	183.4 HV 0.5	89.7 HRB	73.4 µm	68.8 µm	
187	-	176.3 HV 0.5	88.1 HRB	71.2 µm	73.8 µm	
188	-	194.4 HV 0.5	91.9 HRB	68.4 µm	69.7 µm	
189	-	184.7 HV 0.5	89.9 HRB	70.6 µm	71.1 µm	
190	-	180.4 HV 0.5	89.1 HRB	70.2 µm	73.2 µm	
191	-	203.8 HV 0.5	93.8 HRB	67.0 µm	67.9 µm	
192	-	205.0 HV 0.5	94.0 HRB	67.6 µm	66.9 µm	
193	-	209.1 HV 0.5	94.8 HRB	65.6 µm	67.6 µm	
194	-	174.1 HV 0.5	87.5 HRB	74.3 µm	71.7 µm	
195	-	175.0 HV 0.5	87.8 HRB	73.6 µm	71.9 µm	
196	-	172.7 HV 0.5	87.2 HRB	73.4 µm	73.1 µm	
197	-	155.9 HV 0.5	82.0 HRB	77.6 µm	76.6 µm	
198	-	157.3 HV 0.5	82.4 HRB	77.4 µm	76.2 µm	
199	-	155.7 HV 0.5	81.9 HRB	78.1 µm	76.3 µm	
200	-	155.6 HV 0.5	81.9 HRB	76.9 µm	77.5 µm	
201	-	154.1 HV 0.5	81.4 HRB	78.0 µm	77.1 µm	
202	-	155.5 HV 0.5	81.8 HRB	77.7 µm	76.7 µm	
203	-	158.2 HV 0.5	82.7 HRB	76.9 µm	76.2 µm	
204	-	152.6 HV 0.5	80.9 HRB	77.5 µm	78.4 µm	
205	-	153.0 HV 0.5	81.0 HRB	77.5 µm	78.2 µm	
206	-	155.1 HV 0.5	81.7 HRB	78.1 µm	76.5 µm	
207	-	153.0 HV 0.5	81.0 HRB	77.5 µm	78.2 µm	
208	-	184.3 HV 0.5	89.9 HRB	70.7 µm	71.2 µm	
209	-	199.4 HV 0.5	92.9 HRB	66.2 µm	70.2 µm	
210	-	197.1 HV 0.5	92.4 HRB	68.4 µm	68.8 µm	
211	-	187.3 HV 0.5	90.5 HRB	68.7 µm	72.0 µm	
212	-	198.7 HV 0.5	92.7 HRB	67.8 µm	68.8 µm	
213	-	193.8 HV 0.5	91.8 HRB	68.6 µm	69.7 µm	
214	-	190.7 HV 0.5	91.1 HRB	69.0 µm	70.5 µm	
215	-	184.3 HV 0.5	89.9 HRB	69.4 µm	72.5 µm	
216	-	182.0 HV 0.5	89.4 HRB	69.8 µm	73.0 µm	

Date: 05-25-2023
Tester: Admin
Program: Hardness Map

Point	Distance	Hardness	Converted	Diagonal X	Diagonal Y	Comments
217	-	179.1 HV 0.5	88.8 HRB	70.5 µm	73.4 µm	
218	-	175.0 HV 0.5	87.8 HRB	71.7 µm	73.8 µm	
219	-	182.8 HV 0.5	89.6 HRB	71.9 µm	70.5 µm	
220	-	173.2 HV 0.5	87.3 HRB	71.5 µm	74.8 µm	
221	-	180.9 HV 0.5	89.2 HRB	70.4 µm	72.8 µm	
222	-	184.7 HV 0.5	89.9 HRB	72.3 µm	69.4 µm	
223	-	177.3 HV 0.5	88.3 HRB	73.2 µm	71.4 µm	
224	-	183.7 HV 0.5	89.7 HRB	70.0 µm	72.0 µm	
225	-	171.4 HV 0.5	86.8 HRB	72.5 µm	74.6 µm	
226	-	201.3 HV 0.5	93.3 HRB	66.5 µm	69.2 µm	
227	-	206.8 HV 0.5	94.4 HRB	67.4 µm	66.6 µm	
228	-	190.0 HV 0.5	91.0 HRB	68.8 µm	70.9 µm	
229	-	190.0 HV 0.5	91.0 HRB	69.0 µm	70.8 µm	
230	-	201.9 HV 0.5	93.4 HRB	67.4 µm	68.1 µm	
231	-	225.5 HV 0.5	97.6 HRB	66.1 µm	62.1 µm	
232	-	211.7 HV 0.5	95.3 HRB	66.9 µm	65.5 µm	
233	-	205.3 HV 0.5	94.1 HRB	66.3 µm	68.1 µm	
234	-	192.9 HV 0.5	91.6 HRB	67.7 µm	71.0 µm	
235	-	188.5 HV 0.5	90.7 HRB	69.9 µm	70.4 µm	
236	-	180.7 HV 0.5	89.1 HRB	72.5 µm	70.8 µm	
237	-	177.3 HV 0.5	88.3 HRB	72.6 µm	72.0 µm	
238	-	182.7 HV 0.5	89.5 HRB	68.9 µm	73.6 µm	
239	-	208.4 HV 0.5	94.7 HRB	66.9 µm	66.5 µm	
240	-	174.1 HV 0.5	87.5 HRB	72.5 µm	73.5 µm	
241	-	170.1 HV 0.5	86.4 HRB	71.7 µm	75.9 µm	
242	-	164.5 HV 0.5	84.8 HRB	75.8 µm	74.3 µm	
243	-	173.4 HV 0.5	87.3 HRB	74.5 µm	71.7 µm	
244	-	153.0 HV 0.5	81.0 HRB	80.8 µm	74.9 µm	
245	-	169.6 HV 0.5	86.2 HRB	74.1 µm	73.8 µm	
246	-	150.5 HV 0.5	80.2 HRB	76.8 µm	80.2 µm	
247	-	152.0 HV 0.5	80.7 HRB	78.4 µm	77.8 µm	
248	-	149.5 HV 0.5	79.8 HRB	79.7 µm	77.8 µm	
249	-	149.4 HV 0.5	79.8 HRB	80.0 µm	77.5 µm	
250	-	156.4 HV 0.5	82.1 HRB	78.1 µm	75.9 µm	
251	-	162.1 HV 0.5	84.0 HRB	75.3 µm	76.0 µm	
252	-	180.9 HV 0.5	89.2 HRB	71.3 µm	71.8 µm	
253	-	163.0 HV 0.5	84.3 HRB	76.0 µm	74.9 µm	
254	-	204.6 HV 0.5	93.9 HRB	68.3 µm	66.4 µm	
255	-	196.8 HV 0.5	92.4 HRB	68.1 µm	69.2 µm	

Date: 05-25-2023
Tester: Admin
Program: Hardness Map

Point	Distance	Hardness	Converted	Diagonal X	Diagonal Y	Comments
256	-	175.9 HV 0.5	88.0 HRB	70.5 µm	74.7 µm	
257	-	187.2 HV 0.5	90.4 HRB	70.9 µm	69.9 µm	
258	-	174.3 HV 0.5	87.6 HRB	76.0 µm	69.8 µm	
259	-	187.5 HV 0.5	90.5 HRB	70.2 µm	70.5 µm	
260	-	164.8 HV 0.5	84.9 HRB	74.4 µm	75.7 µm	
261	-	165.2 HV 0.5	85.0 HRB	72.2 µm	77.6 µm	
262	-	157.9 HV 0.5	82.6 HRB	77.2 µm	76.1 µm	
263	-	165.1 HV 0.5	85.0 HRB	75.4 µm	74.5 µm	
264	-	158.7 HV 0.5	82.9 HRB	77.5 µm	75.4 µm	
265	-	172.1 HV 0.5	87.0 HRB	72.8 µm	74.0 µm	
266	-	169.9 HV 0.5	86.3 HRB	74.1 µm	73.7 µm	
267	-	177.2 HV 0.5	88.3 HRB	72.6 µm	72.1 µm	
268	-	186.9 HV 0.5	90.4 HRB	70.0 µm	70.8 µm	
269	-	169.6 HV 0.5	86.2 HRB	73.4 µm	74.4 µm	
270	-	178.2 HV 0.5	88.5 HRB	70.7 µm	73.6 µm	
271	-	183.1 HV 0.5	89.6 HRB	70.5 µm	71.8 µm	
272	-	195.8 HV 0.5	92.2 HRB	69.1 µm	68.5 µm	
273	-	180.9 HV 0.5	89.2 HRB	72.0 µm	71.2 µm	
274	-	187.0 HV 0.5	90.4 HRB	68.9 µm	72.0 µm	
275	-	179.8 HV 0.5	88.9 HRB	71.7 µm	71.9 µm	
276	-	183.9 HV 0.5	89.8 HRB	68.1 µm	73.9 µm	
277	-	196.8 HV 0.5	92.4 HRB	68.6 µm	68.7 µm	
278	-	187.3 HV 0.5	90.5 HRB	69.8 µm	70.9 µm	
279	-	178.6 HV 0.5	88.7 HRB	71.8 µm	72.3 µm	
280	-	176.1 HV 0.5	88.0 HRB	72.1 µm	73.0 µm	
281	-	166.9 HV 0.5	85.5 HRB	73.4 µm	75.7 µm	
282	-	167.7 HV 0.5	85.7 HRB	72.5 µm	76.2 µm	
283	-	175.2 HV 0.5	87.8 HRB	72.5 µm	73.0 µm	
284	-	181.9 HV 0.5	89.4 HRB	71.1 µm	71.8 µm	
285	-	186.8 HV 0.5	90.4 HRB	71.5 µm	69.4 µm	
286	-	177.4 HV 0.5	88.4 HRB	71.5 µm	73.1 µm	
287	-	167.4 HV 0.5	85.6 HRB	73.1 µm	75.7 µm	
288	-	166.7 HV 0.5	85.4 HRB	73.6 µm	75.6 µm	
289	-	163.4 HV 0.5	84.5 HRB	75.0 µm	75.6 µm	
290	-	176.0 HV 0.5	88.0 HRB	72.9 µm	72.2 µm	
291	-	169.2 HV 0.5	86.1 HRB	73.5 µm	74.5 µm	
292	-	171.7 HV 0.5	86.9 HRB	73.9 µm	73.1 µm	
293	-	163.4 HV 0.5	84.5 HRB	74.7 µm	76.0 µm	
294	-	165.5 HV 0.5	85.1 HRB	75.1 µm	74.6 µm	

Date: 05-25-2023
Tester: Admin
Program: Hardness Map

Point	Distance	Hardness	Converted	Diagonal X	Diagonal Y	Comments
295	-	170.9 HV 0.5	86.6 HRB	73.6 µm	73.7 µm	
296	-	166.7 HV 0.5	85.4 HRB	74.2 µm	75.0 µm	
297	-	167.0 HV 0.5	85.5 HRB	73.0 µm	76.1 µm	
298	-	167.2 HV 0.5	85.6 HRB	73.3 µm	75.6 µm	
299	-	169.5 HV 0.5	86.2 HRB	74.4 µm	73.5 µm	
300	-	172.1 HV 0.5	87.0 HRB	74.7 µm	72.1 µm	
301	-	174.5 HV 0.5	87.6 HRB	75.3 µm	70.5 µm	
302	-	179.7 HV 0.5	88.9 HRB	72.1 µm	71.6 µm	
303	-	178.4 HV 0.5	88.6 HRB	72.7 µm	71.5 µm	
304	-	162.8 HV 0.5	84.3 HRB	76.7 µm	74.3 µm	
305	-	180.2 HV 0.5	89.0 HRB	71.9 µm	71.5 µm	
306	-	168.6 HV 0.5	85.9 HRB	74.1 µm	74.2 µm	
307	-	164.4 HV 0.5	84.8 HRB	73.3 µm	76.9 µm	
308	-	162.2 HV 0.5	84.1 HRB	74.5 µm	76.7 µm	
309	-	158.4 HV 0.5	82.8 HRB	75.5 µm	77.5 µm	
310	-	169.8 HV 0.5	86.3 HRB	74.8 µm	73.0 µm	
311	-	187.2 HV 0.5	90.4 HRB	68.7 µm	72.1 µm	
312	-	168.3 HV 0.5	85.8 HRB	73.7 µm	74.7 µm	
313	-	177.5 HV 0.5	88.4 HRB	70.4 µm	74.2 µm	
314	-	177.0 HV 0.5	88.2 HRB	70.6 µm	74.2 µm	
315	-	178.1 HV 0.5	88.5 HRB	73.3 µm	71.0 µm	
316	-	182.5 HV 0.5	89.5 HRB	73.7 µm	68.8 µm	
317	-	174.8 HV 0.5	87.7 HRB	71.8 µm	73.8 µm	
318	-	196.2 HV 0.5	92.2 HRB	70.4 µm	67.1 µm	
319	-	194.0 HV 0.5	91.8 HRB	66.9 µm	71.4 µm	
320	-	185.5 HV 0.5	90.1 HRB	68.4 µm	73.0 µm	
321	-	189.1 HV 0.5	90.8 HRB	68.6 µm	71.4 µm	
322	-	183.9 HV 0.5	89.8 HRB	72.3 µm	69.7 µm	
323	-	185.5 HV 0.5	90.1 HRB	69.3 µm	72.1 µm	
324	-	180.2 HV 0.5	89.0 HRB	69.8 µm	73.6 µm	
325	-	180.4 HV 0.5	89.1 HRB	71.4 µm	72.0 µm	
326	-	176.8 HV 0.5	88.2 HRB	70.0 µm	74.9 µm	
327	-	169.9 HV 0.5	86.3 HRB	74.7 µm	73.0 µm	
328	-	179.3 HV 0.5	88.8 HRB	70.8 µm	73.1 µm	
329	-	159.5 HV 0.5	83.2 HRB	74.9 µm	77.6 µm	
330	-	169.2 HV 0.5	86.1 HRB	73.4 µm	74.6 µm	
331	-	182.7 HV 0.5	89.5 HRB	70.5 µm	72.0 µm	
332	-	184.2 HV 0.5	89.8 HRB	69.6 µm	72.3 µm	
333	-	167.1 HV 0.5	85.5 HRB	74.5 µm	74.4 µm	

Date: 05-25-2023
Tester: Admin
Program: Hardness Map

Point	Distance	Hardness	Converted	Diagonal X	Diagonal Y	Comments
334	-	166.4 HV 0.5	85.4 HRB	73.1 µm	76.2 µm	
335	-	163.1 HV 0.5	84.4 HRB	75.1 µm	75.7 µm	
336	-	164.4 HV 0.5	84.8 HRB	76.1 µm	74.1 µm	
337	-	170.8 HV 0.5	86.6 HRB	73.4 µm	74.0 µm	
338	-	159.4 HV 0.5	83.1 HRB	76.1 µm	76.4 µm	
339	-	169.0 HV 0.5	86.0 HRB	73.5 µm	74.6 µm	
340	-	171.0 HV 0.5	86.7 HRB	73.9 µm	73.4 µm	
341	-	163.4 HV 0.5	84.5 HRB	75.6 µm	75.1 µm	
342	-	160.6 HV 0.5	83.5 HRB	77.3 µm	74.6 µm	
343	-	172.7 HV 0.5	87.2 HRB	73.1 µm	73.5 µm	
344	-	156.6 HV 0.5	82.2 HRB	77.4 µm	76.5 µm	
345	-	182.4 HV 0.5	89.5 HRB	73.4 µm	69.2 µm	
346	-	163.5 HV 0.5	84.5 HRB	74.4 µm	76.2 µm	
347	-	160.2 HV 0.5	83.4 HRB	76.0 µm	76.1 µm	
348	-	182.1 HV 0.5	89.4 HRB	70.8 µm	72.0 µm	
349	-	172.0 HV 0.5	87.0 HRB	75.0 µm	71.8 µm	
350	-	164.2 HV 0.5	84.7 HRB	76.1 µm	74.2 µm	
351	-	163.1 HV 0.5	84.4 HRB	74.1 µm	76.7 µm	
352	-	166.7 HV 0.5	85.4 HRB	73.1 µm	76.0 µm	
353	-	163.3 HV 0.5	84.4 HRB	75.4 µm	75.2 µm	
354	-	164.5 HV 0.5	84.8 HRB	74.3 µm	75.9 µm	
355	-	165.1 HV 0.5	85.0 HRB	74.9 µm	75.0 µm	
356	-	171.5 HV 0.5	86.8 HRB	74.5 µm	72.6 µm	
357	-	167.2 HV 0.5	85.5 HRB	74.7 µm	74.3 µm	
358	-	164.0 HV 0.5	84.7 HRB	72.1 µm	78.3 µm	
359	-	176.7 HV 0.5	88.2 HRB	71.4 µm	73.5 µm	
360	-	169.6 HV 0.5	86.2 HRB	71.2 µm	76.7 µm	
361	-	169.0 HV 0.5	86.0 HRB	71.1 µm	77.0 µm	
362	-	172.8 HV 0.5	87.2 HRB	71.5 µm	75.0 µm	
363	-	171.3 HV 0.5	86.8 HRB	73.2 µm	74.0 µm	
364	-	176.9 HV 0.5	88.2 HRB	71.6 µm	73.2 µm	
365	-	182.1 HV 0.5	89.4 HRB	71.2 µm	71.5 µm	
366	-	182.2 HV 0.5	89.4 HRB	70.8 µm	71.9 µm	
367	-	180.1 HV 0.5	89.0 HRB	70.5 µm	73.0 µm	
368	-	184.5 HV 0.5	89.9 HRB	69.5 µm	72.3 µm	
369	-	180.2 HV 0.5	89.0 HRB	72.4 µm	71.1 µm	
370	-	171.5 HV 0.5	86.8 HRB	72.5 µm	74.5 µm	
371	-	171.9 HV 0.5	87.0 HRB	73.7 µm	73.2 µm	
372	-	165.8 HV 0.5	85.2 HRB	74.3 µm	75.3 µm	

Date: 05-25-2023
Tester: Admin
Program: Hardness Map

Point	Distance	Hardness	Converted	Diagonal X	Diagonal Y	Comments
373	-	171.8 HV 0.5	86.9 HRB	75.0 µm	71.9 µm	
374	-	163.4 HV 0.5	84.5 HRB	73.4 µm	77.3 µm	
375	-	165.9 HV 0.5	85.2 HRB	74.8 µm	74.8 µm	
376	-	176.5 HV 0.5	88.1 HRB	73.0 µm	72.0 µm	
377	-	164.9 HV 0.5	85.0 HRB	73.7 µm	76.2 µm	
378	-	164.3 HV 0.5	84.8 HRB	75.5 µm	74.8 µm	
379	-	169.5 HV 0.5	86.2 HRB	73.9 µm	74.0 µm	
380	-	172.8 HV 0.5	87.2 HRB	73.2 µm	73.3 µm	
381	-	163.7 HV 0.5	84.6 HRB	74.3 µm	76.2 µm	
382	-	158.7 HV 0.5	82.9 HRB	75.9 µm	77.0 µm	
383	-	164.7 HV 0.5	84.9 HRB	76.3 µm	73.8 µm	
384	-	159.2 HV 0.5	83.1 HRB	76.6 µm	76.0 µm	
385	-	166.4 HV 0.5	85.4 HRB	75.2 µm	74.1 µm	
386	-	164.0 HV 0.5	84.7 HRB	74.7 µm	75.7 µm	
387	-	157.9 HV 0.5	82.6 HRB	75.5 µm	77.8 µm	
388	-	173.8 HV 0.5	87.5 HRB	72.7 µm	73.3 µm	
389	-	171.3 HV 0.5	86.8 HRB	74.0 µm	73.2 µm	
390	-	158.3 HV 0.5	82.8 HRB	76.3 µm	76.8 µm	
391	-	175.0 HV 0.5	87.7 HRB	72.3 µm	73.3 µm	
392	-	175.0 HV 0.5	87.8 HRB	73.5 µm	72.0 µm	
393	-	170.2 HV 0.5	86.4 HRB	73.7 µm	73.9 µm	
394	-	174.4 HV 0.5	87.6 HRB	71.9 µm	73.9 µm	
395	-	163.8 HV 0.5	84.6 HRB	74.8 µm	75.6 µm	
396	-	161.4 HV 0.5	83.8 HRB	76.3 µm	75.2 µm	
397	-	159.3 HV 0.5	83.1 HRB	76.1 µm	76.5 µm	
398	-	165.5 HV 0.5	85.1 HRB	73.7 µm	76.0 µm	
399	-	160.3 HV 0.5	83.4 HRB	73.6 µm	78.5 µm	
400	-	161.8 HV 0.5	83.9 HRB	76.1 µm	75.2 µm	
401	-	166.1 HV 0.5	85.3 HRB	73.8 µm	75.7 µm	
402	-	163.4 HV 0.5	84.5 HRB	74.9 µm	75.8 µm	
403	-	170.0 HV 0.5	86.3 HRB	74.7 µm	73.0 µm	
404	-	167.4 HV 0.5	85.6 HRB	75.9 µm	72.9 µm	
405	-	168.5 HV 0.5	85.9 HRB	73.4 µm	75.0 µm	
406	-	172.2 HV 0.5	87.0 HRB	71.9 µm	74.8 µm	
407	-	174.2 HV 0.5	87.5 HRB	72.9 µm	73.1 µm	
408	-	172.8 HV 0.5	87.2 HRB	73.0 µm	73.5 µm	
409	-	168.9 HV 0.5	86.0 HRB	75.9 µm	72.3 µm	
410	-	189.2 HV 0.5	90.8 HRB	69.6 µm	70.5 µm	
411	-	179.0 HV 0.5	88.7 HRB	71.3 µm	72.6 µm	

Date: 05-25-2023
Tester: Admin
Program: Hardness Map

Point	Distance	Hardness	Converted	Diagonal X	Diagonal Y	Comments
412	-	182.6 HV 0.5	89.5 HRB	71.7 µm	70.9 µm	
413	-	182.2 HV 0.5	89.4 HRB	70.7 µm	72.0 µm	
414	-	175.7 HV 0.5	87.9 HRB	70.6 µm	74.7 µm	
415	-	174.1 HV 0.5	87.5 HRB	72.6 µm	73.3 µm	
416	-	175.2 HV 0.5	87.8 HRB	70.4 µm	75.1 µm	
417	-	169.1 HV 0.5	86.0 HRB	72.6 µm	75.5 µm	
418	-	180.9 HV 0.5	89.2 HRB	71.0 µm	72.2 µm	
419	-	170.8 HV 0.5	86.6 HRB	73.1 µm	74.3 µm	
420	-	166.3 HV 0.5	85.3 HRB	73.7 µm	75.6 µm	
421	-	161.8 HV 0.5	83.9 HRB	74.9 µm	76.5 µm	
422	-	172.6 HV 0.5	87.2 HRB	72.6 µm	73.9 µm	
423	-	172.8 HV 0.5	87.2 HRB	71.3 µm	75.2 µm	
424	-	166.7 HV 0.5	85.4 HRB	73.8 µm	75.3 µm	
425	-	162.8 HV 0.5	84.3 HRB	77.0 µm	74.0 µm	
426	-	166.3 HV 0.5	85.3 HRB	74.3 µm	75.0 µm	
427	-	166.7 HV 0.5	85.4 HRB	75.7 µm	73.4 µm	
428	-	164.6 HV 0.5	84.9 HRB	75.0 µm	75.2 µm	
429	-	177.3 HV 0.5	88.3 HRB	73.4 µm	71.3 µm	
430	-	164.7 HV 0.5	84.9 HRB	73.8 µm	76.2 µm	
431	-	165.1 HV 0.5	85.0 HRB	75.3 µm	74.6 µm	
432	-	165.4 HV 0.5	85.1 HRB	74.4 µm	75.3 µm	
433	-	165.1 HV 0.5	85.0 HRB	75.0 µm	74.9 µm	
434	-	167.8 HV 0.5	85.7 HRB	73.8 µm	74.9 µm	
435	-	170.7 HV 0.5	86.6 HRB	73.3 µm	74.1 µm	
436	-	176.3 HV 0.5	88.1 HRB	72.2 µm	72.9 µm	
437	-	171.0 HV 0.5	86.7 HRB	73.3 µm	74.0 µm	
438	-	176.3 HV 0.5	88.1 HRB	72.8 µm	72.3 µm	
439	-	175.1 HV 0.5	87.8 HRB	72.8 µm	72.7 µm	
440	-	156.7 HV 0.5	82.2 HRB	78.0 µm	75.8 µm	
441	-	165.0 HV 0.5	85.0 HRB	73.1 µm	76.8 µm	
442	-	161.6 HV 0.5	83.9 HRB	74.2 µm	77.3 µm	
443	-	156.3 HV 0.5	82.1 HRB	75.9 µm	78.2 µm	
444	-	161.9 HV 0.5	84.0 HRB	75.2 µm	76.2 µm	
445	-	165.3 HV 0.5	85.1 HRB	73.9 µm	75.9 µm	
446	-	157.5 HV 0.5	82.5 HRB	75.8 µm	77.7 µm	
447	-	163.1 HV 0.5	84.4 HRB	74.6 µm	76.2 µm	
448	-	179.8 HV 0.5	89.0 HRB	71.5 µm	72.1 µm	
449	-	171.0 HV 0.5	86.7 HRB	72.4 µm	74.9 µm	
450	-	160.4 HV 0.5	83.5 HRB	75.0 µm	77.0 µm	

Date: 05-25-2023
Tester: Admin
Program: Hardness Map

Point	Distance	Hardness	Converted	Diagonal X	Diagonal Y	Comments
451	-	174.5 HV 0.5	87.6 HRB	72.3 µm	73.5 µm	
452	-	184.1 HV 0.5	89.8 HRB	71.5 µm	70.4 µm	
453	-	169.4 HV 0.5	86.1 HRB	72.5 µm	75.4 µm	
454	-	163.2 HV 0.5	84.4 HRB	73.4 µm	77.3 µm	
455	-	178.6 HV 0.5	88.6 HRB	71.8 µm	72.3 µm	
456	-	186.8 HV 0.5	90.4 HRB	71.9 µm	69.0 µm	
457	-	181.8 HV 0.5	89.4 HRB	72.0 µm	70.8 µm	
458	-	178.5 HV 0.5	88.6 HRB	71.1 µm	73.1 µm	
459	-	173.0 HV 0.5	87.2 HRB	71.2 µm	75.2 µm	
460	-	178.5 HV 0.5	88.6 HRB	72.1 µm	72.1 µm	
461	-	182.4 HV 0.5	89.5 HRB	70.8 µm	71.8 µm	
462	-	191.3 HV 0.5	91.3 HRB	71.5 µm	67.8 µm	
463	-	191.7 HV 0.5	91.3 HRB	68.7 µm	70.4 µm	
464	-	182.9 HV 0.5	89.6 HRB	71.3 µm	71.1 µm	
465	-	174.4 HV 0.5	87.6 HRB	72.9 µm	72.9 µm	
466	-	180.9 HV 0.5	89.2 HRB	71.7 µm	71.5 µm	
467	-	175.2 HV 0.5	87.8 HRB	72.0 µm	73.5 µm	
468	-	171.5 HV 0.5	86.8 HRB	73.1 µm	74.0 µm	
469	-	169.5 HV 0.5	86.2 HRB	72.4 µm	75.5 µm	
470	-	171.6 HV 0.5	86.9 HRB	73.5 µm	73.5 µm	
471	-	169.6 HV 0.5	86.2 HRB	73.9 µm	74.0 µm	
472	-	182.5 HV 0.5	89.5 HRB	71.2 µm	71.3 µm	
473	-	168.7 HV 0.5	85.9 HRB	74.0 µm	74.3 µm	
474	-	158.5 HV 0.5	82.8 HRB	76.1 µm	76.9 µm	
475	-	171.9 HV 0.5	87.0 HRB	74.6 µm	72.3 µm	
476	-	170.9 HV 0.5	86.6 HRB	74.3 µm	73.0 µm	
477	-	166.8 HV 0.5	85.4 HRB	75.2 µm	73.9 µm	
478	-	160.0 HV 0.5	83.3 HRB	76.4 µm	75.9 µm	
479	-	155.3 HV 0.5	81.8 HRB	73.1 µm	81.4 µm	
480	-	173.7 HV 0.5	87.4 HRB	74.0 µm	72.1 µm	
481	-	180.5 HV 0.5	89.1 HRB	72.6 µm	70.8 µm	
482	-	176.5 HV 0.5	88.1 HRB	73.7 µm	71.3 µm	
483	-	162.2 HV 0.5	84.1 HRB	76.3 µm	74.9 µm	
484	-	167.2 HV 0.5	85.5 HRB	72.3 µm	76.6 µm	
485	-	165.2 HV 0.5	85.1 HRB	72.8 µm	77.0 µm	
486	-	162.3 HV 0.5	84.1 HRB	75.3 µm	75.9 µm	
487	-	168.7 HV 0.5	85.9 HRB	72.9 µm	75.4 µm	
488	-	158.6 HV 0.5	82.9 HRB	77.5 µm	75.4 µm	
489	-	163.5 HV 0.5	84.5 HRB	74.7 µm	75.9 µm	

Date: 05-25-2023
Tester: Admin
Program: Hardness Map

Point	Distance	Hardness	Converted	Diagonal X	Diagonal Y	Comments
490	-	173.5 HV 0.5	87.4 HRB	74.6 µm	71.6 µm	
491	-	180.0 HV 0.5	89.0 HRB	71.4 µm	72.1 µm	
492	-	166.7 HV 0.5	85.4 HRB	72.3 µm	76.8 µm	
493	-	173.4 HV 0.5	87.4 HRB	69.6 µm	76.6 µm	
494	-	175.3 HV 0.5	87.8 HRB	72.0 µm	73.5 µm	
495	-	179.8 HV 0.5	89.0 HRB	71.3 µm	72.3 µm	
496	-	178.1 HV 0.5	88.5 HRB	73.7 µm	70.6 µm	
497	-	179.0 HV 0.5	88.8 HRB	72.5 µm	71.5 µm	
498	-	184.7 HV 0.5	89.9 HRB	70.2 µm	71.5 µm	
499	-	183.9 HV 0.5	89.8 HRB	69.2 µm	72.8 µm	
500	-	184.5 HV 0.5	89.9 HRB	70.6 µm	71.2 µm	
501	-	167.6 HV 0.5	85.6 HRB	75.7 µm	73.0 µm	
502	-	181.9 HV 0.5	89.4 HRB	70.5 µm	72.3 µm	
503	-	177.2 HV 0.5	88.3 HRB	71.0 µm	73.6 µm	
504	-	191.1 HV 0.5	91.2 HRB	69.1 µm	70.2 µm	
505	-	179.3 HV 0.5	88.8 HRB	70.1 µm	73.7 µm	
506	-	168.8 HV 0.5	86.0 HRB	75.3 µm	73.0 µm	
507	-	182.4 HV 0.5	89.5 HRB	69.7 µm	72.9 µm	
508	-	175.4 HV 0.5	87.9 HRB	72.7 µm	72.7 µm	
509	-	176.7 HV 0.5	88.2 HRB	72.2 µm	72.7 µm	
510	-	163.3 HV 0.5	84.4 HRB	75.4 µm	75.2 µm	
511	-	175.7 HV 0.5	87.9 HRB	71.0 µm	74.2 µm	
512	-	171.5 HV 0.5	86.8 HRB	71.2 µm	75.8 µm	
513	-	176.0 HV 0.5	88.0 HRB	71.8 µm	73.4 µm	
514	-	181.6 HV 0.5	89.3 HRB	72.2 µm	70.7 µm	
515	-	171.0 HV 0.5	86.7 HRB	72.2 µm	75.1 µm	
516	-	174.3 HV 0.5	87.6 HRB	74.0 µm	71.9 µm	
517	-	165.8 HV 0.5	85.2 HRB	76.4 µm	73.1 µm	
518	-	167.7 HV 0.5	85.7 HRB	73.5 µm	75.2 µm	
519	-	184.3 HV 0.5	89.9 HRB	71.6 µm	70.3 µm	
520	-	162.7 HV 0.5	84.2 HRB	75.3 µm	75.7 µm	
521	-	177.2 HV 0.5	88.3 HRB	71.6 µm	73.1 µm	
522	-	164.6 HV 0.5	84.9 HRB	74.9 µm	75.2 µm	
523	-	172.6 HV 0.5	87.2 HRB	73.0 µm	73.6 µm	
524	-	162.7 HV 0.5	84.2 HRB	75.2 µm	75.8 µm	
525	-	175.1 HV 0.5	87.8 HRB	73.4 µm	72.1 µm	
526	-	166.7 HV 0.5	85.4 HRB	74.4 µm	74.8 µm	
527	-	168.1 HV 0.5	85.8 HRB	73.1 µm	75.4 µm	
528	-	158.8 HV 0.5	82.9 HRB	75.5 µm	77.3 µm	

Date: 05-25-2023
Tester: Admin
Program: Hardness Map

Point	Distance	Hardness	Converted	Diagonal X	Diagonal Y	Comments
529	-	176.9 HV 0.5	88.2 HRB	73.0 µm	71.7 µm	
530	-	156.6 HV 0.5	82.2 HRB	76.6 µm	77.3 µm	
531	-	157.9 HV 0.5	82.6 HRB	75.8 µm	77.5 µm	
532	-	157.3 HV 0.5	82.4 HRB	76.2 µm	77.3 µm	
533	-	163.8 HV 0.5	84.6 HRB	74.9 µm	75.6 µm	
534	-	151.6 HV 0.5	80.5 HRB	75.5 µm	80.9 µm	
535	-	172.5 HV 0.5	87.1 HRB	73.8 µm	72.8 µm	
536	-	162.8 HV 0.5	84.3 HRB	73.6 µm	77.4 µm	
537	-	161.2 HV 0.5	83.7 HRB	74.4 µm	77.3 µm	
538	-	156.5 HV 0.5	82.2 HRB	77.1 µm	76.9 µm	
539	-	183.9 HV 0.5	89.8 HRB	70.6 µm	71.4 µm	
540	-	164.6 HV 0.5	84.9 HRB	73.6 µm	76.5 µm	
541	-	162.7 HV 0.5	84.2 HRB	74.4 µm	76.6 µm	
542	-	167.7 HV 0.5	85.7 HRB	73.6 µm	75.1 µm	
543	-	166.4 HV 0.5	85.4 HRB	72.5 µm	76.7 µm	
544	-	172.7 HV 0.5	87.2 HRB	73.0 µm	73.5 µm	
545	-	168.7 HV 0.5	85.9 HRB	73.9 µm	74.3 µm	
546	-	180.4 HV 0.5	89.1 HRB	69.9 µm	73.5 µm	
547	-	172.0 HV 0.5	87.0 HRB	70.6 µm	76.2 µm	
548	-	190.2 HV 0.5	91.0 HRB	67.5 µm	72.2 µm	
549	-	193.4 HV 0.5	91.7 HRB	67.8 µm	70.7 µm	
550	-	182.3 HV 0.5	89.5 HRB	68.3 µm	74.3 µm	
551	-	183.4 HV 0.5	89.7 HRB	71.1 µm	71.1 µm	
552	-	190.2 HV 0.5	91.0 HRB	68.4 µm	71.2 µm	
553	-	175.1 HV 0.5	87.8 HRB	70.2 µm	75.3 µm	
554	-	186.9 HV 0.5	90.4 HRB	69.2 µm	71.7 µm	
555	-	181.1 HV 0.5	89.2 HRB	70.7 µm	72.4 µm	
556	-	171.4 HV 0.5	86.8 HRB	72.2 µm	74.9 µm	
557	-	175.3 HV 0.5	87.8 HRB	71.8 µm	73.7 µm	
558	-	177.5 HV 0.5	88.4 HRB	71.2 µm	73.3 µm	
559	-	173.8 HV 0.5	87.5 HRB	71.4 µm	74.7 µm	
560	-	163.9 HV 0.5	84.6 HRB	72.9 µm	77.5 µm	
561	-	174.0 HV 0.5	87.5 HRB	72.0 µm	74.0 µm	
562	-	179.8 HV 0.5	88.9 HRB	71.7 µm	71.9 µm	
563	-	183.7 HV 0.5	89.7 HRB	71.5 µm	70.5 µm	
564	-	182.7 HV 0.5	89.5 HRB	71.1 µm	71.4 µm	
565	-	171.6 HV 0.5	86.9 HRB	73.9 µm	73.1 µm	
566	-	183.4 HV 0.5	89.7 HRB	70.6 µm	71.6 µm	
567	-	185.6 HV 0.5	90.1 HRB	70.9 µm	70.5 µm	

Date: 05-25-2023
Tester: Admin
Program: Hardness Map

Point	Distance	Hardness	Converted	Diagonal X	Diagonal Y	Comments
568	-	181.4 HV 0.5	89.3 HRB	71.1 µm	71.9 µm	
569	-	168.2 HV 0.5	85.8 HRB	74.2 µm	74.3 µm	
570	-	182.8 HV 0.5	89.6 HRB	70.8 µm	71.6 µm	
571	-	179.4 HV 0.5	88.8 HRB	72.0 µm	71.8 µm	
572	-	170.6 HV 0.5	86.5 HRB	73.7 µm	73.7 µm	
573	-	173.5 HV 0.5	87.4 HRB	73.2 µm	73.0 µm	
574	-	164.3 HV 0.5	84.8 HRB	75.4 µm	74.9 µm	
575	-	167.1 HV 0.5	85.5 HRB	75.3 µm	73.7 µm	
576	-	169.1 HV 0.5	86.0 HRB	73.5 µm	74.6 µm	
577	-	160.9 HV 0.5	83.6 HRB	76.6 µm	75.2 µm	
578	-	169.1 HV 0.5	86.0 HRB	73.8 µm	74.3 µm	
579	-	164.2 HV 0.5	84.7 HRB	75.4 µm	74.9 µm	
580	-	165.3 HV 0.5	85.1 HRB	75.2 µm	74.6 µm	
581	-	162.7 HV 0.5	84.2 HRB	74.8 µm	76.2 µm	
582	-	163.7 HV 0.5	84.6 HRB	75.6 µm	74.9 µm	
583	-	155.9 HV 0.5	82.0 HRB	75.5 µm	78.7 µm	
584	-	163.0 HV 0.5	84.3 HRB	74.9 µm	75.9 µm	
585	-	155.1 HV 0.5	81.7 HRB	79.0 µm	75.6 µm	
586	-	172.0 HV 0.5	87.0 HRB	72.0 µm	74.8 µm	
587	-	166.8 HV 0.5	85.4 HRB	72.0 µm	77.1 µm	
588	-	169.0 HV 0.5	86.0 HRB	74.7 µm	73.4 µm	
589	-	164.6 HV 0.5	84.9 HRB	75.0 µm	75.1 µm	
590	-	170.0 HV 0.5	86.3 HRB	71.5 µm	76.2 µm	
591	-	173.8 HV 0.5	87.4 HRB	72.5 µm	73.6 µm	
592	-	183.2 HV 0.5	89.6 HRB	72.1 µm	70.2 µm	
593	-	184.3 HV 0.5	89.9 HRB	71.5 µm	70.4 µm	
594	-	187.3 HV 0.5	90.5 HRB	68.9 µm	71.8 µm	
595	-	182.2 HV 0.5	89.4 HRB	70.0 µm	72.7 µm	
596	-	176.6 HV 0.5	88.2 HRB	71.0 µm	73.9 µm	
597	-	197.5 HV 0.5	92.5 HRB	69.7 µm	67.3 µm	
598	-	198.1 HV 0.5	92.6 HRB	67.7 µm	69.1 µm	
599	-	185.6 HV 0.5	90.1 HRB	70.9 µm	70.5 µm	
600	-	193.3 HV 0.5	91.7 HRB	69.1 µm	69.4 µm	
601	-	185.2 HV 0.5	90.0 HRB	71.1 µm	70.4 µm	
602	-	192.0 HV 0.5	91.4 HRB	70.1 µm	68.9 µm	
603	-	189.3 HV 0.5	90.9 HRB	70.0 µm	69.9 µm	
604	-	189.1 HV 0.5	90.8 HRB	69.8 µm	70.2 µm	
605	-	169.9 HV 0.5	86.3 HRB	73.4 µm	74.4 µm	
606	-	181.0 HV 0.5	89.2 HRB	71.4 µm	71.7 µm	

Date: 05-25-2023
Tester: Admin
Program: Hardness Map

Point	Distance	Hardness	Converted	Diagonal X	Diagonal Y	Comments
607	-	166.6 HV 0.5	85.4 HRB	71.4 µm	77.8 µm	
608	-	175.1 HV 0.5	87.8 HRB	71.4 µm	74.1 µm	
609	-	184.9 HV 0.5	90.0 HRB	70.1 µm	71.5 µm	
610	-	179.5 HV 0.5	88.9 HRB	73.4 µm	70.3 µm	
611	-	174.1 HV 0.5	87.5 HRB	70.0 µm	76.0 µm	
612	-	163.1 HV 0.5	84.4 HRB	76.3 µm	74.5 µm	
613	-	161.0 HV 0.5	83.7 HRB	75.1 µm	76.7 µm	
614	-	167.0 HV 0.5	85.5 HRB	75.2 µm	73.8 µm	
615	-	170.3 HV 0.5	86.4 HRB	71.6 µm	75.9 µm	
616	-	176.9 HV 0.5	88.2 HRB	73.7 µm	71.1 µm	
617	-	163.7 HV 0.5	84.6 HRB	73.7 µm	76.8 µm	
618	-	167.7 HV 0.5	85.7 HRB	76.3 µm	72.4 µm	
619	-	155.8 HV 0.5	81.9 HRB	76.5 µm	77.8 µm	
620	-	156.0 HV 0.5	82.0 HRB	75.0 µm	79.2 µm	
621	-	175.0 HV 0.5	87.7 HRB	73.0 µm	72.6 µm	
622	-	170.4 HV 0.5	86.5 HRB	74.2 µm	73.3 µm	
623	-	180.6 HV 0.5	89.1 HRB	71.6 µm	71.7 µm	
624	-	166.6 HV 0.5	85.4 HRB	74.8 µm	74.4 µm	
625	-	156.6 HV 0.5	82.2 HRB	78.3 µm	75.6 µm	
626	-	174.6 HV 0.5	87.7 HRB	71.5 µm	74.2 µm	
627	-	163.7 HV 0.5	84.6 HRB	76.2 µm	74.3 µm	
628	-	174.5 HV 0.5	87.6 HRB	71.5 µm	74.3 µm	
629	-	184.4 HV 0.5	89.9 HRB	69.5 µm	72.3 µm	
630	-	182.9 HV 0.5	89.6 HRB	71.4 µm	71.0 µm	
631	-	179.7 HV 0.5	88.9 HRB	69.6 µm	74.1 µm	
632	-	165.7 HV 0.5	85.2 HRB	74.4 µm	75.2 µm	
633	-	179.0 HV 0.5	88.8 HRB	72.0 µm	71.9 µm	
634	-	180.0 HV 0.5	89.0 HRB	69.6 µm	74.0 µm	
635	-	185.7 HV 0.5	90.1 HRB	69.9 µm	71.4 µm	
636	-	178.7 HV 0.5	88.7 HRB	72.5 µm	71.6 µm	
637	-	176.7 HV 0.5	88.2 HRB	71.9 µm	73.0 µm	
638	-	178.6 HV 0.5	88.7 HRB	69.3 µm	74.8 µm	
639	-	183.4 HV 0.5	89.7 HRB	70.7 µm	71.5 µm	
640	-	190.5 HV 0.5	91.1 HRB	69.3 µm	70.3 µm	
641	-	195.3 HV 0.5	92.1 HRB	66.7 µm	71.1 µm	
642	-	203.0 HV 0.5	93.6 HRB	68.1 µm	67.1 µm	
643	-	185.1 HV 0.5	90.0 HRB	72.0 µm	69.6 µm	
644	-	199.9 HV 0.5	93.0 HRB	67.8 µm	68.4 µm	
645	-	201.5 HV 0.5	93.3 HRB	68.5 µm	67.1 µm	

Date: 05-25-2023
Tester: Admin
Program: Hardness Map

Point	Distance	Hardness	Converted	Diagonal X	Diagonal Y	Comments
646	-	201.3 HV 0.5	93.3 HRB	65.9 µm	69.8 µm	
647	-	200.8 HV 0.5	93.2 HRB	67.8 µm	68.1 µm	
648	-	185.6 HV 0.5	90.1 HRB	70.2 µm	71.2 µm	
649	-	207.1 HV 0.5	94.4 HRB	66.1 µm	67.7 µm	
650	-	189.7 HV 0.5	90.9 HRB	70.1 µm	69.8 µm	
651	-	199.7 HV 0.5	92.9 HRB	67.7 µm	68.6 µm	
652	-	191.8 HV 0.5	91.4 HRB	71.8 µm	67.2 µm	
653	-	190.9 HV 0.5	91.2 HRB	71.5 µm	67.9 µm	
654	-	182.4 HV 0.5	89.5 HRB	68.3 µm	74.3 µm	
655	-	187.5 HV 0.5	90.5 HRB	71.2 µm	69.4 µm	
656	-	197.3 HV 0.5	92.5 HRB	68.6 µm	68.5 µm	
657	-	197.1 HV 0.5	92.4 HRB	69.7 µm	67.5 µm	
658	-	164.5 HV 0.5	84.8 HRB	74.1 µm	76.1 µm	
659	-	155.9 HV 0.5	82.0 HRB	76.9 µm	77.3 µm	
660	-	161.5 HV 0.5	83.8 HRB	74.1 µm	77.4 µm	
661	-	161.0 HV 0.5	83.7 HRB	75.1 µm	76.7 µm	
662	-	163.5 HV 0.5	84.5 HRB	73.8 µm	76.8 µm	
663	-	182.1 HV 0.5	89.4 HRB	71.1 µm	71.7 µm	
664	-	181.0 HV 0.5	89.2 HRB	71.0 µm	72.2 µm	
665	-	176.6 HV 0.5	88.2 HRB	70.7 µm	74.2 µm	
666	-	173.6 HV 0.5	87.4 HRB	71.0 µm	75.2 µm	
667	-	188.6 HV 0.5	90.7 HRB	69.7 µm	70.5 µm	
668	-	187.8 HV 0.5	90.6 HRB	68.7 µm	71.8 µm	
669	-	183.0 HV 0.5	89.6 HRB	69.9 µm	72.5 µm	
670	-	177.5 HV 0.5	88.4 HRB	70.9 µm	73.6 µm	
671	-	174.1 HV 0.5	87.5 HRB	73.9 µm	72.0 µm	
672	-	190.8 HV 0.5	91.2 HRB	69.0 µm	70.4 µm	
673	-	184.4 HV 0.5	89.9 HRB	72.0 µm	69.8 µm	
674	-	179.6 HV 0.5	88.9 HRB	71.9 µm	71.8 µm	
675	-	174.3 HV 0.5	87.6 HRB	72.4 µm	73.4 µm	
676	-	173.0 HV 0.5	87.2 HRB	73.7 µm	72.7 µm	
677	-	199.3 HV 0.5	92.9 HRB	66.3 µm	70.1 µm	
678	-	188.4 HV 0.5	90.7 HRB	69.3 µm	71.0 µm	
679	-	190.4 HV 0.5	91.1 HRB	69.8 µm	69.8 µm	
680	-	180.7 HV 0.5	89.1 HRB	70.9 µm	72.3 µm	
681	-	180.6 HV 0.5	89.1 HRB	72.8 µm	70.5 µm	
682	-	191.3 HV 0.5	91.3 HRB	70.4 µm	68.9 µm	
683	-	189.7 HV 0.5	90.9 HRB	69.9 µm	70.0 µm	
684	-	179.5 HV 0.5	88.9 HRB	72.5 µm	71.3 µm	

Date: 05-25-2023
Tester: Admin
Program: Hardness Map

Point	Distance	Hardness	Converted	Diagonal X	Diagonal Y	Comments
685	-	180.6 HV 0.5	89.1 HRB	69.4 µm	73.9 µm	
686	-	206.1 HV 0.5	94.2 HRB	67.1 µm	67.0 µm	
687	-	193.4 HV 0.5	91.7 HRB	69.6 µm	68.9 µm	
688	-	203.9 HV 0.5	93.8 HRB	66.9 µm	68.0 µm	
689	-	198.3 HV 0.5	92.7 HRB	68.0 µm	68.7 µm	
690	-	191.9 HV 0.5	91.4 HRB	66.4 µm	72.6 µm	
691	-	198.4 HV 0.5	92.7 HRB	67.5 µm	69.2 µm	
692	-	174.8 HV 0.5	87.7 HRB	73.1 µm	72.6 µm	
693	-	190.8 HV 0.5	91.2 HRB	70.0 µm	69.4 µm	
694	-	174.5 HV 0.5	87.6 HRB	73.6 µm	72.2 µm	
695	-	189.6 HV 0.5	90.9 HRB	70.4 µm	69.5 µm	
696	-	189.3 HV 0.5	90.9 HRB	69.4 µm	70.6 µm	
697	-	178.0 HV 0.5	88.5 HRB	72.5 µm	71.9 µm	
698	-	193.3 HV 0.5	91.7 HRB	66.7 µm	71.8 µm	
699	-	186.5 HV 0.5	90.3 HRB	71.5 µm	69.5 µm	
700	-	176.5 HV 0.5	88.1 HRB	72.3 µm	72.7 µm	
701	-	191.7 HV 0.5	91.3 HRB	70.1 µm	69.0 µm	
702	-	203.5 HV 0.5	93.7 HRB	68.2 µm	66.8 µm	
703	-	186.4 HV 0.5	90.3 HRB	72.2 µm	68.9 µm	
704	-	178.6 HV 0.5	88.7 HRB	72.2 µm	71.9 µm	
705	-	160.2 HV 0.5	83.4 HRB	74.9 µm	77.2 µm	
706	-	162.6 HV 0.5	84.2 HRB	76.9 µm	74.1 µm	
707	-	164.6 HV 0.5	84.9 HRB	76.6 µm	73.5 µm	
708	-	167.5 HV 0.5	85.6 HRB	74.5 µm	74.3 µm	
709	-	158.1 HV 0.5	82.7 HRB	76.5 µm	76.7 µm	
710	-	179.0 HV 0.5	88.7 HRB	72.4 µm	71.6 µm	
711	-	167.8 HV 0.5	85.7 HRB	74.5 µm	74.2 µm	
712	-	180.7 HV 0.5	89.1 HRB	71.7 µm	71.5 µm	
713	-	199.1 HV 0.5	92.8 HRB	67.7 µm	68.8 µm	
714	-	173.5 HV 0.5	87.4 HRB	73.8 µm	72.4 µm	
715	-	175.6 HV 0.5	87.9 HRB	71.7 µm	73.6 µm	
716	-	171.2 HV 0.5	86.7 HRB	74.0 µm	73.2 µm	
717	-	190.7 HV 0.5	91.1 HRB	69.1 µm	70.4 µm	
718	-	179.7 HV 0.5	88.9 HRB	70.4 µm	73.2 µm	
719	-	175.4 HV 0.5	87.9 HRB	71.7 µm	73.7 µm	
720	-	177.8 HV 0.5	88.4 HRB	72.3 µm	72.1 µm	
721	-	183.9 HV 0.5	89.8 HRB	70.4 µm	71.6 µm	
722	-	179.3 HV 0.5	88.8 HRB	69.9 µm	73.9 µm	
723	-	187.5 HV 0.5	90.5 HRB	70.6 µm	70.1 µm	

Date: 05-25-2023
Tester: Admin
Program: Hardness Map

Point	Distance	Hardness	Converted	Diagonal X	Diagonal Y	Comments
724	-	194.9 HV 0.5	92.0 HRB	69.2 µm	68.7 µm	
725	-	189.9 HV 0.5	91.0 HRB	69.5 µm	70.2 µm	
726	-	193.6 HV 0.5	91.7 HRB	68.1 µm	70.3 µm	
727	-	196.4 HV 0.5	92.3 HRB	67.8 µm	69.6 µm	
728	-	197.7 HV 0.5	92.5 HRB	67.3 µm	69.6 µm	
729	-	167.9 HV 0.5	85.7 HRB	69.4 µm	79.2 µm	
730	-	187.1 HV 0.5	90.4 HRB	70.3 µm	70.5 µm	
731	-	193.9 HV 0.5	91.8 HRB	67.7 µm	70.6 µm	
732	-	210.1 HV 0.5	95.0 HRB	65.4 µm	67.5 µm	
733	-	205.8 HV 0.5	94.2 HRB	67.5 µm	66.7 µm	
734	-	198.7 HV 0.5	92.7 HRB	68.9 µm	67.7 µm	
735	-	192.6 HV 0.5	91.5 HRB	67.7 µm	71.1 µm	
736	-	204.7 HV 0.5	93.9 HRB	67.4 µm	67.2 µm	
737	-	197.4 HV 0.5	92.5 HRB	68.4 µm	68.7 µm	
738	-	189.8 HV 0.5	91.0 HRB	70.5 µm	69.3 µm	
739	-	191.9 HV 0.5	91.4 HRB	69.0 µm	70.0 µm	
740	-	194.7 HV 0.5	91.9 HRB	66.8 µm	71.2 µm	
741	-	201.1 HV 0.5	93.2 HRB	68.0 µm	67.8 µm	
742	-	189.9 HV 0.5	91.0 HRB	69.6 µm	70.1 µm	
743	-	176.7 HV 0.5	88.2 HRB	74.1 µm	70.7 µm	
744	-	189.4 HV 0.5	90.9 HRB	69.8 µm	70.2 µm	
745	-	188.7 HV 0.5	90.7 HRB	69.6 µm	70.6 µm	
746	-	179.9 HV 0.5	89.0 HRB	71.8 µm	71.8 µm	
747	-	184.5 HV 0.5	89.9 HRB	70.3 µm	71.4 µm	
748	-	183.9 HV 0.5	89.8 HRB	70.4 µm	71.7 µm	
749	-	197.1 HV 0.5	92.4 HRB	68.2 µm	69.0 µm	
750	-	196.1 HV 0.5	92.2 HRB	68.2 µm	69.3 µm	
751	-	156.9 HV 0.5	82.3 HRB	75.0 µm	78.7 µm	
752	-	171.6 HV 0.5	86.9 HRB	73.9 µm	73.1 µm	
753	-	169.5 HV 0.5	86.2 HRB	73.3 µm	74.6 µm	
754	-	175.4 HV 0.5	87.8 HRB	72.3 µm	73.1 µm	
755	-	162.5 HV 0.5	84.2 HRB	75.0 µm	76.1 µm	
756	-	169.5 HV 0.5	86.2 HRB	74.3 µm	73.6 µm	
757	-	183.5 HV 0.5	89.7 HRB	71.1 µm	71.1 µm	
758	-	176.6 HV 0.5	88.2 HRB	70.1 µm	74.8 µm	
759	-	201.8 HV 0.5	93.4 HRB	67.2 µm	68.4 µm	
760	-	188.3 HV 0.5	90.7 HRB	69.1 µm	71.2 µm	
761	-	182.2 HV 0.5	89.4 HRB	70.6 µm	72.0 µm	
762	-	161.1 HV 0.5	83.7 HRB	74.0 µm	77.8 µm	

Date: 05-25-2023
Tester: Admin
Program: Hardness Map

Point	Distance	Hardness	Converted	Diagonal X	Diagonal Y	Comments
763	-	173.3 HV 0.5	87.3 HRB	74.0 µm	72.3 µm	
764	-	170.1 HV 0.5	86.4 HRB	73.8 µm	73.9 µm	
765	-	179.8 HV 0.5	88.9 HRB	72.2 µm	71.4 µm	
766	-	188.5 HV 0.5	90.7 HRB	69.3 µm	71.0 µm	
767	-	182.4 HV 0.5	89.5 HRB	70.9 µm	71.7 µm	
768	-	190.1 HV 0.5	91.0 HRB	70.2 µm	69.4 µm	
769	-	191.3 HV 0.5	91.3 HRB	69.9 µm	69.3 µm	
770	-	186.7 HV 0.5	90.3 HRB	70.0 µm	71.0 µm	
771	-	193.3 HV 0.5	91.7 HRB	69.0 µm	69.5 µm	
772	-	197.9 HV 0.5	92.6 HRB	68.7 µm	68.2 µm	
773	-	186.7 HV 0.5	90.3 HRB	70.2 µm	70.7 µm	
774	-	192.5 HV 0.5	91.5 HRB	68.5 µm	70.3 µm	
775	-	185.7 HV 0.5	90.1 HRB	70.2 µm	71.1 µm	
776	-	191.0 HV 0.5	91.2 HRB	68.6 µm	70.7 µm	
777	-	194.9 HV 0.5	92.0 HRB	68.3 µm	69.6 µm	
778	-	194.0 HV 0.5	91.8 HRB	65.4 µm	72.9 µm	
779	-	191.1 HV 0.5	91.2 HRB	68.5 µm	70.8 µm	
780	-	183.1 HV 0.5	89.6 HRB	69.5 µm	72.8 µm	
781	-	196.3 HV 0.5	92.3 HRB	70.5 µm	67.0 µm	
782	-	188.6 HV 0.5	90.7 HRB	68.8 µm	71.4 µm	
783	-	200.9 HV 0.5	93.2 HRB	68.4 µm	67.4 µm	
784	-	203.3 HV 0.5	93.7 HRB	66.5 µm	68.6 µm	
785	-	205.2 HV 0.5	94.0 HRB	67.2 µm	67.2 µm	
786	-	195.5 HV 0.5	92.1 HRB	69.2 µm	68.5 µm	
787	-	176.9 HV 0.5	88.2 HRB	72.2 µm	72.6 µm	
788	-	182.6 HV 0.5	89.5 HRB	71.0 µm	71.5 µm	
789	-	188.5 HV 0.5	90.7 HRB	69.3 µm	71.0 µm	
790	-	191.3 HV 0.5	91.3 HRB	69.6 µm	69.6 µm	
791	-	194.4 HV 0.5	91.9 HRB	67.8 µm	70.3 µm	
792	-	177.6 HV 0.5	88.4 HRB	69.6 µm	74.9 µm	
793	-	193.1 HV 0.5	91.6 HRB	70.0 µm	68.6 µm	
794	-	182.9 HV 0.5	89.6 HRB	70.5 µm	71.9 µm	
795	-	192.1 HV 0.5	91.4 HRB	68.7 µm	70.2 µm	
796	-	189.4 HV 0.5	90.9 HRB	70.1 µm	69.9 µm	
797	-	177.4 HV 0.5	88.4 HRB	72.6 µm	72.0 µm	
798	-	172.9 HV 0.5	87.2 HRB	72.3 µm	74.1 µm	
799	-	169.2 HV 0.5	86.1 HRB	74.2 µm	73.9 µm	
800	-	171.4 HV 0.5	86.8 HRB	72.1 µm	75.0 µm	
801	-	176.5 HV 0.5	88.1 HRB	73.8 µm	71.2 µm	

Date: 05-25-2023
Tester: Admin
Program: Hardness Map

Point	Distance	Hardness	Converted	Diagonal X	Diagonal Y	Comments
802	-	189.5 HV 0.5	90.9 HRB	70.3 µm	69.6 µm	
803	-	191.3 HV 0.5	91.3 HRB	69.5 µm	69.7 µm	
804	-	182.9 HV 0.5	89.6 HRB	70.5 µm	71.9 µm	
805	-	206.2 HV 0.5	94.2 HRB	66.4 µm	67.7 µm	
806	-	183.6 HV 0.5	89.7 HRB	71.0 µm	71.2 µm	
807	-	179.3 HV 0.5	88.8 HRB	71.5 µm	72.3 µm	
808	-	173.4 HV 0.5	87.3 HRB	74.6 µm	71.7 µm	
809	-	169.4 HV 0.5	86.1 HRB	73.8 µm	74.2 µm	
810	-	189.4 HV 0.5	90.9 HRB	68.6 µm	71.4 µm	
811	-	157.9 HV 0.5	82.6 HRB	82.0 µm	71.3 µm	
812	-	177.2 HV 0.5	88.3 HRB	71.1 µm	73.6 µm	
813	-	187.9 HV 0.5	90.6 HRB	70.5 µm	70.0 µm	
814	-	173.0 HV 0.5	87.3 HRB	71.9 µm	74.5 µm	
815	-	184.9 HV 0.5	90.0 HRB	69.6 µm	72.1 µm	
816	-	178.5 HV 0.5	88.6 HRB	72.9 µm	71.3 µm	
817	-	191.4 HV 0.5	91.3 HRB	67.6 µm	71.6 µm	
818	-	217.0 HV 0.5	96.2 HRB	65.3 µm	65.4 µm	
819	-	217.7 HV 0.5	96.3 HRB	64.7 µm	65.8 µm	
820	-	218.2 HV 0.5	96.4 HRB	65.4 µm	64.9 µm	
821	-	203.8 HV 0.5	93.8 HRB	67.7 µm	67.2 µm	
822	-	192.3 HV 0.5	91.5 HRB	68.3 µm	70.5 µm	
823	-	192.4 HV 0.5	91.5 HRB	69.4 µm	69.4 µm	
824	-	197.8 HV 0.5	92.6 HRB	65.8 µm	71.2 µm	
825	-	239.2 HV 0.5	99.9 HRB	61.8 µm	62.7 µm	
826	-	221.1 HV 0.5	96.8 HRB	64.1 µm	65.4 µm	

Hardness Map

ADV PN 100794 3:00 o'clock

Date: 05-24-2023
Tester: Admin
Program: Hardness Map

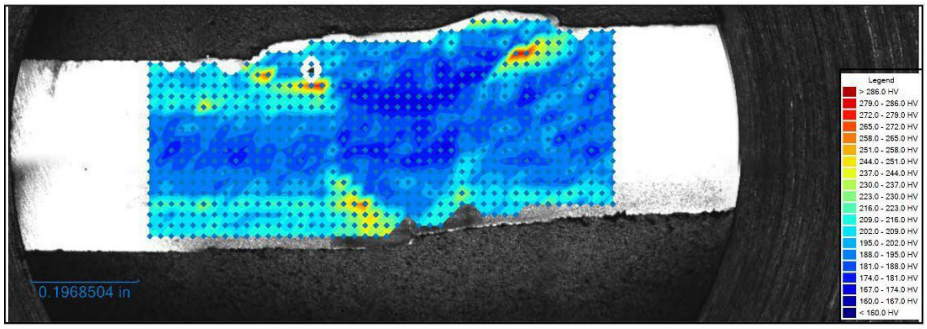

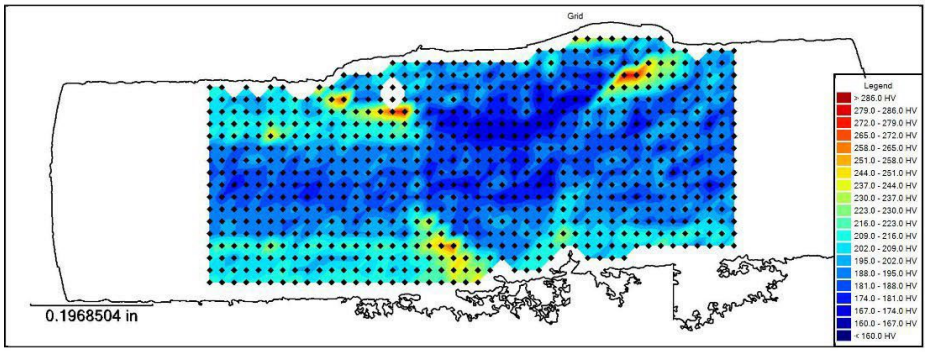

Date: 05-24-2023
Tester: Admin
Program: Hardness Map

Grid

Mean	Minimum	Maximum	Range	Std. deviation
197.2	166.4	283.7	117.3	16.9

Hardness Trace

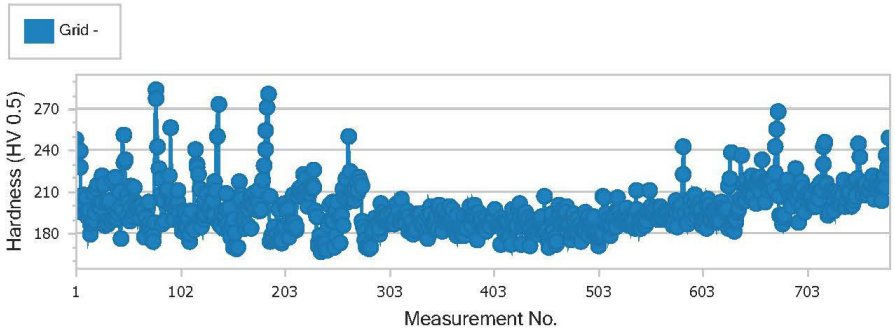

Point	Distance	Hardness	Converted	Diagonal X	Diagonal Y	Comments
1	-	247.8 HV 0.5	-	61.4 µm	61.0 µm	
2	-	241.5 HV 0.5	-	61.2 µm	62.8 µm	
3	-	227.3 HV 0.5	97.9 HRB	63.9 µm	63.8 µm	
4	-	239.9 HV 0.5	100.0 HRB	61.2 µm	63.2 µm	
5	-	227.3 HV 0.5	97.9 HRB	63.6 µm	64.1 µm	
6	-	195.1 HV 0.5	92.0 HRB	68.3 µm	69.5 µm	
7	-	207.3 HV 0.5	94.5 HRB	67.1 µm	66.7 µm	
8	-	198.9 HV 0.5	92.8 HRB	69.3 µm	67.3 µm	
9	-	200.6 HV 0.5	93.1 HRB	67.4 µm	68.6 µm	
10	-	205.4 HV 0.5	94.1 HRB	67.4 µm	67.0 µm	
11	-	191.6 HV 0.5	91.3 HRB	68.7 µm	70.5 µm	
12	-	196.0 HV 0.5	92.2 HRB	68.0 µm	69.5 µm	
13	-	196.0 HV 0.5	92.2 HRB	67.7 µm	69.8 µm	
14	-	179.1 HV 0.5	88.8 HRB	72.8 µm	71.1 µm	
15	-	186.5 HV 0.5	90.3 HRB	71.5 µm	69.5 µm	
16	-	188.1 HV 0.5	90.6 HRB	70.6 µm	69.8 µm	
17	-	208.3 HV 0.5	94.7 HRB	66.8 µm	66.7 µm	
18	-	188.1 HV 0.5	90.6 HRB	69.6 µm	70.8 µm	
19	-	195.3 HV 0.5	92.1 HRB	68.9 µm	68.9 µm	
20	-	211.4 HV 0.5	95.2 HRB	66.1 µm	66.3 µm	
21	-	215.4 HV 0.5	95.9 HRB	64.9 µm	66.4 µm	

Date: 05-24-2023
Tester: Admin
Program: Hardness Map

Point	Distance	Hardness	Converted	Diagonal X	Diagonal Y	Comments
22	-	200.5 HV 0.5	93.1 HRB	66.8 µm	69.2 µm	
23	-	197.6 HV 0.5	92.5 HRB	66.5 µm	70.5 µm	
24	-	198.3 HV 0.5	92.7 HRB	67.4 µm	69.4 µm	
25	-	221.8 HV 0.5	97.0 HRB	64.5 µm	64.8 µm	
26	-	202.5 HV 0.5	93.5 HRB	66.4 µm	68.9 µm	
27	-	215.4 HV 0.5	95.9 HRB	65.2 µm	66.0 µm	
28	-	188.2 HV 0.5	90.6 HRB	70.9 µm	69.5 µm	
29	-	185.0 HV 0.5	90.0 HRB	71.2 µm	70.4 µm	
30	-	202.5 HV 0.5	93.5 HRB	66.8 µm	68.6 µm	
31	-	186.4 HV 0.5	90.3 HRB	69.6 µm	71.4 µm	
32	-	201.6 HV 0.5	93.3 HRB	67.1 µm	68.6 µm	
33	-	203.4 HV 0.5	93.7 HRB	66.8 µm	68.3 µm	
34	-	188.2 HV 0.5	90.6 HRB	67.7 µm	72.7 µm	
35	-	193.0 HV 0.5	91.6 HRB	69.7 µm	68.9 µm	
36	-	218.7 HV 0.5	96.4 HRB	65.8 µm	64.4 µm	
37	-	190.7 HV 0.5	91.1 HRB	68.7 µm	70.8 µm	
38	-	220.7 HV 0.5	96.8 HRB	65.8 µm	63.9 µm	
39	-	189.8 HV 0.5	91.0 HRB	68.7 µm	71.1 µm	
40	-	190.8 HV 0.5	91.2 HRB	67.7 µm	71.7 µm	
41	-	194.2 HV 0.5	91.8 HRB	69.6 µm	68.6 µm	
42	-	197.9 HV 0.5	92.6 HRB	69.0 µm	67.9 µm	
43	-	209.3 HV 0.5	94.9 HRB	67.7 µm	65.4 µm	
44	-	176.0 HV 0.5	88.0 HRB	73.1 µm	72.1 µm	
45	-	195.8 HV 0.5	92.2 HRB	68.7 µm	68.9 µm	
46	-	250.7 HV 0.5	-	62.0 µm	59.6 µm	
47	-	231.3 HV 0.5	98.5 HRB	64.1 µm	62.5 µm	
48	-	232.7 HV 0.5	98.8 HRB	62.4 µm	63.8 µm	
49	-	207.0 HV 0.5	94.4 HRB	68.2 µm	65.6 µm	
50	-	191.6 HV 0.5	91.3 HRB	69.5 µm	69.7 µm	
51	-	202.4 HV 0.5	93.5 HRB	68.1 µm	67.3 µm	
52	-	188.4 HV 0.5	90.7 HRB	67.1 µm	73.2 µm	
53	-	197.8 HV 0.5	92.6 HRB	66.8 µm	70.2 µm	
54	-	214.0 HV 0.5	95.7 HRB	65.3 µm	66.4 µm	
55	-	191.6 HV 0.5	91.3 HRB	69.6 µm	69.5 µm	
56	-	195.1 HV 0.5	92.0 HRB	68.3 µm	69.5 µm	
57	-	213.4 HV 0.5	95.6 HRB	65.8 µm	66.0 µm	
58	-	202.5 HV 0.5	93.5 HRB	68.0 µm	67.3 µm	
59	-	195.6 HV 0.5	92.1 HRB	67.7 µm	70.0 µm	
60	-	196.9 HV 0.5	92.4 HRB	69.9 µm	67.3 µm	

Date: 05-24-2023
Tester: Admin
Program: Hardness Map

Point	Distance	Hardness	Converted	Diagonal X	Diagonal Y	Comments
61	-	200.6 HV 0.5	93.1 HRB	66.8 µm	69.2 µm	
62	-	190.9 HV 0.5	91.2 HRB	70.2 µm	69.1 µm	
63	-	196.9 HV 0.5	92.4 HRB	68.3 µm	68.9 µm	
64	-	200.6 HV 0.5	93.1 HRB	67.1 µm	68.9 µm	
65	-	195.6 HV 0.5	92.1 HRB	69.2 µm	68.5 µm	
66	-	177.1 HV 0.5	88.3 HRB	70.1 µm	74.6 µm	
67	-	191.6 HV 0.5	91.3 HRB	69.3 µm	69.8 µm	
68	-	191.2 HV 0.5	91.2 HRB	69.9 µm	69.4 µm	
69	-	184.0 HV 0.5	89.8 HRB	70.9 µm	71.1 µm	
70	-	186.6 HV 0.5	90.3 HRB	70.5 µm	70.5 µm	
71	-	202.5 HV 0.5	93.5 HRB	68.0 µm	67.3 µm	
72	-	182.2 HV 0.5	89.4 HRB	72.4 µm	70.2 µm	
73	-	180.7 HV 0.5	89.1 HRB	72.1 µm	71.1 µm	
74	-	178.4 HV 0.5	88.6 HRB	74.0 µm	70.2 µm	
75	-	173.9 HV 0.5	87.5 HRB	72.4 µm	73.7 µm	
76	-	187.3 HV 0.5	90.5 HRB	70.2 µm	70.5 µm	
77	-	283.7 HV 0.5	-	57.3 µm	57.0 µm	
78	-	277.4 HV 0.5	-	59.5 µm	56.1 µm	
79	-	242.3 HV 0.5	-	61.2 µm	62.5 µm	
80	-	226.3 HV 0.5	97.7 HRB	63.6 µm	64.4 µm	
81	-	218.7 HV 0.5	96.5 HRB	65.1 µm	65.1 µm	
82	-	207.8 HV 0.5	94.6 HRB	67.6 µm	66.0 µm	
83	-	186.1 HV 0.5	90.2 HRB	70.4 µm	70.7 µm	
84	-	203.9 HV 0.5	93.8 HRB	67.5 µm	67.3 µm	
85	-	203.5 HV 0.5	93.7 HRB	68.7 µm	66.4 µm	
86	-	188.9 HV 0.5	90.8 HRB	70.0 µm	70.2 µm	
87	-	209.8 HV 0.5	95.0 HRB	66.7 µm	66.2 µm	
88	-	210.6 HV 0.5	95.1 HRB	66.9 µm	65.9 µm	
89	-	211.5 HV 0.5	95.3 HRB	65.1 µm	67.3 µm	
90	-	221.0 HV 0.5	96.8 HRB	65.6 µm	63.9 µm	
91	-	200.6 HV 0.5	93.1 HRB	65.9 µm	70.1 µm	
92	-	256.3 HV 0.5	-	59.5 µm	60.8 µm	
93	-	202.5 HV 0.5	93.5 HRB	67.4 µm	67.9 µm	
94	-	189.8 HV 0.5	91.0 HRB	68.7 µm	71.1 µm	
95	-	200.0 HV 0.5	93.0 HRB	67.6 µm	68.6 µm	
96	-	197.8 HV 0.5	92.6 HRB	67.4 µm	69.5 µm	
97	-	201.6 HV 0.5	93.3 HRB	68.0 µm	67.6 µm	
98	-	Deleted	-	-	-	
99	-	202.5 HV 0.5	93.5 HRB	67.4 µm	67.9 µm	

Date: 05-24-2023
Tester: Admin
Program: Hardness Map

Point	Distance	Hardness	Converted	Diagonal X	Diagonal Y	Comments
100	-	210.3 HV 0.5	95.1 HRB	67.1 µm	65.7 µm	
101	-	195.1 HV 0.5	92.0 HRB	69.9 µm	67.9 µm	
102	-	187.3 HV 0.5	90.5 HRB	70.6 µm	70.2 µm	
103	-	181.5 HV 0.5	89.3 HRB	70.9 µm	72.1 µm	
104	-	184.0 HV 0.5	89.8 HRB	70.9 µm	71.1 µm	
105	-	196.0 HV 0.5	92.2 HRB	69.0 µm	68.6 µm	
106	-	193.3 HV 0.5	91.7 HRB	68.7 µm	69.8 µm	
107	-	184.3 HV 0.5	89.9 HRB	72.0 µm	69.8 µm	
108	-	184.8 HV 0.5	90.0 HRB	69.9 µm	71.8 µm	
109	-	190.6 HV 0.5	91.1 HRB	69.3 µm	70.2 µm	
110	-	173.7 HV 0.5	87.4 HRB	73.1 µm	73.0 µm	
111	-	179.1 HV 0.5	88.8 HRB	72.4 µm	71.4 µm	
112	-	196.0 HV 0.5	92.2 HRB	68.0 µm	69.5 µm	
113	-	184.8 HV 0.5	90.0 HRB	69.9 µm	71.8 µm	
114	-	183.0 HV 0.5	89.6 HRB	71.8 µm	70.6 µm	
115	-	182.4 HV 0.5	89.5 HRB	71.2 µm	71.4 µm	
116	-	240.6 HV 0.5	-	62.1 µm	62.0 µm	
117	-	229.7 HV 0.5	98.3 HRB	62.2 µm	64.8 µm	
118	-	228.2 HV 0.5	98.0 HRB	64.0 µm	63.4 µm	
119	-	222.3 HV 0.5	97.1 HRB	63.7 µm	65.4 µm	
120	-	211.4 HV 0.5	95.2 HRB	66.1 µm	66.4 µm	
121	-	190.5 HV 0.5	91.1 HRB	69.1 µm	70.5 µm	
122	-	184.1 HV 0.5	89.8 HRB	72.4 µm	69.5 µm	
123	-	191.8 HV 0.5	91.4 HRB	68.7 µm	70.4 µm	
124	-	203.2 HV 0.5	93.6 HRB	65.2 µm	69.9 µm	
125	-	190.1 HV 0.5	91.0 HRB	68.5 µm	71.2 µm	
126	-	192.4 HV 0.5	91.5 HRB	70.6 µm	68.3 µm	
127	-	210.1 HV 0.5	95.0 HRB	64.9 µm	67.9 µm	
128	-	207.3 HV 0.5	94.5 HRB	66.6 µm	67.2 µm	
129	-	198.0 HV 0.5	92.6 HRB	67.4 µm	69.5 µm	
130	-	197.8 HV 0.5	92.6 HRB	68.6 µm	68.3 µm	
131	-	192.5 HV 0.5	91.5 HRB	72.1 µm	66.7 µm	
132	-	204.7 HV 0.5	93.9 HRB	67.9 µm	66.7 µm	
133	-	203.6 HV 0.5	93.7 HRB	67.7 µm	67.2 µm	
134	-	217.1 HV 0.5	96.2 HRB	66.7 µm	64.0 µm	
135	-	193.3 HV 0.5	91.7 HRB	68.2 µm	70.4 µm	
136	-	210.7 HV 0.5	95.1 HRB	65.0 µm	67.7 µm	
137	-	249.8 HV 0.5	-	60.6 µm	61.2 µm	
138	-	273.1 HV 0.5	-	59.0 µm	57.5 µm	

Date: 05-24-2023
Tester: Admin
Program: Hardness Map

Point	Distance	Hardness	Converted	Diagonal X	Diagonal Y	Comments
139	-	187.3 HV 0.5	90.5 HRB	71.8 µm	68.9 µm	
140	-	185.6 HV 0.5	90.1 HRB	69.0 µm	72.4 µm	
141	-	193.3 HV 0.5	91.7 HRB	67.4 µm	71.1 µm	
142	-	Deleted	-	-	-	
143	-	195.1 HV 0.5	92.0 HRB	69.0 µm	68.9 µm	
144	-	183.5 HV 0.5	89.7 HRB	70.2 µm	71.9 µm	
145	-	192.5 HV 0.5	91.5 HRB	68.7 µm	70.2 µm	
146	-	196.9 HV 0.5	92.4 HRB	67.7 µm	69.5 µm	
147	-	208.3 HV 0.5	94.7 HRB	68.0 µm	65.4 µm	
148	-	186.5 HV 0.5	90.3 HRB	70.2 µm	70.8 µm	
149	-	198.6 HV 0.5	92.7 HRB	67.4 µm	69.2 µm	
150	-	180.7 HV 0.5	89.1 HRB	71.8 µm	71.4 µm	
151	-	177.2 HV 0.5	88.3 HRB	72.8 µm	71.9 µm	
152	-	185.7 HV 0.5	90.1 HRB	70.5 µm	70.8 µm	
153	-	189.8 HV 0.5	91.0 HRB	69.3 µm	70.5 µm	
154	-	169.6 HV 0.5	86.2 HRB	74.0 µm	73.9 µm	
155	-	179.9 HV 0.5	89.0 HRB	71.8 µm	71.8 µm	
156	-	168.6 HV 0.5	85.9 HRB	74.3 µm	74.0 µm	
157	-	168.4 HV 0.5	85.8 HRB	74.1 µm	74.3 µm	
158	-	170.0 HV 0.5	86.3 HRB	73.7 µm	74.0 µm	
159	-	216.6 HV 0.5	96.1 HRB	65.4 µm	65.4 µm	
160	-	208.0 HV 0.5	94.6 HRB	67.7 µm	65.9 µm	
161	-	204.5 HV 0.5	93.9 HRB	67.4 µm	67.3 µm	
162	-	189.3 HV 0.5	90.9 HRB	68.5 µm	71.4 µm	
163	-	189.7 HV 0.5	90.9 HRB	68.1 µm	71.8 µm	
164	-	186.1 HV 0.5	90.2 HRB	72.1 µm	69.1 µm	
165	-	183.7 HV 0.5	89.7 HRB	67.9 µm	74.1 µm	
166	-	199.2 HV 0.5	92.8 HRB	69.0 µm	67.4 µm	
167	-	185.0 HV 0.5	90.0 HRB	70.2 µm	71.4 µm	
168	-	196.5 HV 0.5	92.3 HRB	66.2 µm	71.2 µm	
169	-	201.0 HV 0.5	93.2 HRB	66.9 µm	68.9 µm	
170	-	182.9 HV 0.5	89.6 HRB	70.6 µm	71.9 µm	
171	-	205.7 HV 0.5	94.1 HRB	66.3 µm	68.0 µm	
172	-	201.8 HV 0.5	93.4 HRB	67.0 µm	68.6 µm	
173	-	208.5 HV 0.5	94.7 HRB	65.8 µm	67.5 µm	
174	-	202.7 HV 0.5	93.5 HRB	66.5 µm	68.8 µm	
175	-	197.4 HV 0.5	92.5 HRB	67.9 µm	69.1 µm	
176	-	204.3 HV 0.5	93.9 HRB	66.1 µm	68.6 µm	
177	-	202.6 HV 0.5	93.5 HRB	66.8 µm	68.5 µm	

Date: 05-24-2023
Tester: Admin
Program: Hardness Map

Point	Distance	Hardness	Converted	Diagonal X	Diagonal Y	Comments
178	-	211.0 HV 0.5	95.2 HRB	65.9 µm	66.7 µm	
179	-	195.4 HV 0.5	92.1 HRB	68.3 µm	69.5 µm	
180	-	197.5 HV 0.5	92.5 HRB	67.6 µm	69.5 µm	
181	-	217.9 HV 0.5	96.3 HRB	66.1 µm	64.3 µm	
182	-	217.8 HV 0.5	96.3 HRB	66.1 µm	64.4 µm	
183	-	228.9 HV 0.5	98.2 HRB	62.2 µm	65.1 µm	
184	-	240.2 HV 0.5	-	61.9 µm	62.3 µm	
185	-	254.0 HV 0.5	-	59.8 µm	61.0 µm	
186	-	271.4 HV 0.5	-	59.4 µm	57.5 µm	
187	-	280.7 HV 0.5	-	57.8 µm	57.1 µm	
188	-	206.5 HV 0.5	94.3 HRB	66.1 µm	67.9 µm	
189	-	173.5 HV 0.5	87.4 HRB	72.9 µm	73.3 µm	
190	-	177.6 HV 0.5	88.4 HRB	71.8 µm	72.7 µm	
191	-	174.7 HV 0.5	87.7 HRB	73.1 µm	72.6 µm	
192	-	177.4 HV 0.5	88.3 HRB	71.6 µm	73.0 µm	
193	-	184.7 HV 0.5	89.9 HRB	71.1 µm	70.6 µm	
194	-	178.3 HV 0.5	88.6 HRB	71.8 µm	72.4 µm	
195	-	176.0 HV 0.5	88.0 HRB	71.8 µm	73.3 µm	
196	-	179.1 HV 0.5	88.8 HRB	70.6 µm	73.3 µm	
197	-	196.9 HV 0.5	92.4 HRB	68.7 µm	68.6 µm	
198	-	176.8 HV 0.5	88.2 HRB	72.8 µm	72.1 µm	
199	-	172.9 HV 0.5	87.2 HRB	73.2 µm	73.2 µm	
200	-	175.2 HV 0.5	87.8 HRB	71.8 µm	73.7 µm	
201	-	182.7 HV 0.5	89.5 HRB	69.0 µm	73.4 µm	
202	-	201.0 HV 0.5	93.2 HRB	68.0 µm	67.9 µm	
203	-	185.4 HV 0.5	90.1 HRB	69.3 µm	72.2 µm	
204	-	198.6 HV 0.5	92.7 HRB	69.3 µm	67.4 µm	
205	-	196.5 HV 0.5	92.3 HRB	67.7 µm	69.7 µm	
206	-	177.4 HV 0.5	88.3 HRB	72.4 µm	72.3 µm	
207	-	188.4 HV 0.5	90.7 HRB	69.9 µm	70.4 µm	
208	-	185.6 HV 0.5	90.1 HRB	69.6 µm	71.7 µm	
209	-	187.6 HV 0.5	90.5 HRB	69.6 µm	71.0 µm	
210	-	185.6 HV 0.5	90.1 HRB	69.3 µm	72.1 µm	
211	-	207.4 HV 0.5	94.5 HRB	66.3 µm	67.4 µm	
212	-	187.4 HV 0.5	90.5 HRB	71.2 µm	69.4 µm	
213	-	182.6 HV 0.5	89.5 HRB	71.3 µm	71.3 µm	
214	-	184.2 HV 0.5	89.8 HRB	71.7 µm	70.2 µm	
215	-	206.8 HV 0.5	94.4 HRB	65.9 µm	68.1 µm	
216	-	209.3 HV 0.5	94.9 HRB	66.4 µm	66.7 µm	

Date: 05-24-2023
Tester: Admin
Program: Hardness Map

Point	Distance	Hardness	Converted	Diagonal X	Diagonal Y	Comments
217	-	211.5 HV 0.5	95.2 HRB	66.4 µm	66.0 µm	
218	-	212.4 HV 0.5	95.4 HRB	65.3 µm	66.9 µm	
219	-	209.1 HV 0.5	94.8 HRB	65.3 µm	67.8 µm	
220	-	222.0 HV 0.5	97.0 HRB	64.7 µm	64.6 µm	
221	-	206.7 HV 0.5	94.3 HRB	66.1 µm	67.9 µm	
222	-	218.9 HV 0.5	96.5 HRB	65.9 µm	64.3 µm	
223	-	208.1 HV 0.5	94.6 HRB	67.9 µm	65.6 µm	
224	-	211.6 HV 0.5	95.3 HRB	66.1 µm	66.3 µm	
225	-	198.9 HV 0.5	92.8 HRB	68.7 µm	67.9 µm	
226	-	208.4 HV 0.5	94.7 HRB	68.5 µm	64.9 µm	
227	-	212.4 HV 0.5	95.4 HRB	65.5 µm	66.6 µm	
228	-	214.4 HV 0.5	95.7 HRB	65.6 µm	65.9 µm	
229	-	215.2 HV 0.5	95.9 HRB	65.3 µm	65.9 µm	
230	-	213.0 HV 0.5	95.5 HRB	65.7 µm	66.2 µm	
231	-	226.0 HV 0.5	97.7 HRB	64.5 µm	63.6 µm	
232	-	196.0 HV 0.5	92.2 HRB	68.7 µm	68.9 µm	
233	-	192.1 HV 0.5	91.4 HRB	70.2 µm	68.7 µm	
234	-	173.0 HV 0.5	87.2 HRB	72.8 µm	73.7 µm	
235	-	170.5 HV 0.5	86.5 HRB	73.7 µm	73.8 µm	
236	-	178.2 HV 0.5	88.6 HRB	72.1 µm	72.1 µm	
237	-	166.4 HV 0.5	85.4 HRB	72.4 µm	76.8 µm	
238	-	173.0 HV 0.5	87.2 HRB	72.8 µm	73.7 µm	
239	-	171.3 HV 0.5	86.8 HRB	73.2 µm	74.0 µm	
240	-	170.6 HV 0.5	86.5 HRB	74.1 µm	73.3 µm	
241	-	172.2 HV 0.5	87.1 HRB	73.1 µm	73.7 µm	
242	-	167.0 HV 0.5	85.5 HRB	74.0 µm	75.0 µm	
243	-	167.6 HV 0.5	85.7 HRB	75.4 µm	73.3 µm	
244	-	188.9 HV 0.5	90.8 HRB	69.6 µm	70.5 µm	
245	-	185.0 HV 0.5	90.0 HRB	70.9 µm	70.7 µm	
246	-	200.2 HV 0.5	93.0 HRB	68.7 µm	67.4 µm	
247	-	188.8 HV 0.5	90.8 HRB	70.4 µm	69.8 µm	
248	-	202.3 HV 0.5	93.5 HRB	67.9 µm	67.5 µm	
249	-	188.9 HV 0.5	90.8 HRB	70.7 µm	69.4 µm	
250	-	169.7 HV 0.5	86.2 HRB	73.3 µm	74.5 µm	
251	-	177.8 HV 0.5	88.4 HRB	67.8 µm	76.6 µm	
252	-	195.9 HV 0.5	92.2 HRB	69.1 µm	68.5 µm	
253	-	202.5 HV 0.5	93.5 HRB	66.7 µm	68.7 µm	
254	-	190.7 HV 0.5	91.1 HRB	67.7 µm	71.7 µm	
255	-	192.1 HV 0.5	91.4 HRB	70.9 µm	68.1 µm	

Date: 05-24-2023
Tester: Admin
Program: Hardness Map

Point	Distance	Hardness	Converted	Diagonal X	Diagonal Y	Comments
256	-	172.5 HV 0.5	87.1 HRB	71.8 µm	74.9 µm	
257	-	193.2 HV 0.5	91.6 HRB	69.3 µm	69.3 µm	
258	-	185.2 HV 0.5	90.0 HRB	70.6 µm	70.9 µm	
259	-	211.4 HV 0.5	95.2 HRB	66.1 µm	66.4 µm	
260	-	205.3 HV 0.5	94.1 HRB	67.8 µm	66.6 µm	
261	-	219.1 HV 0.5	96.5 HRB	65.2 µm	64.9 µm	
262	-	202.4 HV 0.5	93.5 HRB	67.2 µm	68.2 µm	
263	-	204.7 HV 0.5	93.9 HRB	67.8 µm	66.8 µm	
264	-	249.6 HV 0.5	-	59.6 µm	62.3 µm	
265	-	224.3 HV 0.5	97.4 HRB	64.5 µm	64.1 µm	
266	-	205.0 HV 0.5	94.0 HRB	65.0 µm	69.5 µm	
267	-	210.9 HV 0.5	95.1 HRB	67.0 µm	65.6 µm	
268	-	204.5 HV 0.5	93.9 HRB	65.2 µm	69.5 µm	
269	-	203.0 HV 0.5	93.6 HRB	65.2 µm	69.9 µm	
270	-	211.9 HV 0.5	95.3 HRB	66.3 µm	66.0 µm	
271	-	217.0 HV 0.5	96.2 HRB	65.9 µm	64.8 µm	
272	-	208.9 HV 0.5	94.8 HRB	66.2 µm	67.1 µm	
273	-	210.3 HV 0.5	95.0 HRB	63.9 µm	69.0 µm	
274	-	219.9 HV 0.5	96.7 HRB	64.4 µm	65.4 µm	
275	-	216.7 HV 0.5	96.1 HRB	67.1 µm	63.7 µm	
276	-	214.3 HV 0.5	95.7 HRB	64.9 µm	66.7 µm	
277	-	188.1 HV 0.5	90.6 HRB	69.1 µm	71.3 µm	
278	-	184.7 HV 0.5	89.9 HRB	71.3 µm	70.4 µm	
279	-	181.3 HV 0.5	89.3 HRB	71.3 µm	71.8 µm	
280	-	174.6 HV 0.5	87.6 HRB	74.7 µm	71.0 µm	
281	-	169.7 HV 0.5	86.2 HRB	71.4 µm	76.4 µm	
282	-	169.4 HV 0.5	86.1 HRB	74.6 µm	73.3 µm	
283	-	171.5 HV 0.5	86.8 HRB	74.5 µm	72.6 µm	
284	-	168.2 HV 0.5	85.8 HRB	74.6 µm	73.9 µm	
285	-	169.3 HV 0.5	86.1 HRB	73.4 µm	74.6 µm	
286	-	182.3 HV 0.5	89.5 HRB	70.9 µm	71.7 µm	
287	-	179.6 HV 0.5	88.9 HRB	71.9 µm	71.8 µm	
288	-	181.5 HV 0.5	89.3 HRB	71.5 µm	71.4 µm	
289	-	190.6 HV 0.5	91.1 HRB	69.2 µm	70.3 µm	
290	-	186.4 HV 0.5	90.3 HRB	70.3 µm	70.8 µm	
291	-	185.9 HV 0.5	90.2 HRB	69.7 µm	71.5 µm	
292	-	185.7 HV 0.5	90.1 HRB	69.3 µm	72.0 µm	
293	-	179.4 HV 0.5	88.8 HRB	71.9 µm	71.9 µm	
294	-	183.1 HV 0.5	89.6 HRB	69.6 µm	72.7 µm	

Date: 05-24-2023
Tester: Admin
Program: Hardness Map

Point	Distance	Hardness	Converted	Diagonal X	Diagonal Y	Comments
295	-	201.0 HV 0.5	93.2 HRB	68.6 µm	67.2 µm	
296	-	194.4 HV 0.5	91.9 HRB	68.3 µm	69.8 µm	
297	-	191.5 HV 0.5	91.3 HRB	68.7 µm	70.5 µm	
298	-	188.9 HV 0.5	90.8 HRB	68.7 µm	71.4 µm	
299	-	190.7 HV 0.5	91.1 HRB	69.3 µm	70.2 µm	
300	-	187.4 HV 0.5	90.5 HRB	68.1 µm	72.6 µm	
301	-	193.1 HV 0.5	91.6 HRB	68.4 µm	70.2 µm	
302	-	186.4 HV 0.5	90.3 HRB	71.6 µm	69.5 µm	
303	-	187.4 HV 0.5	90.5 HRB	69.6 µm	71.1 µm	
304	-	193.2 HV 0.5	91.6 HRB	68.0 µm	70.5 µm	
305	-	188.0 HV 0.5	90.6 HRB	68.7 µm	71.8 µm	
306	-	187.0 HV 0.5	90.4 HRB	70.1 µm	70.7 µm	
307	-	190.1 HV 0.5	91.0 HRB	70.5 µm	69.2 µm	
308	-	186.5 HV 0.5	90.3 HRB	69.5 µm	71.6 µm	
309	-	189.7 HV 0.5	90.9 HRB	68.2 µm	71.7 µm	
310	-	201.1 HV 0.5	93.2 HRB	67.0 µm	68.8 µm	
311	-	195.6 HV 0.5	92.1 HRB	68.6 µm	69.1 µm	
312	-	195.8 HV 0.5	92.2 HRB	67.8 µm	69.8 µm	
313	-	190.0 HV 0.5	91.0 HRB	68.6 µm	71.1 µm	
314	-	204.8 HV 0.5	94.0 HRB	66.5 µm	68.1 µm	
315	-	187.1 HV 0.5	90.4 HRB	69.7 µm	71.1 µm	
316	-	192.1 HV 0.5	91.4 HRB	67.9 µm	71.0 µm	
317	-	190.0 HV 0.5	91.0 HRB	70.9 µm	68.8 µm	
318	-	192.5 HV 0.5	91.5 HRB	70.2 µm	68.6 µm	
319	-	186.6 HV 0.5	90.3 HRB	69.2 µm	71.8 µm	
320	-	195.6 HV 0.5	92.1 HRB	68.3 µm	69.4 µm	
321	-	191.4 HV 0.5	91.3 HRB	70.1 µm	69.1 µm	
322	-	181.7 HV 0.5	89.3 HRB	71.0 µm	71.9 µm	
323	-	183.5 HV 0.5	89.7 HRB	71.5 µm	70.6 µm	
324	-	188.1 HV 0.5	90.6 HRB	70.2 µm	70.2 µm	
325	-	179.0 HV 0.5	88.8 HRB	72.1 µm	71.8 µm	
326	-	182.6 HV 0.5	89.5 HRB	71.1 µm	71.4 µm	
327	-	182.4 HV 0.5	89.5 HRB	71.5 µm	71.1 µm	
328	-	180.9 HV 0.5	89.2 HRB	71.4 µm	71.8 µm	
329	-	181.8 HV 0.5	89.4 HRB	71.4 µm	71.4 µm	
330	-	193.8 HV 0.5	91.8 HRB	68.4 µm	69.9 µm	
331	-	193.0 HV 0.5	91.6 HRB	70.0 µm	68.6 µm	
332	-	189.3 HV 0.5	90.9 HRB	69.8 µm	70.2 µm	
333	-	193.8 HV 0.5	91.8 HRB	68.1 µm	70.2 µm	

Date: 05-24-2023
Tester: Admin
Program: Hardness Map

Point	Distance	Hardness	Converted	Diagonal X	Diagonal Y	Comments
334	-	185.6 HV 0.5	90.1 HRB	70.3 µm	71.1 µm	
335	-	183.8 HV 0.5	89.8 HRB	70.8 µm	71.3 µm	
336	-	186.4 HV 0.5	90.3 HRB	70.7 µm	70.3 µm	
337	-	189.2 HV 0.5	90.8 HRB	70.1 µm	69.9 µm	
338	-	178.9 HV 0.5	88.7 HRB	69.8 µm	74.2 µm	
339	-	193.2 HV 0.5	91.6 HRB	67.8 µm	70.7 µm	
340	-	175.9 HV 0.5	88.0 HRB	72.0 µm	73.2 µm	
341	-	184.5 HV 0.5	89.9 HRB	70.2 µm	71.6 µm	
342	-	199.4 HV 0.5	92.9 HRB	67.1 µm	69.2 µm	
343	-	193.6 HV 0.5	91.7 HRB	69.3 µm	69.1 µm	
344	-	186.9 HV 0.5	90.4 HRB	70.7 µm	70.2 µm	
345	-	184.5 HV 0.5	89.9 HRB	71.2 µm	70.6 µm	
346	-	182.4 HV 0.5	89.5 HRB	70.5 µm	72.1 µm	
347	-	187.5 HV 0.5	90.5 HRB	70.0 µm	70.7 µm	
348	-	191.3 HV 0.5	91.3 HRB	68.9 µm	70.3 µm	
349	-	181.7 HV 0.5	89.3 HRB	71.1 µm	71.8 µm	
350	-	199.1 HV 0.5	92.8 HRB	67.1 µm	69.4 µm	
351	-	200.1 HV 0.5	93.0 HRB	67.9 µm	68.2 µm	
352	-	192.3 HV 0.5	91.5 HRB	68.5 µm	70.4 µm	
353	-	194.3 HV 0.5	91.9 HRB	68.2 µm	70.0 µm	
354	-	181.2 HV 0.5	89.2 HRB	70.2 µm	72.9 µm	
355	-	197.3 HV 0.5	92.5 HRB	69.0 µm	68.2 µm	
356	-	192.1 HV 0.5	91.4 HRB	69.0 µm	70.0 µm	
357	-	187.8 HV 0.5	90.6 HRB	70.0 µm	70.6 µm	
358	-	189.9 HV 0.5	91.0 HRB	68.2 µm	71.6 µm	
359	-	195.4 HV 0.5	92.1 HRB	68.0 µm	69.7 µm	
360	-	188.1 HV 0.5	90.6 HRB	70.2 µm	70.2 µm	
361	-	199.0 HV 0.5	92.8 HRB	67.1 µm	69.4 µm	
362	-	190.7 HV 0.5	91.1 HRB	69.7 µm	69.7 µm	
363	-	192.4 HV 0.5	91.5 HRB	68.8 µm	70.0 µm	
364	-	196.6 HV 0.5	92.3 HRB	68.3 µm	69.0 µm	
365	-	181.2 HV 0.5	89.2 HRB	72.8 µm	70.3 µm	
366	-	183.8 HV 0.5	89.8 HRB	70.9 µm	71.1 µm	
367	-	177.9 HV 0.5	88.5 HRB	73.6 µm	70.8 µm	
368	-	193.2 HV 0.5	91.6 HRB	69.4 µm	69.1 µm	
369	-	183.6 HV 0.5	89.7 HRB	71.5 µm	70.6 µm	
370	-	181.6 HV 0.5	89.3 HRB	71.8 µm	71.1 µm	
371	-	181.5 HV 0.5	89.3 HRB	70.9 µm	72.1 µm	
372	-	178.6 HV 0.5	88.7 HRB	72.2 µm	71.9 µm	

Date: 05-24-2023
Tester: Admin
Program: Hardness Map

Point	Distance	Hardness	Converted	Diagonal X	Diagonal Y	Comments
373	-	177.6 HV 0.5	88.4 HRB	72.8 µm	71.8 µm	
374	-	192.6 HV 0.5	91.5 HRB	67.9 µm	70.9 µm	
375	-	177.9 HV 0.5	88.5 HRB	73.1 µm	71.3 µm	
376	-	183.7 HV 0.5	89.7 HRB	70.6 µm	71.5 µm	
377	-	182.3 HV 0.5	89.5 HRB	71.8 µm	70.8 µm	
378	-	182.8 HV 0.5	89.6 HRB	71.8 µm	70.6 µm	
379	-	192.4 HV 0.5	91.5 HRB	67.9 µm	70.9 µm	
380	-	198.9 HV 0.5	92.8 HRB	70.0 µm	66.6 µm	
381	-	193.3 HV 0.5	91.7 HRB	69.2 µm	69.3 µm	
382	-	185.1 HV 0.5	90.0 HRB	70.1 µm	71.4 µm	
383	-	191.8 HV 0.5	91.4 HRB	67.7 µm	71.4 µm	
384	-	199.7 HV 0.5	92.9 HRB	68.2 µm	68.1 µm	
385	-	193.7 HV 0.5	91.7 HRB	68.9 µm	69.4 µm	
386	-	190.6 HV 0.5	91.1 HRB	68.1 µm	71.4 µm	
387	-	174.9 HV 0.5	87.7 HRB	71.5 µm	74.1 µm	
388	-	186.5 HV 0.5	90.3 HRB	70.0 µm	71.1 µm	
389	-	195.2 HV 0.5	92.0 HRB	68.5 µm	69.3 µm	
390	-	191.0 HV 0.5	91.2 HRB	68.7 µm	70.7 µm	
391	-	184.6 HV 0.5	89.9 HRB	70.4 µm	71.3 µm	
392	-	188.3 HV 0.5	90.7 HRB	70.1 µm	70.2 µm	
393	-	183.7 HV 0.5	89.7 HRB	70.6 µm	71.5 µm	
394	-	182.6 HV 0.5	89.5 HRB	70.4 µm	72.1 µm	
395	-	180.6 HV 0.5	89.1 HRB	71.3 µm	72.0 µm	
396	-	190.2 HV 0.5	91.0 HRB	67.6 µm	72.1 µm	
397	-	186.8 HV 0.5	90.4 HRB	69.3 µm	71.6 µm	
398	-	187.8 HV 0.5	90.6 HRB	68.2 µm	72.4 µm	
399	-	185.4 HV 0.5	90.1 HRB	70.6 µm	70.8 µm	
400	-	184.4 HV 0.5	89.9 HRB	69.3 µm	72.5 µm	
401	-	191.2 HV 0.5	91.2 HRB	68.3 µm	70.9 µm	
402	-	190.7 HV 0.5	91.1 HRB	67.6 µm	71.8 µm	
403	-	192.2 HV 0.5	91.4 HRB	68.7 µm	70.2 µm	
404	-	196.8 HV 0.5	92.4 HRB	67.4 µm	69.8 µm	
405	-	185.8 HV 0.5	90.2 HRB	69.6 µm	71.7 µm	
406	-	185.4 HV 0.5	90.1 HRB	70.6 µm	70.9 µm	
407	-	186.2 HV 0.5	90.2 HRB	70.8 µm	70.3 µm	
408	-	188.0 HV 0.5	90.6 HRB	70.2 µm	70.3 µm	
409	-	172.0 HV 0.5	87.0 HRB	72.6 µm	74.2 µm	
410	-	190.6 HV 0.5	91.1 HRB	69.3 µm	70.2 µm	
411	-	187.3 HV 0.5	90.5 HRB	69.9 µm	70.8 µm	

Date: 05-24-2023
Tester: Admin
Program: Hardness Map

Point	Distance	Hardness	Converted	Diagonal X	Diagonal Y	Comments
412	-	186.1 HV 0.5	90.2 HRB	70.2 µm	70.9 µm	
413	-	185.6 HV 0.5	90.1 HRB	70.2 µm	71.1 µm	
414	-	178.8 HV 0.5	88.7 HRB	71.3 µm	72.8 µm	
415	-	187.1 HV 0.5	90.4 HRB	70.6 µm	70.2 µm	
416	-	176.9 HV 0.5	88.2 HRB	71.5 µm	73.3 µm	
417	-	188.1 HV 0.5	90.6 HRB	69.9 µm	70.5 µm	
418	-	177.8 HV 0.5	88.5 HRB	72.3 µm	72.1 µm	
419	-	172.0 HV 0.5	87.0 HRB	73.4 µm	73.4 µm	
420	-	196.9 HV 0.5	92.4 HRB	68.9 µm	68.3 µm	
421	-	188.1 HV 0.5	90.6 HRB	70.6 µm	69.8 µm	
422	-	182.8 HV 0.5	89.6 HRB	71.9 µm	70.6 µm	
423	-	190.5 HV 0.5	91.1 HRB	69.6 µm	70.0 µm	
424	-	184.2 HV 0.5	89.8 HRB	70.6 µm	71.3 µm	
425	-	185.4 HV 0.5	90.1 HRB	69.7 µm	71.8 µm	
426	-	197.2 HV 0.5	92.4 HRB	68.2 µm	68.9 µm	
427	-	191.6 HV 0.5	91.3 HRB	69.7 µm	69.4 µm	
428	-	200.8 HV 0.5	93.2 HRB	67.1 µm	68.8 µm	
429	-	171.8 HV 0.5	86.9 HRB	77.1 µm	69.8 µm	
430	-	185.7 HV 0.5	90.1 HRB	68.5 µm	72.8 µm	
431	-	193.5 HV 0.5	91.7 HRB	69.4 µm	69.0 µm	
432	-	188.7 HV 0.5	90.7 HRB	68.5 µm	71.7 µm	
433	-	195.1 HV 0.5	92.0 HRB	69.6 µm	68.3 µm	
434	-	185.6 HV 0.5	90.1 HRB	69.6 µm	71.8 µm	
435	-	188.4 HV 0.5	90.7 HRB	70.8 µm	69.5 µm	
436	-	190.4 HV 0.5	91.1 HRB	70.6 µm	68.9 µm	
437	-	170.8 HV 0.5	86.6 HRB	77.5 µm	69.8 µm	
438	-	182.1 HV 0.5	89.4 HRB	72.6 µm	70.1 µm	
439	-	183.1 HV 0.5	89.6 HRB	71.5 µm	70.9 µm	
440	-	189.2 HV 0.5	90.8 HRB	69.5 µm	70.6 µm	
441	-	186.7 HV 0.5	90.3 HRB	70.4 µm	70.6 µm	
442	-	179.9 HV 0.5	89.0 HRB	69.3 µm	74.3 µm	
443	-	181.0 HV 0.5	89.2 HRB	70.1 µm	73.0 µm	
444	-	178.7 HV 0.5	88.7 HRB	70.3 µm	73.8 µm	
445	-	188.6 HV 0.5	90.7 HRB	69.1 µm	71.1 µm	
446	-	182.4 HV 0.5	89.5 HRB	68.8 µm	73.8 µm	
447	-	188.7 HV 0.5	90.7 HRB	68.6 µm	71.6 µm	
448	-	183.4 HV 0.5	89.7 HRB	71.1 µm	71.1 µm	
449	-	191.7 HV 0.5	91.3 HRB	68.9 µm	70.2 µm	
450	-	183.0 HV 0.5	89.6 HRB	69.7 µm	72.6 µm	

Date: 05-24-2023
Tester: Admin
Program: Hardness Map

Point	Distance	Hardness	Converted	Diagonal X	Diagonal Y	Comments
451	-	183.3 HV 0.5	89.7 HRB	71.6 µm	70.6 µm	
452	-	206.1 HV 0.5	94.2 HRB	67.5 µm	66.6 µm	
453	-	181.6 HV 0.5	89.3 HRB	70.5 µm	72.4 µm	
454	-	174.7 HV 0.5	87.7 HRB	72.4 µm	73.3 µm	
455	-	174.9 HV 0.5	87.7 HRB	72.1 µm	73.5 µm	
456	-	169.1 HV 0.5	86.0 HRB	73.9 µm	74.2 µm	
457	-	178.7 HV 0.5	88.7 HRB	71.4 µm	72.7 µm	
458	-	191.1 HV 0.5	91.2 HRB	69.0 µm	70.3 µm	
459	-	194.1 HV 0.5	91.8 HRB	68.6 µm	69.6 µm	
460	-	181.4 HV 0.5	89.3 HRB	71.0 µm	72.0 µm	
461	-	176.9 HV 0.5	88.2 HRB	73.5 µm	71.2 µm	
462	-	172.1 HV 0.5	87.0 HRB	72.6 µm	74.2 µm	
463	-	173.6 HV 0.5	87.4 HRB	72.7 µm	73.4 µm	
464	-	189.7 HV 0.5	90.9 HRB	70.1 µm	69.7 µm	
465	-	194.4 HV 0.5	91.9 HRB	69.0 µm	69.2 µm	
466	-	200.7 HV 0.5	93.1 HRB	67.4 µm	68.6 µm	
467	-	186.4 HV 0.5	90.3 HRB	70.6 µm	70.5 µm	
468	-	197.4 HV 0.5	92.5 HRB	70.1 µm	67.0 µm	
469	-	194.2 HV 0.5	91.8 HRB	68.4 µm	69.8 µm	
470	-	187.2 HV 0.5	90.4 HRB	70.4 µm	70.3 µm	
471	-	188.8 HV 0.5	90.8 HRB	69.1 µm	71.0 µm	
472	-	199.1 HV 0.5	92.8 HRB	68.0 µm	68.4 µm	
473	-	194.8 HV 0.5	92.0 HRB	67.4 µm	70.6 µm	
474	-	187.9 HV 0.5	90.6 HRB	70.5 µm	70.0 µm	
475	-	186.6 HV 0.5	90.3 HRB	69.7 µm	71.2 µm	
476	-	174.4 HV 0.5	87.6 HRB	73.2 µm	72.6 µm	
477	-	180.1 HV 0.5	89.0 HRB	70.1 µm	73.4 µm	
478	-	191.9 HV 0.5	91.4 HRB	68.6 µm	70.4 µm	
479	-	193.9 HV 0.5	91.8 HRB	66.3 µm	72.0 µm	
480	-	181.6 HV 0.5	89.3 HRB	71.2 µm	71.7 µm	
481	-	189.0 HV 0.5	90.8 HRB	69.5 µm	70.6 µm	
482	-	180.6 HV 0.5	89.1 HRB	70.3 µm	73.0 µm	
483	-	191.0 HV 0.5	91.2 HRB	67.7 µm	71.6 µm	
484	-	179.9 HV 0.5	89.0 HRB	70.9 µm	72.7 µm	
485	-	185.1 HV 0.5	90.0 HRB	69.1 µm	72.5 µm	
486	-	182.7 HV 0.5	89.5 HRB	71.1 µm	71.4 µm	
487	-	173.5 HV 0.5	87.4 HRB	69.0 µm	77.2 µm	
488	-	182.8 HV 0.5	89.6 HRB	69.0 µm	73.4 µm	
489	-	181.5 HV 0.5	89.3 HRB	71.4 µm	71.6 µm	

Date: 05-24-2023
Tester: Admin
Program: Hardness Map

Point	Distance	Hardness	Converted	Diagonal X	Diagonal Y	Comments
490	-	182.7 HV 0.5	89.5 HRB	70.7 µm	71.8 µm	
491	-	194.5 HV 0.5	91.9 HRB	67.3 µm	70.8 µm	
492	-	186.1 HV 0.5	90.2 HRB	68.4 µm	72.7 µm	
493	-	178.2 HV 0.5	88.6 HRB	70.1 µm	74.2 µm	
494	-	191.9 HV 0.5	91.4 HRB	68.9 µm	70.1 µm	
495	-	185.2 HV 0.5	90.0 HRB	70.2 µm	71.3 µm	
496	-	187.3 HV 0.5	90.5 HRB	70.8 µm	69.9 µm	
497	-	180.1 HV 0.5	89.0 HRB	71.6 µm	71.9 µm	
498	-	188.9 HV 0.5	90.8 HRB	70.0 µm	70.2 µm	
499	-	191.6 HV 0.5	91.3 HRB	69.1 µm	70.0 µm	
500	-	182.3 HV 0.5	89.5 HRB	71.8 µm	70.8 µm	
501	-	179.8 HV 0.5	89.0 HRB	72.3 µm	71.3 µm	
502	-	180.0 HV 0.5	89.0 HRB	72.0 µm	71.5 µm	
503	-	170.5 HV 0.5	86.5 HRB	73.9 µm	73.6 µm	
504	-	176.0 HV 0.5	88.0 HRB	71.6 µm	73.5 µm	
505	-	176.5 HV 0.5	88.1 HRB	72.1 µm	72.9 µm	
506	-	177.8 HV 0.5	88.4 HRB	71.8 µm	72.6 µm	
507	-	180.5 HV 0.5	89.1 HRB	71.4 µm	72.0 µm	
508	-	206.4 HV 0.5	94.3 HRB	66.4 µm	67.6 µm	
509	-	205.5 HV 0.5	94.1 HRB	67.0 µm	67.3 µm	
510	-	194.1 HV 0.5	91.8 HRB	70.6 µm	67.7 µm	
511	-	189.9 HV 0.5	91.0 HRB	70.0 µm	69.8 µm	
512	-	185.4 HV 0.5	90.1 HRB	70.2 µm	71.2 µm	
513	-	184.9 HV 0.5	90.0 HRB	69.8 µm	71.8 µm	
514	-	177.7 HV 0.5	88.4 HRB	71.5 µm	73.0 µm	
515	-	183.7 HV 0.5	89.7 HRB	68.1 µm	74.0 µm	
516	-	185.3 HV 0.5	90.1 HRB	70.7 µm	70.8 µm	
517	-	190.3 HV 0.5	91.1 HRB	69.4 µm	70.2 µm	
518	-	188.2 HV 0.5	90.6 HRB	67.5 µm	72.9 µm	
519	-	193.1 HV 0.5	91.6 HRB	68.6 µm	70.0 µm	
520	-	183.8 HV 0.5	89.8 HRB	67.9 µm	74.2 µm	
521	-	196.5 HV 0.5	92.3 HRB	68.8 µm	68.6 µm	
522	-	206.0 HV 0.5	94.2 HRB	68.0 µm	66.2 µm	
523	-	196.2 HV 0.5	92.2 HRB	68.3 µm	69.2 µm	
524	-	191.0 HV 0.5	91.2 HRB	69.0 µm	70.4 µm	
525	-	188.6 HV 0.5	90.7 HRB	68.5 µm	71.8 µm	
526	-	188.8 HV 0.5	90.8 HRB	70.6 µm	69.6 µm	
527	-	188.1 HV 0.5	90.6 HRB	68.7 µm	71.7 µm	
528	-	191.5 HV 0.5	91.3 HRB	68.0 µm	71.1 µm	

Date: 05-24-2023
Tester: Admin
Program: Hardness Map

Point	Distance	Hardness	Converted	Diagonal X	Diagonal Y	Comments
529	-	188.9 HV 0.5	90.8 HRB	69.6 µm	70.5 µm	
530	-	198.6 HV 0.5	92.7 HRB	67.4 µm	69.2 µm	
531	-	189.5 HV 0.5	90.9 HRB	69.6 µm	70.3 µm	
532	-	191.9 HV 0.5	91.4 HRB	67.6 µm	71.4 µm	
533	-	185.2 HV 0.5	90.0 HRB	70.8 µm	70.7 µm	
534	-	186.7 HV 0.5	90.3 HRB	69.0 µm	72.0 µm	
535	-	190.2 HV 0.5	91.0 HRB	68.6 µm	71.1 µm	
536	-	188.4 HV 0.5	90.7 HRB	69.2 µm	71.1 µm	
537	-	188.1 HV 0.5	90.6 HRB	68.1 µm	72.4 µm	
538	-	183.5 HV 0.5	89.7 HRB	70.7 µm	71.5 µm	
539	-	196.8 HV 0.5	92.4 HRB	68.1 µm	69.2 µm	
540	-	210.5 HV 0.5	95.1 HRB	65.6 µm	67.1 µm	
541	-	184.2 HV 0.5	89.8 HRB	72.7 µm	69.2 µm	
542	-	186.1 HV 0.5	90.2 HRB	70.1 µm	71.1 µm	
543	-	190.0 HV 0.5	91.0 HRB	70.2 µm	69.5 µm	
544	-	183.3 HV 0.5	89.7 HRB	71.0 µm	71.2 µm	
545	-	190.0 HV 0.5	91.0 HRB	68.9 µm	70.8 µm	
546	-	193.3 HV 0.5	91.7 HRB	68.6 µm	69.9 µm	
547	-	185.3 HV 0.5	90.1 HRB	70.4 µm	71.1 µm	
548	-	185.5 HV 0.5	90.1 HRB	70.9 µm	70.5 µm	
549	-	193.9 HV 0.5	91.8 HRB	70.0 µm	68.3 µm	
550	-	188.7 HV 0.5	90.7 HRB	69.8 µm	70.4 µm	
551	-	195.1 HV 0.5	92.0 HRB	68.8 µm	69.0 µm	
552	-	210.8 HV 0.5	95.1 HRB	66.2 µm	66.5 µm	
553	-	199.1 HV 0.5	92.8 HRB	67.7 µm	68.8 µm	
554	-	193.7 HV 0.5	91.7 HRB	68.5 µm	69.8 µm	
555	-	195.6 HV 0.5	92.1 HRB	69.0 µm	68.7 µm	
556	-	192.7 HV 0.5	91.5 HRB	67.4 µm	71.4 µm	
557	-	194.0 HV 0.5	91.8 HRB	67.8 µm	70.5 µm	
558	-	197.8 HV 0.5	92.6 HRB	68.7 µm	68.2 µm	
559	-	191.4 HV 0.5	91.3 HRB	67.7 µm	71.5 µm	
560	-	191.2 HV 0.5	91.2 HRB	68.9 µm	70.4 µm	
561	-	189.3 HV 0.5	90.9 HRB	68.6 µm	71.4 µm	
562	-	199.0 HV 0.5	92.8 HRB	68.2 µm	68.3 µm	
563	-	191.0 HV 0.5	91.2 HRB	70.2 µm	69.1 µm	
564	-	198.2 HV 0.5	92.6 HRB	66.3 µm	70.5 µm	
565	-	189.2 HV 0.5	90.8 HRB	68.9 µm	71.2 µm	
566	-	195.4 HV 0.5	92.1 HRB	66.9 µm	70.9 µm	
567	-	189.9 HV 0.5	91.0 HRB	69.7 µm	70.0 µm	

Date: 05-24-2023
Tester: Admin
Program: Hardness Map

Point	Distance	Hardness	Converted	Diagonal X	Diagonal Y	Comments
568	-	195.8 HV 0.5	92.2 HRB	67.1 µm	70.6 µm	
569	-	196.3 HV 0.5	92.3 HRB	69.0 µm	68.5 µm	
570	-	190.8 HV 0.5	91.2 HRB	69.6 µm	69.8 µm	
571	-	194.9 HV 0.5	92.0 HRB	68.3 µm	69.6 µm	
572	-	190.8 HV 0.5	91.2 HRB	69.6 µm	69.8 µm	
573	-	187.5 HV 0.5	90.5 HRB	68.6 µm	72.1 µm	
574	-	185.6 HV 0.5	90.1 HRB	68.2 µm	73.1 µm	
575	-	194.8 HV 0.5	92.0 HRB	69.8 µm	68.2 µm	
576	-	191.8 HV 0.5	91.4 HRB	68.6 µm	70.5 µm	
577	-	202.9 HV 0.5	93.6 HRB	66.2 µm	69.0 µm	
578	-	194.6 HV 0.5	91.9 HRB	68.3 µm	69.8 µm	
579	-	184.8 HV 0.5	90.0 HRB	69.6 µm	72.1 µm	
580	-	198.3 HV 0.5	92.7 HRB	67.7 µm	69.1 µm	
581	-	198.4 HV 0.5	92.7 HRB	67.3 µm	69.4 µm	
582	-	193.6 HV 0.5	91.7 HRB	67.5 µm	71.0 µm	
583	-	200.3 HV 0.5	93.1 HRB	66.8 µm	69.2 µm	
584	-	222.3 HV 0.5	97.0 HRB	64.3 µm	64.8 µm	
585	-	242.8 HV 0.5	-	62.4 µm	61.2 µm	
586	-	193.5 HV 0.5	91.7 HRB	69.0 µm	69.5 µm	
587	-	187.5 HV 0.5	90.5 HRB	70.2 µm	70.4 µm	
588	-	188.2 HV 0.5	90.6 HRB	69.8 µm	70.6 µm	
589	-	186.1 HV 0.5	90.2 HRB	69.4 µm	71.8 µm	
590	-	197.9 HV 0.5	92.6 HRB	68.3 µm	68.6 µm	
591	-	204.6 HV 0.5	93.9 HRB	67.8 µm	66.8 µm	
592	-	194.5 HV 0.5	91.9 HRB	69.3 µm	68.7 µm	
593	-	195.4 HV 0.5	92.1 HRB	69.7 µm	68.1 µm	
594	-	189.7 HV 0.5	90.9 HRB	69.8 µm	70.0 µm	
595	-	201.1 HV 0.5	93.2 HRB	69.5 µm	66.3 µm	
596	-	207.7 HV 0.5	94.5 HRB	67.6 µm	66.0 µm	
597	-	192.0 HV 0.5	91.4 HRB	67.0 µm	72.0 µm	
598	-	198.5 HV 0.5	92.7 HRB	68.7 µm	67.9 µm	
599	-	201.6 HV 0.5	93.3 HRB	66.0 µm	69.6 µm	
600	-	195.1 HV 0.5	92.0 HRB	67.8 µm	70.0 µm	
601	-	196.9 HV 0.5	92.4 HRB	69.4 µm	67.9 µm	
602	-	190.0 HV 0.5	91.0 HRB	69.6 µm	70.2 µm	
603	-	185.7 HV 0.5	90.1 HRB	68.6 µm	72.8 µm	
604	-	188.9 HV 0.5	90.8 HRB	69.7 µm	70.5 µm	
605	-	186.6 HV 0.5	90.3 HRB	69.6 µm	71.4 µm	
606	-	183.3 HV 0.5	89.7 HRB	68.2 µm	74.0 µm	

Date: 05-24-2023
Tester: Admin
Program: Hardness Map

Point	Distance	Hardness	Converted	Diagonal X	Diagonal Y	Comments
607	-	200.7 HV 0.5	93.1 HRB	67.9 µm	68.0 µm	
608	-	204.9 HV 0.5	94.0 HRB	66.7 µm	67.8 µm	
609	-	199.8 HV 0.5	93.0 HRB	67.1 µm	69.1 µm	
610	-	189.2 HV 0.5	90.8 HRB	68.0 µm	72.0 µm	
611	-	189.1 HV 0.5	90.8 HRB	69.2 µm	70.8 µm	
612	-	195.5 HV 0.5	92.1 HRB	69.4 µm	68.4 µm	
613	-	195.4 HV 0.5	92.1 HRB	68.1 µm	69.7 µm	
614	-	193.9 HV 0.5	91.8 HRB	69.3 µm	69.0 µm	
615	-	187.7 HV 0.5	90.5 HRB	69.8 µm	70.7 µm	
616	-	192.8 HV 0.5	91.6 HRB	68.4 µm	70.2 µm	
617	-	188.1 HV 0.5	90.6 HRB	71.5 µm	68.9 µm	
618	-	199.9 HV 0.5	93.0 HRB	68.2 µm	68.1 µm	
619	-	188.9 HV 0.5	90.8 HRB	70.1 µm	70.0 µm	
620	-	201.8 HV 0.5	93.4 HRB	67.3 µm	68.3 µm	
621	-	198.4 HV 0.5	92.7 HRB	67.6 µm	69.1 µm	
622	-	195.7 HV 0.5	92.1 HRB	68.5 µm	69.2 µm	
623	-	194.4 HV 0.5	91.9 HRB	70.5 µm	67.7 µm	
624	-	194.9 HV 0.5	92.0 HRB	67.9 µm	70.1 µm	
625	-	196.9 HV 0.5	92.4 HRB	68.0 µm	69.2 µm	
626	-	196.6 HV 0.5	92.3 HRB	70.4 µm	67.0 µm	
627	-	183.2 HV 0.5	89.6 HRB	71.4 µm	70.9 µm	
628	-	213.9 HV 0.5	95.6 HRB	64.3 µm	67.3 µm	
629	-	219.1 HV 0.5	96.5 HRB	65.4 µm	64.7 µm	
630	-	238.1 HV 0.5	99.7 HRB	62.2 µm	62.7 µm	
631	-	183.8 HV 0.5	89.8 HRB	73.2 µm	68.9 µm	
632	-	188.7 HV 0.5	90.7 HRB	70.0 µm	70.2 µm	
633	-	181.1 HV 0.5	89.2 HRB	70.4 µm	72.7 µm	
634	-	187.3 HV 0.5	90.5 HRB	70.6 µm	70.1 µm	
635	-	189.9 HV 0.5	91.0 HRB	67.6 µm	72.1 µm	
636	-	194.6 HV 0.5	91.9 HRB	68.7 µm	69.3 µm	
637	-	197.3 HV 0.5	92.5 HRB	68.7 µm	68.4 µm	
638	-	197.9 HV 0.5	92.6 HRB	69.3 µm	67.6 µm	
639	-	204.6 HV 0.5	93.9 HRB	69.3 µm	65.3 µm	
640	-	236.2 HV 0.5	99.4 HRB	62.7 µm	62.6 µm	
641	-	215.1 HV 0.5	95.9 HRB	65.2 µm	66.1 µm	
642	-	202.2 HV 0.5	93.4 HRB	65.8 µm	69.6 µm	
643	-	210.0 HV 0.5	95.0 HRB	66.4 µm	66.5 µm	
644	-	202.9 HV 0.5	93.6 HRB	66.5 µm	68.7 µm	
645	-	217.9 HV 0.5	96.3 HRB	64.4 µm	66.0 µm	

Date: 05-24-2023
Tester: Admin
Program: Hardness Map

Point	Distance	Hardness	Converted	Diagonal X	Diagonal Y	Comments
646	-	211.7 HV 0.5	95.3 HRB	65.7 µm	66.7 µm	
647	-	210.9 HV 0.5	95.1 HRB	67.4 µm	65.2 µm	
648	-	205.3 HV 0.5	94.1 HRB	66.1 µm	68.3 µm	
649	-	208.7 HV 0.5	94.7 HRB	66.0 µm	67.3 µm	
650	-	221.6 HV 0.5	96.9 HRB	63.9 µm	65.5 µm	
651	-	211.6 HV 0.5	95.3 HRB	65.3 µm	67.1 µm	
652	-	207.6 HV 0.5	94.5 HRB	67.9 µm	65.7 µm	
653	-	214.6 HV 0.5	95.8 HRB	67.4 µm	64.1 µm	
654	-	201.6 HV 0.5	93.3 HRB	65.8 µm	69.8 µm	
655	-	214.1 HV 0.5	95.7 HRB	63.8 µm	67.8 µm	
656	-	220.2 HV 0.5	96.7 HRB	63.3 µm	66.5 µm	
657	-	217.8 HV 0.5	96.3 HRB	63.7 µm	66.8 µm	
658	-	220.6 HV 0.5	96.8 HRB	64.9 µm	64.8 µm	
659	-	210.1 HV 0.5	95.0 HRB	66.4 µm	66.4 µm	
660	-	233.4 HV 0.5	98.9 HRB	65.1 µm	60.9 µm	
661	-	215.8 HV 0.5	96.0 HRB	65.4 µm	65.6 µm	
662	-	201.9 HV 0.5	93.4 HRB	70.4 µm	65.1 µm	
663	-	217.4 HV 0.5	96.2 HRB	64.7 µm	65.9 µm	
664	-	217.5 HV 0.5	96.3 HRB	64.8 µm	65.7 µm	
665	-	210.6 HV 0.5	95.1 HRB	65.7 µm	67.0 µm	
666	-	218.7 HV 0.5	96.4 HRB	64.5 µm	65.7 µm	
667	-	218.1 HV 0.5	96.3 HRB	64.6 µm	65.8 µm	
668	-	212.5 HV 0.5	95.4 HRB	65.5 µm	66.6 µm	
669	-	219.7 HV 0.5	96.6 HRB	64.4 µm	65.5 µm	
670	-	217.2 HV 0.5	96.2 HRB	65.2 µm	65.5 µm	
671	-	212.2 HV 0.5	95.4 HRB	64.1 µm	68.1 µm	
672	-	223.2 HV 0.5	97.2 HRB	63.4 µm	65.5 µm	
673	-	242.7 HV 0.5	-	61.3 µm	62.3 µm	
674	-	255.7 HV 0.5	-	60.3 µm	60.1 µm	
675	-	268.3 HV 0.5	-	58.9 µm	58.7 µm	
676	-	206.2 HV 0.5	94.2 HRB	66.6 µm	67.5 µm	
677	-	192.3 HV 0.5	91.5 HRB	69.2 µm	69.7 µm	
678	-	192.2 HV 0.5	91.4 HRB	69.4 µm	69.5 µm	
679	-	186.9 HV 0.5	90.4 HRB	70.3 µm	70.5 µm	
680	-	190.4 HV 0.5	91.1 HRB	70.0 µm	69.5 µm	
681	-	192.5 HV 0.5	91.5 HRB	69.9 µm	68.9 µm	
682	-	213.1 HV 0.5	95.5 HRB	65.5 µm	66.4 µm	
683	-	216.1 HV 0.5	96.0 HRB	65.4 µm	65.6 µm	
684	-	218.2 HV 0.5	96.4 HRB	65.4 µm	65.0 µm	

Date: 05-24-2023
Tester: Admin
Program: Hardness Map

Point	Distance	Hardness	Converted	Diagonal X	Diagonal Y	Comments
685	-	209.5 HV 0.5	94.9 HRB	65.5 µm	67.6 µm	
686	-	206.3 HV 0.5	94.3 HRB	66.1 µm	68.0 µm	
687	-	206.2 HV 0.5	94.2 HRB	66.1 µm	68.0 µm	
688	-	199.2 HV 0.5	92.8 HRB	66.5 µm	70.0 µm	
689	-	207.7 HV 0.5	94.5 HRB	68.1 µm	65.5 µm	
690	-	208.5 HV 0.5	94.7 HRB	65.6 µm	67.8 µm	
691	-	207.9 HV 0.5	94.6 HRB	65.6 µm	67.9 µm	
692	-	226.8 HV 0.5	97.8 HRB	65.0 µm	62.9 µm	
693	-	207.1 HV 0.5	94.4 HRB	67.2 µm	66.6 µm	
694	-	204.6 HV 0.5	93.9 HRB	66.1 µm	68.5 µm	
695	-	188.0 HV 0.5	90.6 HRB	70.5 µm	70.0 µm	
696	-	207.8 HV 0.5	94.6 HRB	67.4 µm	66.2 µm	
697	-	198.8 HV 0.5	92.8 HRB	66.6 µm	70.0 µm	
698	-	217.6 HV 0.5	96.3 HRB	64.4 µm	66.1 µm	
699	-	212.8 HV 0.5	95.5 HRB	66.4 µm	65.6 µm	
700	-	205.4 HV 0.5	94.1 HRB	67.5 µm	66.8 µm	
701	-	194.5 HV 0.5	91.9 HRB	69.3 µm	68.8 µm	
702	-	208.0 HV 0.5	94.6 HRB	66.7 µm	66.8 µm	
703	-	208.8 HV 0.5	94.8 HRB	65.5 µm	67.8 µm	
704	-	209.4 HV 0.5	94.9 HRB	65.5 µm	67.5 µm	
705	-	208.3 HV 0.5	94.7 HRB	66.5 µm	67.0 µm	
706	-	205.9 HV 0.5	94.2 HRB	66.0 µm	68.2 µm	
707	-	207.5 HV 0.5	94.5 HRB	66.3 µm	67.4 µm	
708	-	200.2 HV 0.5	93.0 HRB	68.0 µm	68.1 µm	
709	-	198.8 HV 0.5	92.8 HRB	69.9 µm	66.7 µm	
710	-	199.4 HV 0.5	92.9 HRB	68.2 µm	68.1 µm	
711	-	199.2 HV 0.5	92.8 HRB	68.3 µm	68.2 µm	
712	-	211.3 HV 0.5	95.2 HRB	65.6 µm	66.8 µm	
713	-	209.9 HV 0.5	95.0 HRB	66.0 µm	66.9 µm	
714	-	207.1 HV 0.5	94.4 HRB	64.8 µm	69.0 µm	
715	-	204.9 HV 0.5	94.0 HRB	66.9 µm	67.7 µm	
716	-	215.9 HV 0.5	96.0 HRB	66.5 µm	64.6 µm	
717	-	211.2 HV 0.5	95.2 HRB	67.3 µm	65.2 µm	
718	-	229.7 HV 0.5	98.3 HRB	62.4 µm	64.7 µm	
719	-	242.1 HV 0.5	-	61.9 µm	61.9 µm	
720	-	246.2 HV 0.5	-	61.9 µm	60.9 µm	
721	-	215.7 HV 0.5	95.9 HRB	65.7 µm	65.4 µm	
722	-	214.5 HV 0.5	95.7 HRB	65.1 µm	66.4 µm	
723	-	192.7 HV 0.5	91.5 HRB	69.3 µm	69.5 µm	

Date: 05-24-2023
Tester: Admin
Program: Hardness Map

Point	Distance	Hardness	Converted	Diagonal X	Diagonal Y	Comments
724	-	195.2 HV 0.5	92.0 HRB	68.5 µm	69.3 µm	
725	-	208.8 HV 0.5	94.8 HRB	66.6 µm	66.7 µm	
726	-	210.5 HV 0.5	95.1 HRB	65.9 µm	66.9 µm	
727	-	208.9 HV 0.5	94.8 HRB	66.5 µm	66.8 µm	
728	-	203.2 HV 0.5	93.6 HRB	67.6 µm	67.5 µm	
729	-	196.2 HV 0.5	92.2 HRB	67.1 µm	70.4 µm	
730	-	210.0 HV 0.5	95.0 HRB	67.0 µm	65.8 µm	
731	-	206.9 HV 0.5	94.4 HRB	67.8 µm	66.1 µm	
732	-	201.5 HV 0.5	93.3 HRB	68.0 µm	67.6 µm	
733	-	204.5 HV 0.5	93.9 HRB	66.7 µm	67.9 µm	
734	-	210.2 HV 0.5	95.0 HRB	66.9 µm	65.9 µm	
735	-	205.4 HV 0.5	94.1 HRB	67.3 µm	67.1 µm	
736	-	200.6 HV 0.5	93.1 HRB	69.2 µm	66.8 µm	
737	-	207.1 HV 0.5	94.4 HRB	67.1 µm	66.7 µm	
738	-	217.7 HV 0.5	96.3 HRB	65.5 µm	65.1 µm	
739	-	201.0 HV 0.5	93.2 HRB	68.3 µm	67.5 µm	
740	-	199.3 HV 0.5	92.9 HRB	67.5 µm	69.0 µm	
741	-	203.4 HV 0.5	93.7 HRB	66.8 µm	68.3 µm	
742	-	210.7 HV 0.5	95.1 HRB	64.7 µm	68.0 µm	
743	-	208.6 HV 0.5	94.7 HRB	65.9 µm	67.5 µm	
744	-	210.2 HV 0.5	95.0 HRB	67.4 µm	65.4 µm	
745	-	199.6 HV 0.5	92.9 HRB	65.8 µm	70.5 µm	
746	-	216.9 HV 0.5	96.2 HRB	66.0 µm	64.7 µm	
747	-	200.1 HV 0.5	93.0 HRB	66.1 µm	70.0 µm	
748	-	203.4 HV 0.5	93.7 HRB	65.3 µm	69.7 µm	
749	-	206.7 HV 0.5	94.3 HRB	66.5 µm	67.4 µm	
750	-	218.1 HV 0.5	96.4 HRB	64.9 µm	65.5 µm	
751	-	219.7 HV 0.5	96.6 HRB	64.4 µm	65.5 µm	
752	-	244.7 HV 0.5	-	60.5 µm	62.6 µm	
753	-	234.7 HV 0.5	99.1 HRB	63.8 µm	61.9 µm	
754	-	234.8 HV 0.5	99.1 HRB	62.5 µm	63.2 µm	
755	-	213.6 HV 0.5	95.6 HRB	66.5 µm	65.3 µm	
756	-	207.5 HV 0.5	94.5 HRB	65.4 µm	68.3 µm	
757	-	214.4 HV 0.5	95.7 HRB	65.4 µm	66.1 µm	
758	-	214.4 HV 0.5	95.7 HRB	66.4 µm	65.1 µm	
759	-	215.6 HV 0.5	95.9 HRB	64.9 µm	66.3 µm	
760	-	209.5 HV 0.5	94.9 HRB	66.5 µm	66.5 µm	
761	-	207.9 HV 0.5	94.6 HRB	66.0 µm	67.5 µm	
762	-	211.1 HV 0.5	95.2 HRB	65.6 µm	67.0 µm	

Date: 05-24-2023
Tester: Admin
Program: Hardness Map

Point	Distance	Hardness	Converted	Diagonal X	Diagonal Y	Comments
763	-	212.9 HV 0.5	95.5 HRB	65.3 µm	66.6 µm	
764	-	211.2 HV 0.5	95.2 HRB	65.8 µm	66.7 µm	
765	-	214.6 HV 0.5	95.8 HRB	65.2 µm	66.3 µm	
766	-	221.0 HV 0.5	96.8 HRB	64.5 µm	65.1 µm	
767	-	204.9 HV 0.5	94.0 HRB	67.3 µm	67.2 µm	
768	-	211.8 HV 0.5	95.3 HRB	66.5 µm	65.8 µm	
769	-	211.9 HV 0.5	95.3 HRB	66.0 µm	66.3 µm	
770	-	213.7 HV 0.5	95.6 HRB	65.5 µm	66.2 µm	
771	-	218.2 HV 0.5	96.4 HRB	65.5 µm	64.9 µm	
772	-	213.5 HV 0.5	95.6 HRB	65.5 µm	66.3 µm	
773	-	214.8 HV 0.5	95.8 HRB	66.1 µm	65.3 µm	
774	-	214.6 HV 0.5	95.8 HRB	64.8 µm	66.7 µm	
775	-	203.1 HV 0.5	93.6 HRB	68.0 µm	67.2 µm	
776	-	219.8 HV 0.5	96.6 HRB	65.3 µm	64.6 µm	
777	-	221.3 HV 0.5	96.9 HRB	63.9 µm	65.5 µm	
778	-	212.6 HV 0.5	95.4 HRB	63.8 µm	68.3 µm	
779	-	236.7 HV 0.5	99.4 HRB	62.3 µm	62.8 µm	
780	-	227.4 HV 0.5	97.9 HRB	63.3 µm	64.4 µm	
781	-	249.1 HV 0.5	-	61.6 µm	60.4 µm	

Geosyntec consultants

10777 Westheimer Road, Suite 900
Houston, Texas 77042
PH 281.920.4601
FAX 281.920.4602
www.geosyntec.com

Exhibit B - Memorandum

Date: 7 July 2022

To: [redacted] and [redacted], Marathon Pipe Line, LLC

From: [redacted] and [redacted], Geosyntec Consultants, Inc.

Cc: [redacted], [redacted] and [redacted], Geosyntec Consultants, Inc.

Subject: Memorandum Addressing Cause of Ground Movement
Edwardsville, Illinois
Geosyntec Memorandum: TXG0258-0700-MM-001 (Rev. 1)

INTRODUCTION

Geosyntec Consultants, Inc. (Geosyntec) has prepared this memorandum at the request of Marathon Pipe Line, LLC (MPL) to present our findings regarding the geotechnical and hydrotechnical factors that contributed to ground movement in the vicinity of the Wood River-to-Patoka (WoodPat) 22-inch pipeline (Pipeline) and Cahokia Creek in Edwardsville, Illinois (Site). The rupture location is within MPL right-of-way (ROW) Number (No.) 15 adjacent to the intersection of Edwardsville Road (IL-143) and Cahokia Creek (Creek). The Site is located on the southeast terrace of the Creek and the Pipeline traverses roughly parallel to the Creek in a southwest to northeast orientation.

Geosyntec's team of geotechnical and hydrotechnical engineers has assisted MPL with the following activities related to the Site:

- On 17 March 2022, Geosyntec's engineers conducted a visual inspection of the ground conditions at the Site to inform the development of recommendations for temporary stabilization and geohazard monitoring.
- On 21 March 2022, Geosyntec submitted a technical memorandum summarizing the field observations, recommendations for temporary stabilization and requesting data needed to advance the geohazard mitigation design.
- On 4 April 2022, Geosyntec submitted a memorandum summarizing our preliminary geohazard assessment for the Site.
- On 11 to 13 April 2022, Geosyntec oversaw the drilling and sampling of two geotechnical boreholes at the Site. Inclinometer casing and a vibrating wire piezometer were installed in each of the two boreholes. Subsequently, Geosyntec also installed two ShapeArray

inclinometers, and five sets of primary and redundant strain gauges at the Site, three sets on the WoodPat pipeline and two sets on the adjacent RoxPat pipeline.

- On 13 May 2022, Geosyntec submitted a geotechnical report for the Site, which included interpretations of the subsurface condition and geotechnical design parameter recommendations for stability analysis and mitigation design.
- On 27 May 2022, Geosyntec submitted a slope stability assessment calculation package (dated 26 May 2022) and presented the results of our hydrotechnical analysis (dated 20 May 2022) which was submitted following a call with MPL.

This memorandum builds on Geosyntec's prior activities related to the Site and offers our assessment of the cause of the ground movement.

FIELD OBSERVATIONS

Geosyntec conducted a visual inspection of the Site on 17 March 2022, and our observations are summarized in the *Geohazard Assessment of Edwardsville Site, Illinois* memorandum, dated 21 March 2022.

A few key observations from the site visit include the following:

- Water in the Creek, as it passes underneath the bridge north of the Site, flows directly toward the south stream bank (left bank looking downstream) near the southwestern extent of the ground movement, as shown in Figure 1.
- Sandy flood deposits were observed along the streambank more than 15-feet above the observed water elevation, suggesting episodic high-flow and associated erosional events occur within the Creek.
- Streambank deposits along the Creek are alluvial deposits which are susceptible to scour.

Figure 1 - View Looking Southwest from Edwardsville Road Bridge (Photo Taken 17 March 2022)

DOCUMENT REVIEW

In addition to field observations made during the site visit, the following documents were reviewed and considered in our findings presented herein:

- 2014 slope repair documents, including: (i) Submar Design-Build Proposal dated 9 January 2014; and (ii) Land & Pipe Management Report dated 8 August 2014.
- 2015, 2016, and 2017 slope repair documents, including: (i) MPL documentation checklist dated 13 May 2015; (ii) MPL erosion control – assessment sheet dated 2 June 2016; and (iii) Land & Pipe Management Report dated 17 April 2017.
- Bedrock and surficial geology maps from the Illinois State Geological Survey.
- Nearby water well logs from the Illinois State Geological Survey.

HYDROTECHNICAL ANALYSIS

Geosyntec reviewed historical aerial images, evaluated historical stream gage data, and performed hydraulic analyses for the purpose of assessing the contributions from bank and bed scour on ground stability at the Site.

Historical Aerial Image Review

Review of aerial images from 1991 through 2022 obtained from Google Earth™ and NearMap show riverine behavior at the Site is influenced by historical straightening and natural attempt to re-establish a meander pattern. In the area where scour has resulted in lateral migration of the south streambank, there is evidence of scarp progression and ground instability dating back at least several decades.

Previous repair attempts in 2014 and 2017 using erosion control devices appear to have had little to no impact on preventing scour of the streambank and thus preventing or slowing ground movement.

Figures 2 through 5 present a series of historical aerial images showing changes that occurred at the Site since 2011.

- The image from September 2011 (Figure 2) shows the absence of deep-rooted forest canopy along the streambank, a defined scarp at the head of the ground instability, presence of large woody debris (LWD), and a point bar on the opposite side of the creek that is re-directing the flow hydraulics toward the Site.
- The image from April 2016 (Figure 3) shows the bank conditions without vegetive cover along the streambank, presence of LWD along downstream end of left bank at Site, the development of hydraulic expansion pool created by increased flow velocities downstream from the bridge floodway constriction and grade drop downstream of the bridge, and splay deposits indicative of flooding and outer bend hydraulics. The photo also shows articulated concrete mats that were installed for erosion control above a section of the Pipeline in 2014, but which generally do not appear to be protecting the bank from scour or contributing to the stability of the slope.
- The image from July 2020 (Figure 4) shows an additional area of LWD accumulation at the upstream end of the left bank at the Site. The existence and proximity of LWD to the left bank complicate scour hydraulics creating local scour conditions resulting for localized velocity accelerations and multidirectional flow patterns.
- The image from 1 March 2022 (Figure 5) shows flow through the Illinois Department of Transportation (IDOT) installed scour mitigation riprap directed towards the left bank and accumulations of LWD.

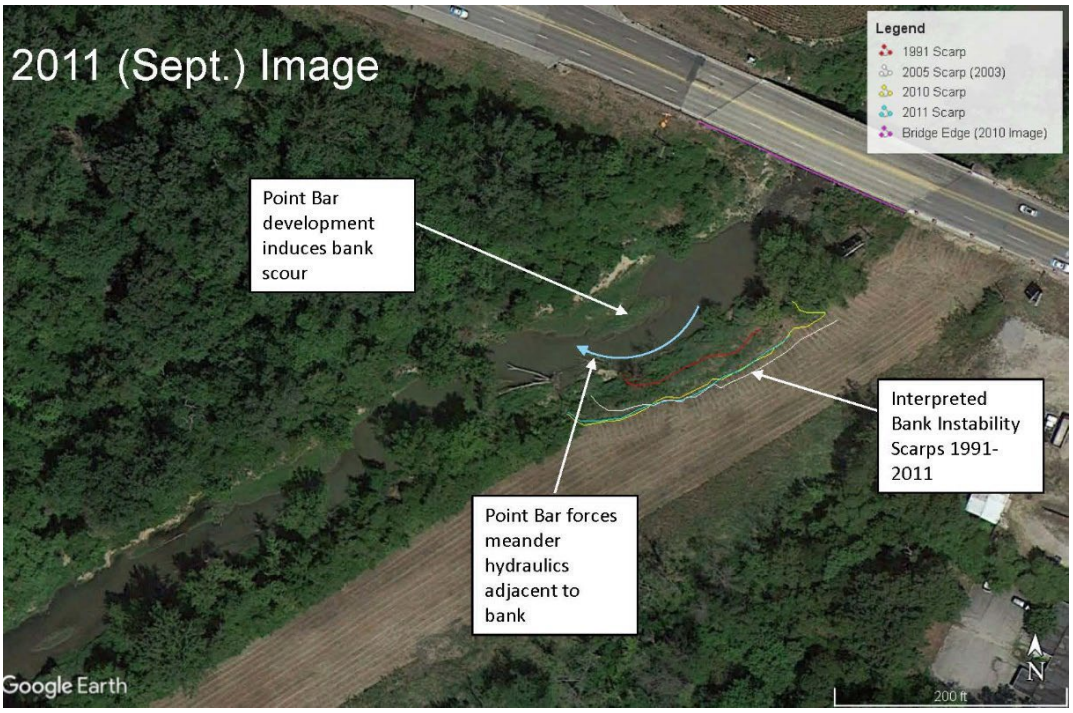

Figure 2 - Aerial Image Dated September 2011 (from Google Earth™)

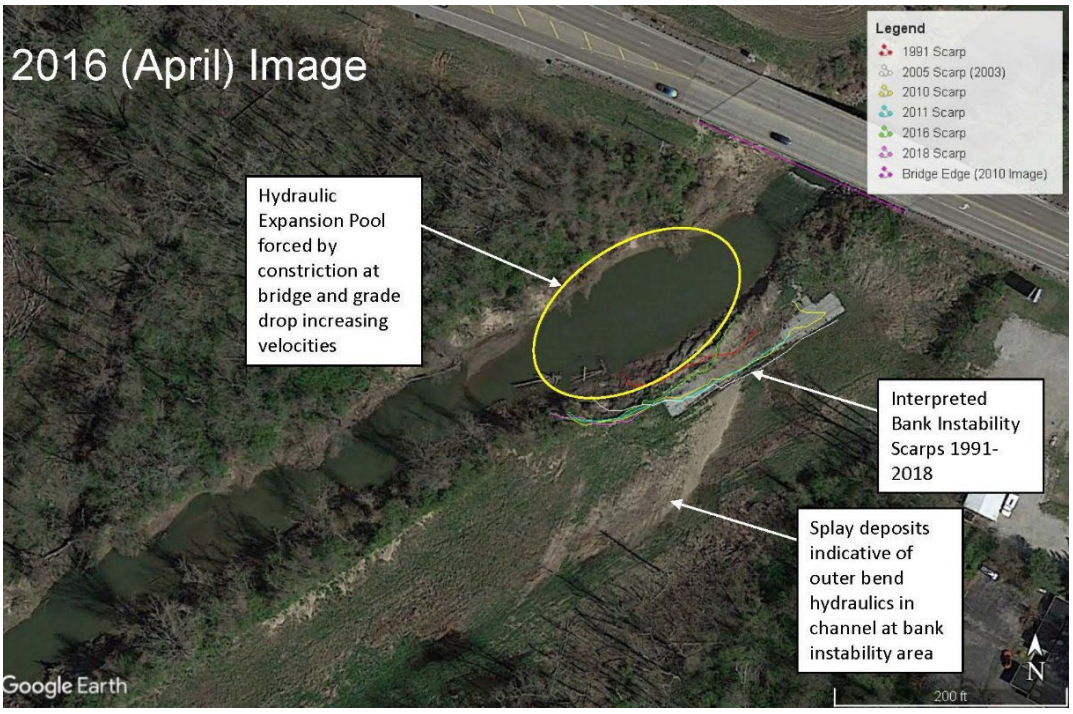

Figure 3 - Aerial Image Dated April 2016 (from Google Earth™)

Figure 4 - Aerial Image Dated July 2020 (from Google Earth™)

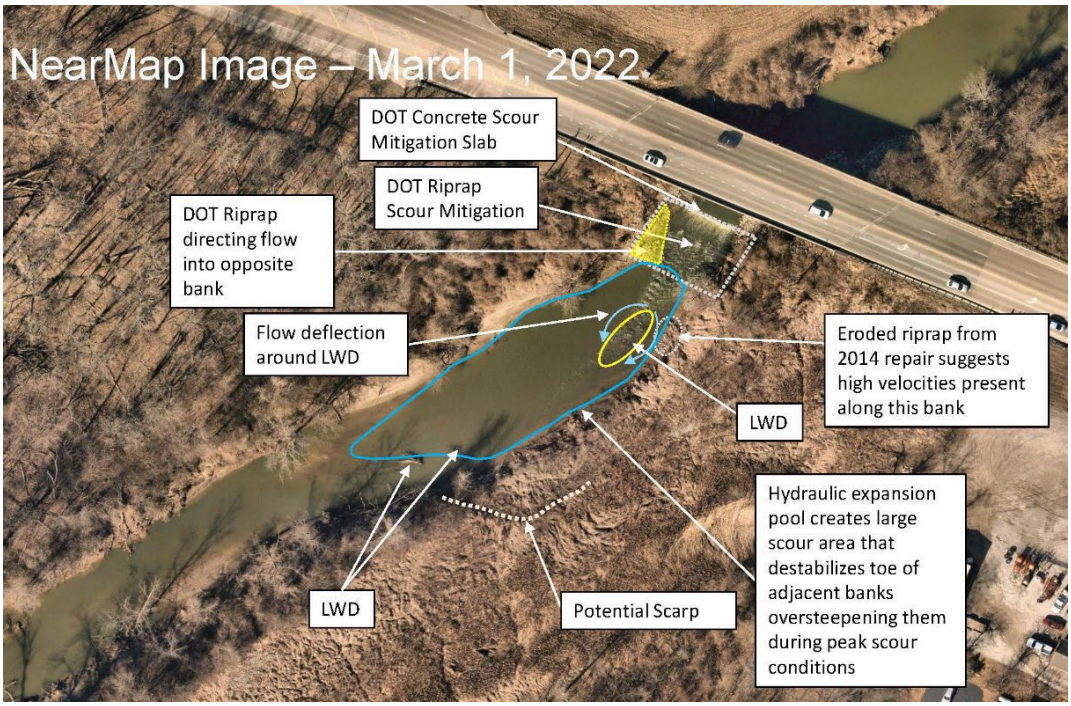

Figure 5 - Aerial Image Dated 1 March 2022 (from NearMap)

Creek Bathymetry and Bank Topography

The creek bathymetry and bank topography collected by DoC Mapping LLC after the 11 March 2022 ground movement is shown in Figure 6. These contours, along with the cross sections in Figure 8, illustrate topographically the impact of scour and ground movement on the left bank relative to the forested upstream and downstream streambanks. The instabilities along the left bank are coincident with deeper creek bed depths (i.e., resulting from bed scour), lateral bank position, and altered bank slope inclination. As shown in Figure 8, in the area of the ground instability, the creek bed depth is about five feet deeper and the bank is recessed laterally about 15 feet, compared to the upstream and downstream streambanks.

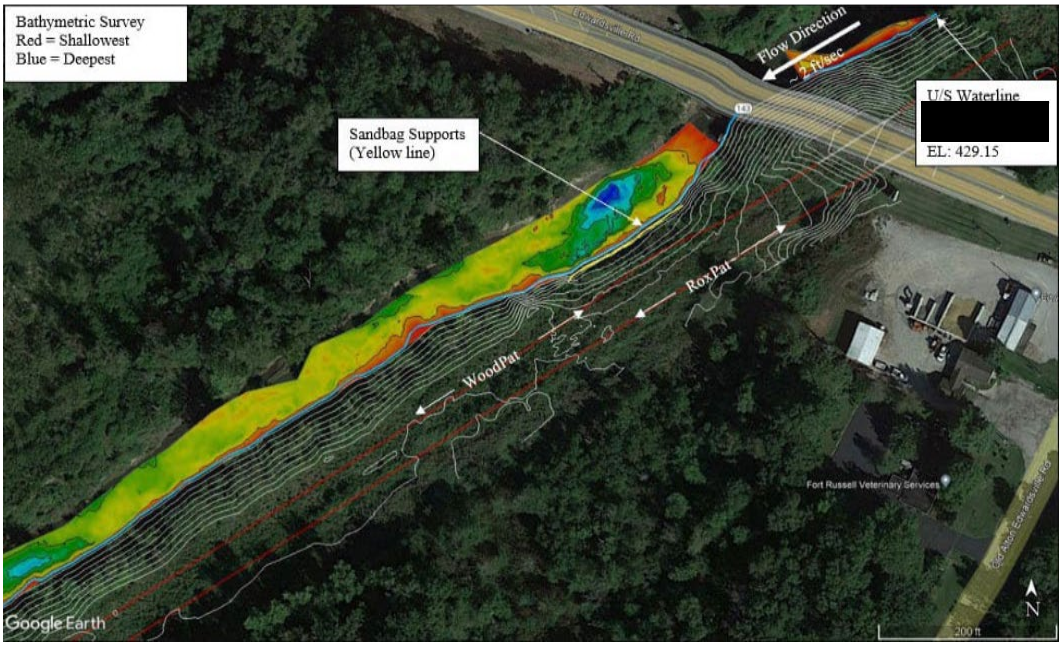

Figure 6 - Site Plan with Bathymetric and Ground Contours Obtained April 2022 (from DoC Mapping LLC)

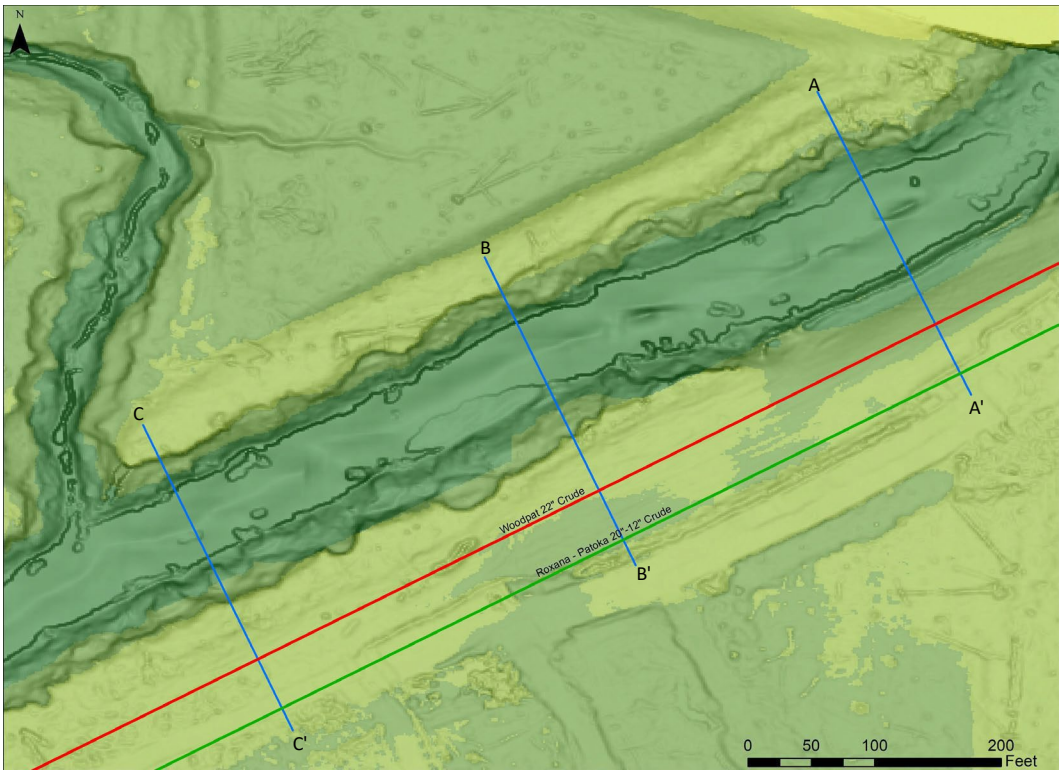

Figure 7 - Plan Showing Locations of Cross Sections

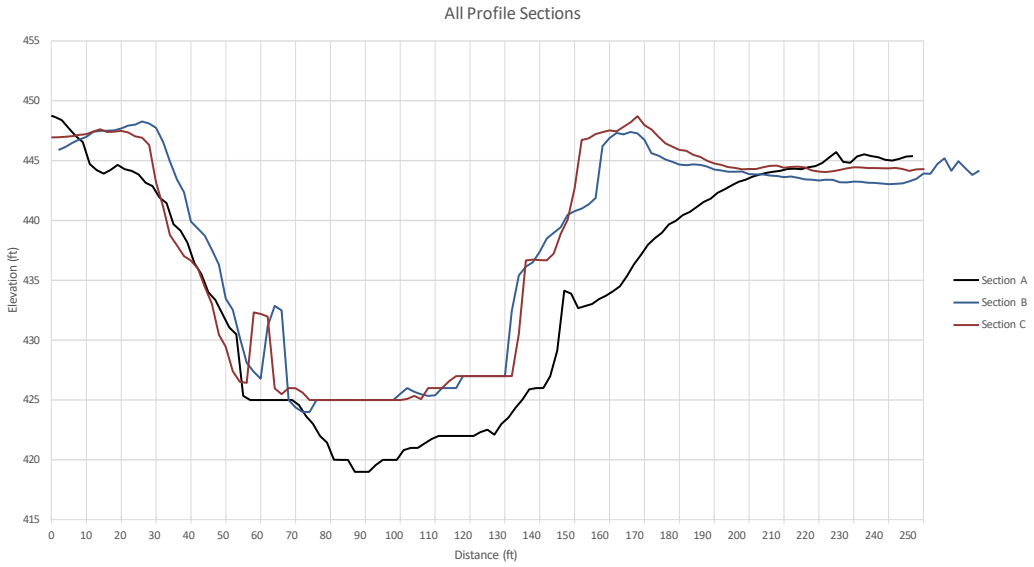

Figure 8 - Cross Section Profiles

Flood Event on 7 March 2022

The flood event which occurred on 7 March 2022, preceding the Pipeline rupture by several days, is reported to have had a stream flow magnitude of 4,070 cubic feet per second (cfs), which corresponds to approximately a 1.5-year return period event. This is equivalent to a "bankfull" event responsible for the dominant sediment transport annually. It is suspected that a single flood event is not responsible for the scour which led to the conditions at the Site, but rather a series of multiple smaller events, such as the 7 March 2022 flood event. Figure 9 contains a hydrograph with stream flow data for the Creek showing the relatively frequency of flood events with stream flows in the range of 4,000 cfs from May 2021 to April 2022.

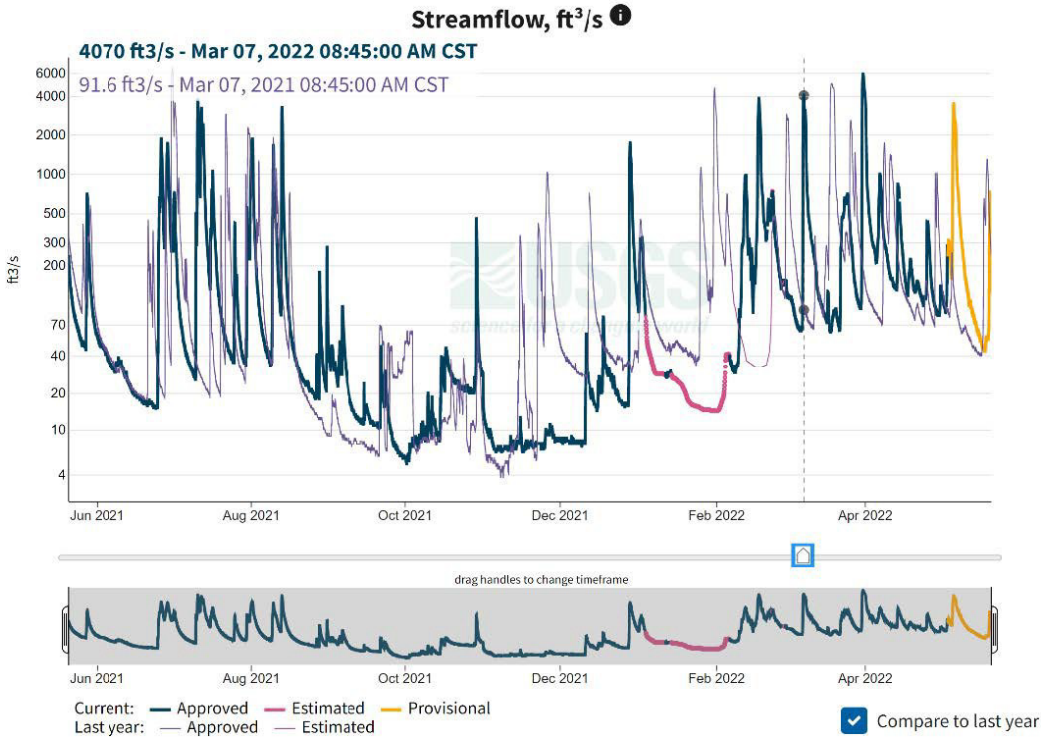

Figure 9 - 1-yr Cahokia Creek Hydrograph (from USGS)

Hydraulic Analyses

The hydraulic analyses were performed using HEC-RAS 2D to model existing hydraulic conditions and one stabilization concept (i.e., an anchored sheet pile wall). The modeling used the bathymetric data collected by DoC Mapping LLC in April 2022 and data from the nearby United States Geological Survey (USGS) stream gage. Geosyntec modeled existing conditions at 2-, 5-, 10-, 25-, 50-, and 100-year flood return interval discharges using the Federal Emergency Management Agency (FEMA) Flood Insurance Study (FIS) hydrology for initial set up and approximation of the model. Follow-on scour modeling using HEC-RAS 2D was conducted for the 50- and 100-year flood return intervals. The scour modeling analyses confirmed the potential

for deep bed scour at the Site, with maximum bed scour depths of 7 to 9 feet (below current bed depths) predicted for large 50- and 100-year return period flood events, enough to scour the creek bed down to the top of the underlying bedrock.

Streambank Instability Root Cause Hypothesis

The hydrotechnical analysis results indicate the following mechanics are the root cause of the streambank instability at the Site:

- Scour mitigation placed to protect the bridge has been preferentially eroded by the Creek, such that the scour mitigation directs flow toward the affected streambank.
- Hydraulic expansion conditions downstream of bridge create a scour pool that destabilizes toe of adjacent streambanks oversteepening them during peak scour conditions.
- Outer bend flow hydraulics force outer bank toe scour. Toe scour over-steepens the streambank setting up conditions for streambank instability.
- Fluctuating water levels in the Creek, especially after extensive high water and/or wet periods is a contributing factor in furthering bank failures of varying magnitudes (see Geosyntec *Slope Stability Assessment* calculation package dated 26 May 2022).
- LWD is prevalent in this system and regularly deposits or is impinged on the affected streambank. The presence of LWD creates local hydraulics inducing scour (i.e., local scour).

Conclusions

The hydraulic and scour conditions noted above and described further in Geosyntec's *Hydrotechnical Analysis (TXG0258-0600)* dated 20 May 2022, are expected to continue at the Site. The streambank instability was caused by ground movement resulting from riverine scour and LWD which influenced local scour along the left bank (looking downstream). Mitigation of future streambank instabilities will need to accommodate the observed scour patterns, occurrence of LWD, and scour depths illustrated in the *Hydrotechnical Analysis (TXG0258-0600)*. Mitigation measures should be designed to minimize destabilizing adjacent streambanks parallel to the Pipeline downstream.

GEOTECHNICAL STABILITY ANALYSIS

Geosyntec performed two-dimensional (2D) limit equilibrium slope stability analyses for the Site using the Slide2 software by Rocscience and a geotechnical model developed following the geotechnical investigation. The analysis is summarized in Geosyntec's *Slope Stability Assessment* calculation package, dated 26 May 2022. The analysis was performed to assess the present condition of the Site and to assess potential causes for the 11 March 2022 ground movement. The analysis included evaluating the slope for changing hydraulic conditions (i.e., fluctuating

groundwater table and rapid drawdown) resulting from flooding and rainfall events, and instability caused by riverine scour along the streambank.

The slope stability analysis results for Section A-A' under the assumed conditions at the time of instability are shown in Figure 10. This scenario considers a streambank slope of approximately 1.2H to 1V with material removed at the slope toe from riverine scour. Groundwater is modeled as a rapid drawdown condition with initial and final water elevations changing from EL. 440 feet[1] to EL. 425 feet within the model to match flooding conditions observed prior to the event on 11 March 2022. The undrained shear strength of the alluvial clay (Unit 2A) below EL. 430 feet was adjusted until a factor of safety equal to 1.0 was achieved. The resulting undrained shear strength is 400 pounds per square foot (lbs/ft^2), a value that is consistent with the range of shear strengths for this material measured from laboratory testing.

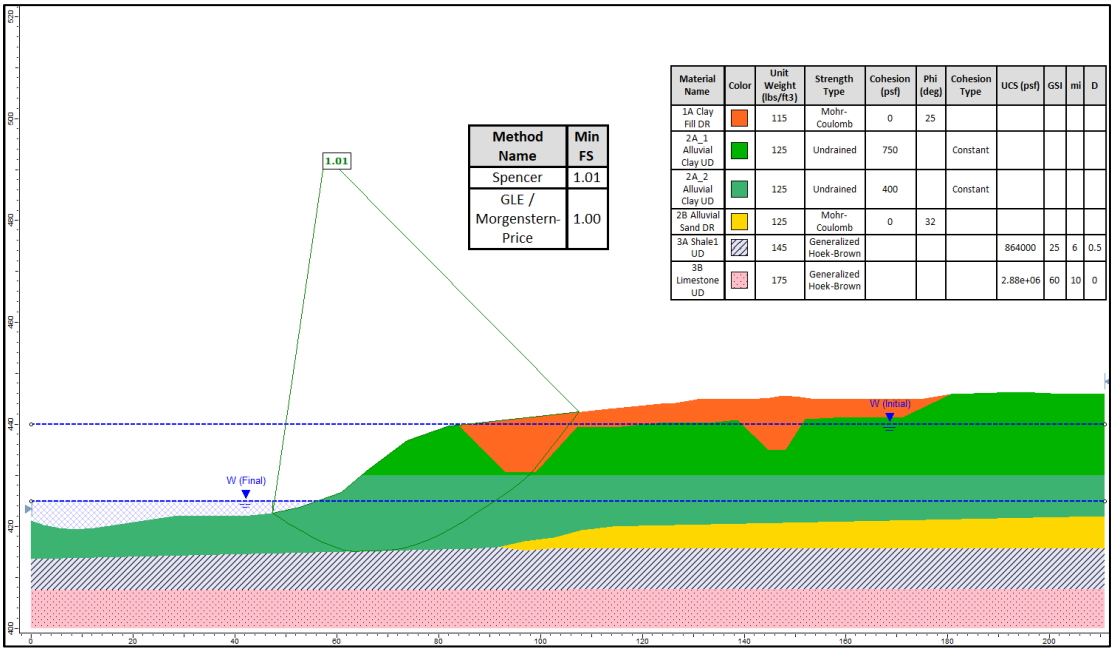

Figure 10 - Limit Equilibrium Slope Stability Analysis at Section A-A'

Conclusions

The slope stability analyses indicate that a combination of streambank scour in the Creek and a reduction of undrained shear strength in the subsurface soil is the plausible cause of instability which led to ground movement. The slope stability sensitivity analysis results presented in Geosyntec's *Slope Stability Assessment* calculation package, dated 26 May 2022, which generally utilize the material parameters provided in the Geosyntec's *Geotechnical Report,* dated 13 May

[1] Elevations (EL) provided herein are in North American Vertical Datum of 1988 (NAVD88)

2022, closely simulate the conditions that are suspected to have led to the 11 March 2022 instability at the Site. The analyzed cross sections indicate a deep-seated sliding surface with entrance/exit locations generally consistent with field observations. As such, mitigation should be designed to address the apparent deep-seated or global instability at the Site.

SUMMARY

The inferred cause of ground movement at the Site is a combination of scour and a reduction of shear strength in the alluvial soils due to softening and repeated shearing. These two mechanisms combined to induce progressive ground movement of upslope soils into the Creek when sediment from the toe of the streambank was removed by scour during subsequent episodic high-flow events. The progressive ground movement over the past decade or more deflected the Pipeline horizontally and vertically downslope toward the Creek.

*****

Exhibit C - Strain Feature Prioritization

Priority 1 Feature:
Initiate site investigation / remediation project immediately. Site must be investigated within 90 days.

Priority 2 Feature:
Investigate site within one year.

Priority 3 Feature:
Strain feature does not appear to be geohazard related and is likely due to original construction or integrity work. No investigation required. Site should be monitored for change during future assessments.

Land Movement Review:

- Review MAUI data base for existing mapped hazards (Span, WWX, GEO, DCM)
- Look at aerial / satellite imagery for current and historic changes
- Cracking
- Hummocky terrain (use MPL or Public LiDAR)
- Tree/vegetation changes, water, etc.
- Review geohazard desktop studies.
- USGS faults
- Look at topography - does strain align with downhill movement?
- Encroaching stream banks?
- Does pipe deflection have “bell shape”?
- Karst Maps

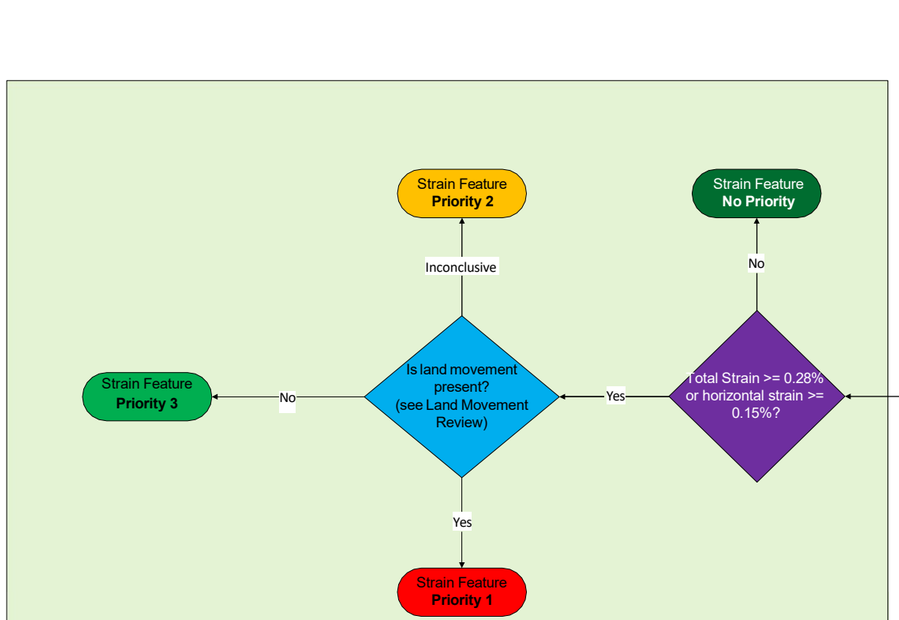

AREAS REPORTED AS STABLE IN STRAIN REPORT

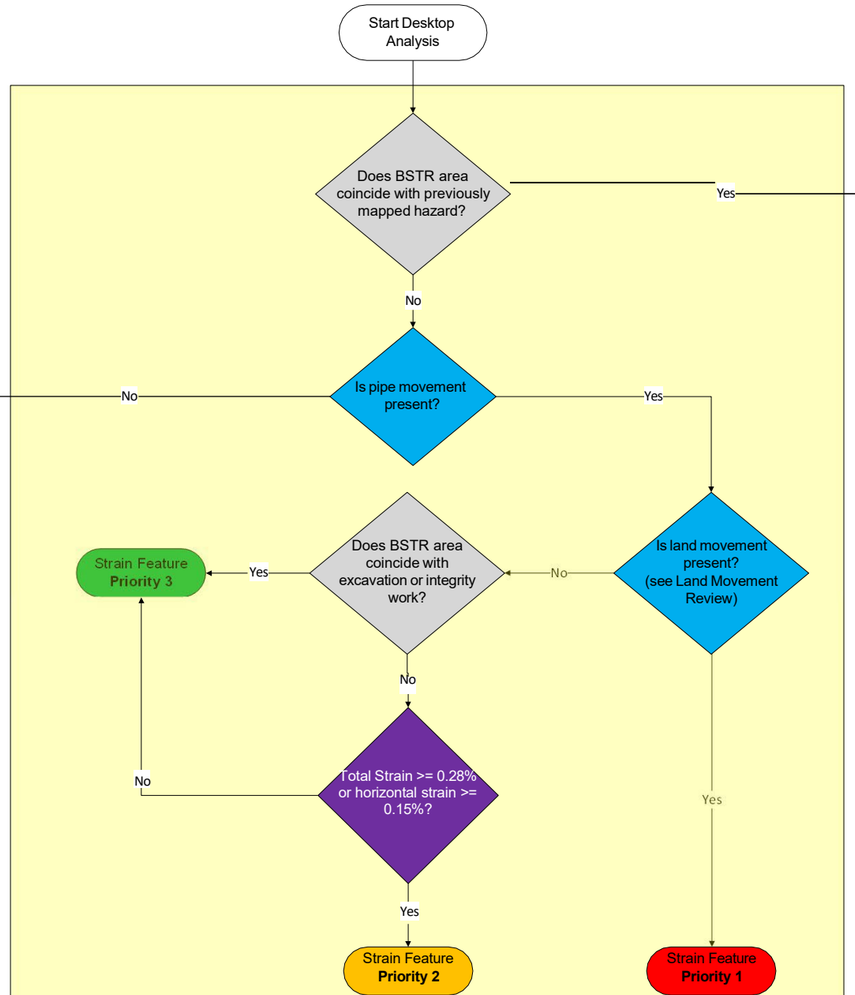

PIPE MOVEMENT PRESENT
NO INTERACTION WITH MAPPED HAZARDS OR HAZARD DATA UNABILABLE

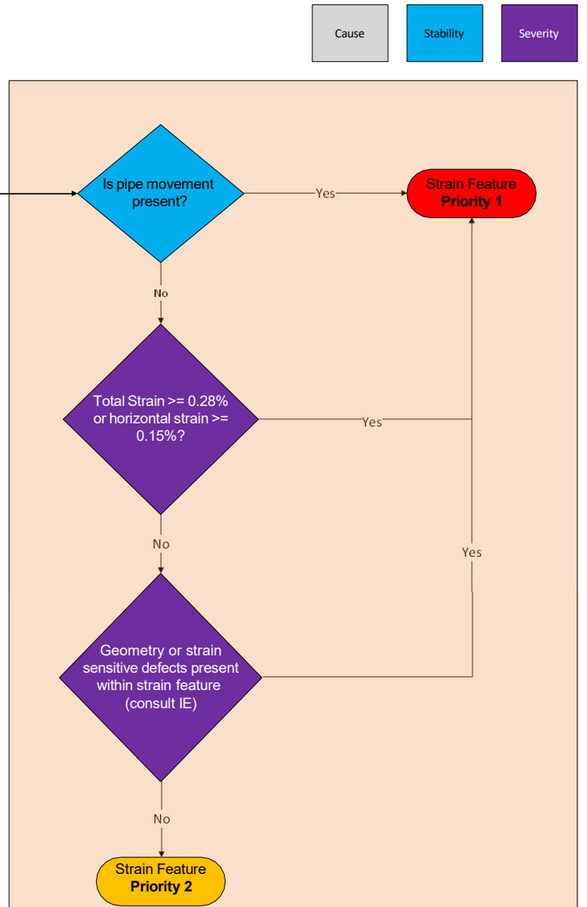

STRAIN FEATURE INTERACTS WITH MAPPED HAZARDS